CHEMICAL REVIEWS

REVIEW

pubs.acs.org/CR

Site Selective and Single Complex Laser-Based Spectroscopies: A Window on Excited State Electronic Structure, Excitation Energy Transfer, and Electron−Phonon Coupling of Selected Photosynthetic Complexes

Ryszard Jankowiak,*[,†] Mike Reppert,[†] Valter Zazubovich,[‡] Jörg Pieper,[§,∥] and Tonu Reinot[†]

[†]Department of Chemistry, Kansas State University, Manhattan, Kansas 66506, United States

[‡]Department of Physics, Concordia University, Montreal H4B1R6 Quebec, Canada

[§]Max-Volmer-Laboratories for Biophysical Chemistry, Technical University of Berlin, Germany

[∥]Institute of Physics, University of Tartu, Riia 142, 51014 Tartu, Estonia

CONTENTS

1. INTRODUCTION

In photosynthesis, light is harvested and its energy is used to produce the various biological components that support nearly all life on earth. It is oxygenic photosynthesis that led to the green and well-oxygenated world that surrounds us today. Plants and cyanobacteria possess a large number of chlorophylls embedded in local environments of two large proteins called photosystem I

Received: July 25, 2010
Published: May 19, 2011

(PSI) and photosystem II (PSII) that work in concert.[1−3] Details of molecular mechanisms at work in these systems continue to be unraveled thanks to the detailed information provided by X-ray diffraction crystallography[4−8] and improved interpretation of various optical spectra[9−19] (vide infra). Details of the structure and function of these two photosystems can be found in the very recent book;[20] see section 2 for more details and additional relevant references. A minireview of functional implications regarding the primary photophysical processes in PSII including discussion of hypotheses regarding electron-transfer pathways has been recently published by Renger and Schlodder.[11] Continued efforts in basic photosynthesis research are of great value, as improved understanding of the photosynthetic process may lead to more efficient biofuel production. It is important to bear in mind that light-driven water oxidation that is catalyzed by PSII is not only responsible for the production of oxygen (O_2) but is also involved in the production of biomass and fossil fuels. It is anticipated that better understanding of these complex multichromophoric assemblies may also help in designing better artificial systems that could find applications in future solar cells. Thus, further advances in fundamental knowledge in various areas of photosynthesis research are extremely important. In this review, we discuss a number of photosynthetic complexes, including the PSI and PSII complexes, as well as the components of bacterial photosynthesis machinery[21−25] with a focus on the information gained from recent high-resolution (site-selective) spectroscopic studies. These studies provide more insight into the excited state electronic structure, excitation energy transfer (EET), electron−phonon (el−ph) coupling, and protein dynamics in the above-mentioned photosynthetic complexes (PC).

At low temperatures, proteins behave as amorphous solids. It is well-known that electronic transitions in amorphous phases are subject to inhomogeneous broadening caused by the variation of local fields.[26] This broadening obscures the information on the dynamics of the system. Several (low-temperature) laser-based techniques that can overcome the inhomogeneous broadening and access the homogeneous (natural) line width have been developed.[27−31] This review provides a brief description and a critical account of site-selective spectroscopies, i.e., spectral hole-burning (SHB)[32−41] and fluorescence line-narrowing (FLN),[42−46] as well as their applications in the area of photosynthesis research (for recent reviews see refs 47, 48). It was Kharlamov and co-workers[49] and Gorokhovskii and co-workers[50] who first observed the nonphotochemical hole-burning (NPHB), as it later came to be called. NPHB is an ideal technique to unravel the optical and dynamic properties of complex biological systems. For previous reviews of the site excitation energy selective techniques, see refs 33, 36, and 46. The site-selective techniques are of great utility, as they improve spectral resolution by a factor of 10^3-10^5 as compared to conventional spectroscopy at room temperature. As a result, HB and FLN spectroscopies [including the delta FLN (ΔFLN) approach,[51−61] i.e., a combination of FLN and SHB] can provide information not available to other spectroscopic techniques and allow one to measure the rates of dynamic processes that normally remain hidden in the broad absorption bands. Low-temperature experiments allow one to trap biomolecules in a physical state in which large-scale motions necessary for crossing the high barriers are frozen out ("physical trapping"), while the motions within the lower hierarchical tiers of the protein energy landscape (vide infra) remain active.[26,62,63] The latter provides valuable information on the dynamics of complex systems.[48,62]

The basic aspects of these specialized techniques, i.e., SHB, FLN, and ΔFLN, are described in order to reach a broad community of spectroscopists and researchers in the area of photosynthesis, bridging the gap between the biophysical and biochemical sciences. The reader interested in structural disorder and configurational tunneling dynamics of amorphous solids at low temperatures or applications in the area of information storage technologies is referred to excellent books and reviews.[26,36,62−64] To broaden the scope of this review, we also describe the basic aspects of single photosynthetic complex spectroscopy (SPCS),[65−81] with an emphasis on how SHB and FLN spectroscopies corroborate or contradict data obtained by SPCS. SPCS continues to be of great help in answering many challenging questions related to various photosynthetic complexes. We focus on the capabilities of the above-mentioned methods to access different phenomena and discuss relevant connections between SPCS and SHB/FLN results obtained for the same systems. In section 4.10 we also briefly discuss the connections between SHB and the new class of experiments collectively known as 2D electronic spectroscopies.

Although a number of issues of interest to specialists in high-resolution spectroscopy will be addressed and many details of new developments are provided, we also try to make our treatment of spectroscopic techniques and results (and their interpretation) accessible to those who are not experts in SHB/FLN/ΔFLN/SPCS. Therefore, a clear description of the limitations and advantages of using these highly specialized techniques is also given, including a summary of the information that can be extracted from photosynthetic reaction centers (RC) and light-harvesting antenna complexes using site-selective and single molecule spectroscopies (SMS). Theoretical sections on various aspects of SHB, FLN, and ΔFLN spectroscopies are self-contained and can be omitted by readers interested only in the implications of the experimental findings for photosynthesis related problems. Basic aspects of SPCS spectroscopy are also briefly discussed. It is anticipated that a comprehensive review of high-resolution spectroscopies will stimulate additional research by making it possible for both experts and nonexperts to profit from the special insight that these techniques offer.

Numerous advances were made in recent years in understanding excited state electronic structure, excitation energy transfer (EET), el−ph coupling, and heterogeneity of various PC/multichromophoric molecular assemblies[9−19] using high-resolution spectroscopy in frequency domain[9−12,48,51,58−61] as well as time domain techniques.[11,13,15,16] A large variety of complexes have been isolated and studied in detail.[9−16,82−84] This review focuses on recent progress in SHB/FLN/ΔFLN spectroscopies and key questions related to PC studied by our groups. The effects of energy disorder on the excitonic structure (localization) are discussed in detail. We emphasize that many issues related to the electronic structure of PSI and PSII complexes still remain to be fully resolved, including the number and origin/composition of the lowest-energy traps, origin of various emission bands, the pigment composition of excitonic states, and the exact nature and parameters of the protein dynamics. For example, various subsections of section 5 discuss the electronic structure and the EET of peripheral antenna systems (LHCI, LHCII, CP29) and the extent of delocalization of the excitons in the CP43 and CP47 antenna pigment complexes of PSII. Issues related to the reaction centers, their electronic structure, and primary charge separation processes in the PSII RC and larger photosystems and supercomplexes are

addressed, along with a brief discussion of possible future developments.

Although significant progress has been made in the studies of single PC[65,67−72] and ensembles via SHB spectroscopy,[9,10,14,17] we believe that much remains to be done (vide infra) before a consistent picture of electronic structure and the EET processes will emerge. Since SHB/FLN and SPCS are complementary techniques, both continue to contribute to a better understanding of PC. In addition, a series of projects under development that are needed to further advance the field of SHB are briefly discussed in section 6. In particular, a better theoretical description of the origin of resonant and nonresonant holes burned in excitonically coupled photosynthetic antenna pigment complexes is needed to provide more insight into the underlying electronic structures of these systems. We argue that simple models recently developed[39,40,69,85,86] can provide a necessary framework for probing the electronic structure of complex systems via SHB spectroscopy.

In section 2, the review begins with general structural information on PSI and PSII (structure−function relationship, basic assignments, and frequently asked questions). This section also addresses the basic aspects of the bacterial photosynthesis, as bacterial RCs and LH2 antenna systems are briefly discussed. General considerations related to EET and charge separation (CS) rates are briefly summarized in section 3. Section 4 describes the fundamentals of SHB/FLN and SPCS. A theory for the hole profiles, hole growth kinetics, the burn frequency (ω_B) dependence of the hole profile, which leads to the determination of inhomogeneous broadening Γ_{inh} (i.e., site distribution function, SDF) and el−ph coupling parameters is presented in sections 4.1−4.4. Equations related to the theoretical description of hole profiles and FLN/ΔFLN spectra are briefly addressed in sections 4.5−4.7, while very recent, new developments regarding modeling of HB spectra in excitonically coupled systems are described in section 4.8. A broad coverage of recent applications is given in section 5. Numerous examples are shown to demonstrate the power of the above spectroscopic approaches in application to biological systems. The discussion is centered around recent experimental and theoretical results with an emphasis on the wealth of information that is not easily obtainable using other techniques. Finally, section 6 discusses the future of SHB spectroscopy in the era of single molecule/complex spectroscopy; here, our attention is focused on continuing developments of high-resolution spectroscopies.

2. GENERAL INFORMATION ON THE STRUCTURE OF PHOTOSYNTHETIC COMPLEXES AND STRUCTURE−FUNCTION RELATIONSHIPS

2.1. Photosystem I (PSI) and Photosystem II (PSII)

The existence of PSI and PSII is of fundamental importance for life and energy flow on Earth, and detailed knowledge about the process of photosynthesis is important both for the understanding of complex ecological phenomena and for practical applications involving solar energy conversion. The latter may involve both natural PC and their artificial mimics.[1,2] PC use identical chlorophyll (Chl) molecules or the magnesium-free equivalents, pheophytins (Pheo), as both donors and acceptors of energy and charge; various other pigments (especially carotenoids) are employed to increase the range of wavelengths accessible for light harvesting and to assist in photoprotection. The specific tasks that each Chl carries out are defined (to a large extent) by its interaction with other Chls and cofactors, as well as with the surrounding protein.[3,20,87]

In very general terms, photosynthetic proteins can be divided into RC proteins (where charge separation takes place) and antenna proteins (where solar radiation is absorbed and transferred to the RC). The details of the energy conversion process vary from system to system, but in general after light harvesting and charge separation have taken place, a variety of redox active carrier proteins are involved in a complex electron transfer pathway to convert the generated proton/electron gradient into useable energy for the system. In oxygenic photosynthesis, electrons are produced in PSII by the light-induced splitting of water molecules; the protons released in this process are isolated on one side of the photosynthetic membrane, producing a cross-membrane electrochemical potential. The electrons produced from the splitting of water are shuttled through a variety of electron carriers to the PSI complex, where a second light-induced reaction occurs, using these free electrons to reduce electron carriers (e.g., $NADP^+$ to NADPH) and to contribute additional protons to the cross-membrane proton gradient. Together, the electrochemical gradient and reduced electron carriers produced by PSII and PSI are then used by metabolic proteins including ATP synthetase to produce usable chemical resources for the organism such as ATP and, via the Calvin cycle, carbohydrates.

To facilitate the interactions necessary for this complex process, in vivo photosynthetic proteins do not exist in isolation but rather in large complexes (or so-called "supercomplexes") of many protein in specific associations with each other. The advent of high-resolution X-ray crystallography has provided crucial insight into the structure and functioning of PSI, PSII, and their associated antenna complexes.[4−7] Figure 1 shows in frames A and B the structures of two plant photosynthetic supercomplexes, one involving PSI (frame B[88]) and the other PSII (frame A[7,89,90]). The PSII supercomplex pictured consists of a *core antenna complex* (the RC along with core antenna proteins CP43 and CP47 and numerous non-Chl binding proteins) together with the associated *peripheral antenna complexes* light harvesting complex II (LHCII or the Lhcb family of proteins), CP24, CP26, and CP29.[89] (The structure shown is adapted from that presented in ref 89 using ref 7 for the PSII core complex and ref 90 for the antenna proteins). These peripheral Chl *a*/*b* binding proteins (which are believed to be structurally homologous) are rather loosely associated with the core antenna complex and can be easily separated from it. The CP43/CP47/RC core complex is bound together somewhat more strongly and can be isolated as a separate preparation, as can the individual constituents CP43, CP47, and the RC, although to what extent the properties of the intact supercomplex are preserved in the isolated monomeric protein constituents is an important question currently under discussion (see section 5.3.2). The plant PSI supercomplex pictured in Figure 1B consists of the core complex (most notably the PsaA and PsaB Chl-binding proteins) together with the LHCI peripheral light harvesting complexes (Lhca 1−4).[88] In plants, the PSI core complex occurs as a monomer, while in cyanobacteria, three such complexes merge to form a PSI trimer. We hasten to note that the list of PC discussed here and pictured in Figure 1 is by no means exhaustive; many other Chl-binding photosynthetic proteins from a wide variety of plants, cyanobacteria, and bacteria have been identified, isolated, and even studied by means of SHB. Indeed, even within a given species, the structure and composition of the PSI or PSII supercomplexes may vary depending on light intensity levels and

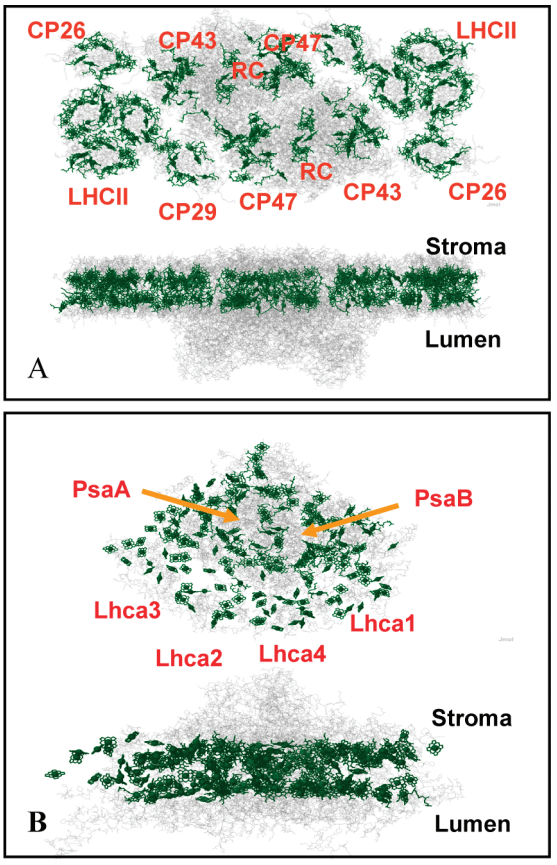

Figure 1. (A) Structure of photosystem II supercomplex based on Figure 4 of Nield and Barber.[89] The view in the upper panel is from the stromal side of the membrane, while the lower panel is from within the membrane. The structures of CP43, CP47, and the RC were taken from the 3BZ1 and 3BZ2 Brookhaven Protein Databank files,[7] while the structure for LHCII was taken from file 1RWT.[90] Estimated structures for CP26 and CP29 were obtained by removing the appropriate pigments from the LHCII monomer structure (following Nield and Barber). (B) Structure of a PSI supercomplex taken from Brookhaven Protein Databank file 2001.[88] The upper view is from the lumenal side of the membrane, while the lower view is from within the membrane.

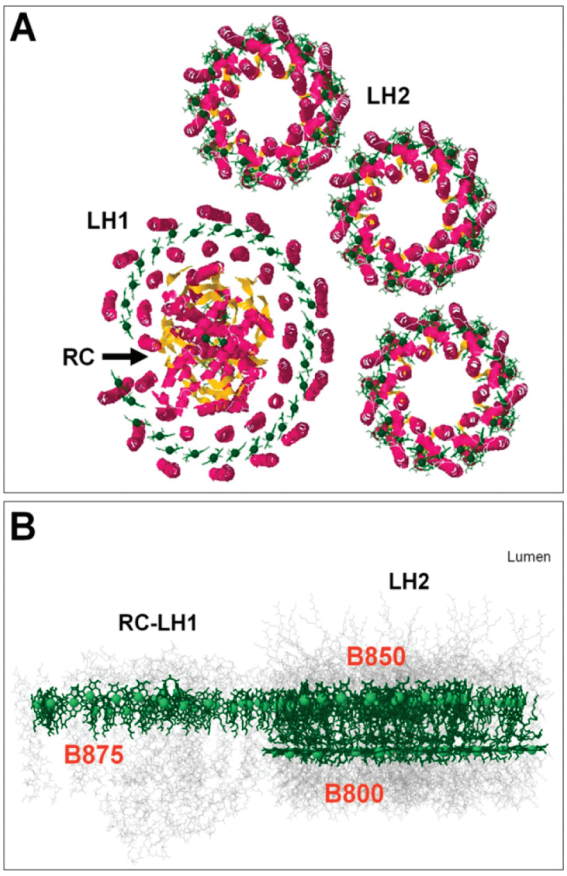

Figure 2. LH1−BRC assembly surrounded by multiple copies of LH2 complexes. The structure shown was created using the crystal structures from refs 23, 96, and 99. (Note that the RC−LH1 structure is taken from *Rhodopseudomonas palustris*, while the LH2 structure is from *Rhodopseudomonas acidophila*.)

available mineral resources. The structures shown here are meant only to give a flavor of the complex structure and organization of these highly efficiently light-harvesting systems.

2.2. Basic Aspects of Bacterial Photosynthesis

Unlike plants, purple bacteria are incapable of oxygenic photosynthesis. However, the basic elements of their photosynthetic apparatus carry great resemblance to those of higher plants and cyanobacteria. The bacterial reaction center (BRC) contains two main subunits, L and M, approximately related to each other by C_2 symmetry, as well as the H-subunit and the cytochrome.[91] L and M proteins provide the scaffold for two symmetrical arrangements of bacteriochlorophyll (BChl) and bacteriopheophytine (BPheo) molecules. Both PSII and PSI RCs exhibit structurally similar arrangement for the primary electron transfer chain. Upon excitation of any RC pigments, the energy is quickly transferred to the pair of strongly coupled BChl *a* molecules ("special pair"), which serves as a primary electron donor. Despite the nearly symmetric two-branch arrangement, the electron transfer occurs along the A- (L-)branch in wild-type organisms. Genetic modifications may be employed to increase the probability of electron transfer along the B- (M)-branch.[92,93] SHB is among the many methods capable of detecting primary charge separation (CS) in the BRC.[94,95] The lowest-energy absorption of the BRC belongs to the special pair and is located from ~870 nm (*Rhodobacter sphaeroides*) to ~960 nm [*Blastochloris viridis* (formerly *Rhodopseudomonas viridis*)].[91−94]

The BRC is surrounded by the LH1 antenna protein. Although initially it was believed that LH1 exhibits nearly perfect C_n symmetry, recent AFM and cryomicroscopy studies indicated that the ring is broken by the PufX protein subunit.[96,97] Nevertheless, the LH1 complex is an assembly of *n* identical protein subunits holding in place an array of strongly coupled BChl *a* molecules. Each subunit holds two BChl *a* molecules in slightly nonidentical environment. The strong interpigment coupling results in absorption and emission spectra of LH1 becoming profound manifestations of excitonic effects (see section 3). The LH1−BRC assembly is surrounded by multiple copies of the LH2 antenna complex, as illustrated in Figure 2 (see also ref 98). The latter arrangement is a cyclic structure possessing the approximate C_n symmetry (with n = 8 or 9 depending on the species).[99] Unlike in LH1, LH2 structure contains two distinct rings of BChl *a* molecules. While in the B850 ring (labeling refers to the wavelengths of the strongest absorption band associated with respective ring) the center-to-center distances between BChl *a* molecules belonging to both the same dimer and the

dx.doi.org/10.1021/cr100234j |*Chem. Rev.* 2011, 111, 4546–4598

adjacent dimers are on the order of 9 Å, the electrostatic couplings are strong, and respective excitations are highly delocalized, the molecules of the B800 ring are relatively weakly interacting. Due to the highly symmetric character of antenna complexes of purple bacteria and strong interactions of BChls within the B850 (LH2) or B875 (LH1) rings, the absorption spectra of these complexes exhibit quite interesting properties. Namely, almost all oscillator strength of the molecules in the ring is concentrated in the transition to the second-lowest doubly degenerate excitonic state. In the absence of static or dynamic energy disorder, this description would be perfect, and the excited states of such a system would be ideally delocalized over the whole ring. Disorder, however, causes other excitonic states to become weakly allowed, as well as partial localization of excitons.[100,101] Interactions with vibrational degrees of freedom cause exciton self-trapping[56,102] and further localization.

Overall, energy harvested by the B800 ring of the LH2 is transferred to the B850 ring in about 1.6 ps at low temperatures[103,104] and in less than 1 ps at physiological temperatures (see, for example, refs 102, 105). In several picoseconds the excitation energy is transferred to the nearby LH1 complexes[97] and then to the BRCs. The energy transfer effectiveness approaches 100% in terms of number of primary charge separation events per number of photons absorbed. As mentioned above, charge separation starts at the special pair with an electron being quickly transported along the A-branch to Q_A (immobile quinone) and to Q_B (mobile quinone).

3. INTERPIGMENT INTERACTIONS, EXCITATION ENERGY TRANSFER (EET), AND CHARGE SEPARATION (CS) RATES—GENERAL CONSIDERATIONS

As evident from the discussion in the previous section, light-harvesting complexes can be considered as networks of interacting pigment molecules. The concept of an exciton, the excited electronic state delocalized over many molecules, proved extremely useful in describing the functioning of light-harvesting complexes and their spectroscopic properties.[44] The concept originates from condensed matter physics, the key feature of the exciton being its quasiparticle nature, with the wavelike property of delocalization, and the particle-like properties of effective mass, definite momentum, and energy. In conventional condensed matter theory, the exciton is just an electron−hole pair that is weakly bound by electrostatic interactions. The separation between electron and hole exceeds the lattice constant. Such excitons, called Wannier−Mott excitons, can propagate in the crystal, carrying momentum and energy.[44,106] The excited state of a single molecule can be imagined as a tightly bound exciton, with electron−hole separation smaller than the molecule size. Due to the coupling interactions between identical molecules in the crystal, the excitation energy could be passed from molecule to molecule like a wave, and excitation becomes delocalized. In quantum-mechanical terms, the resulting excited state becomes a superposition of excited states of multiple molecules (in the case of the perfect crystal, of all molecules in the crystal), so the concept of energy transfer loses its meaning. This type of the exciton is called Frenkel exciton.[106,107] Defects in the crystal structure cause localization of the Frenkel excitons, although exciton theory still can be applied to determine group velocities and the extent of delocalization. And even though the PCs are far from the infinite crystals possessing translation symmetry, they still remain the systems of multiple interacting molecules, and the concepts of exciton theory apply to them as well.

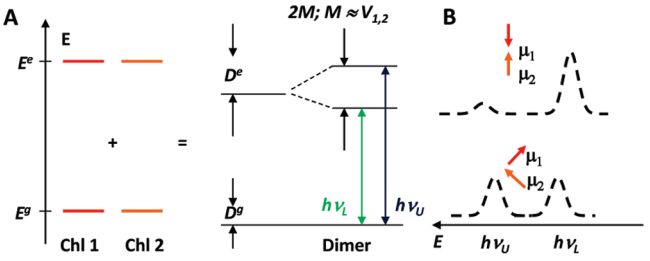

Figure 3. Effects of exciton interaction on the energy levels in a degenerate dimer of Chls. The splitting is equal to $2V_{1,2}$. Schematic spectra on the right are shown for two cases: (1) "head-to-tail" dimer (top spectra) and (2) a dimer with two perpendicular orientations of the dipole moments (lower spectra). $h\nu_L$ and $h\nu_U$ correspond to the energies of transitions to the lower and upper excitonic state, respectively. The same coupling was assumed for both configurations of the dipole moments.

We continue by considering the case of an excitonically coupled dimer. The logic of this simple example can be easily extended to PC containing more than two pigment molecules. Consider an isolated molecule with eigenfunction ϕ^i and eigenenergies E^i defined by the Hamiltonian

$$H\phi^i = E^i\phi^i$$

where i = g or e for ground and excited electronic states, respectively. If one now introduces one more molecule into the system, interacting with the first one with (electrostatic) potential energy V, the total wave functions become the products of the wave functions of the individual molecules. The total wave function for the ground state becomes $\phi_1{}^g\phi_2{}^g$, and the single-excited states localized on molecules 1 and 2 become $\psi_1{}^e = \phi_1{}^e\phi_2{}^g$ and $\psi_2{}^e = \phi_1{}^g\phi_2{}^e$, respectively. The wave functions of the excitonically coupled dimer may be written as $\psi_\pm = 1/2^{1/2}(\psi_1{}^e \pm \psi_2{}^e)$, with

$$\langle\psi^g|H_1 + H_2 + V|\psi^g\rangle = 2E^g + D^g$$
$$\langle\psi_\pm|H_1 + H_2 + V|\psi_\pm\rangle = E^g + E^e + D^e \pm M$$

where $D^g = \langle\psi^g|V|\psi^g\rangle$ is van der Waals interaction or dispersion energy for the ground state, $D^e = \langle\psi_1{}^e|V|\psi_1{}^e\rangle = \langle\psi_2{}^e|V|\psi_2{}^e\rangle$ is the van der Waals interaction for the excited dimer, and $V_{1,2} = \langle\psi_1{}^e|V|\psi_2{}^e\rangle = \langle\psi_2{}^e|V|\psi_1{}^e\rangle$ is the resonance transfer integral determining the excitation energy transfer rate and dimer excitonic splitting. The sign and magnitude of $V_{1,2}$ are determined by the orientation of the transition dipole moment vectors of the two molecules. Ignoring D^g and D^e, one can depict excitonic splitting in case of the dimer, as shown in Figure 3A. Note that the effect of coupling is the splitting of the spectrum into high ($h\nu_U$) and low ($h\nu_L$) energy components. The distribution of the oscillator strength depends on the orientation of the transition dipole moments, as schematically illustrated in Figure 3B.

In PC, due to the electrostatic coupling discussed above, the EET can take place in the excited state from one pigment to another. EET is a radiationless transition process. In general, the EET occurs from a manifold of vibrational states associated with the excited electronic state of the donor molecule into a manifold of vibrational states associated with the ground state of the acceptor molecule. In the area of photosynthesis, Chls form various antenna systems that can funnel energy to the RC, where the photochemistry takes place.[1−3] In simple terms, exciton (vide

supra) is often viewed as an excited electronic state that resides on more than one pigment (or group of molecules) during its lifetime.[44,108] Thus the nature of pigment−pigment and pigment−protein interactions is critical to describe various optical spectra. If the coupling between chromophores is weak (i.e., excitation is localized on a single pigment), energies of the chromophores are considered to be independent, even if there is a finite probability that energy will move from another chromophore to a chromophore (i.e., from donor to acceptor). Such an energy transfer can be described by the Förster theory.[109,110] In the case that the electronic coupling is so weak that inter- and intramolecular relaxation processes occur on a time scale faster than EET, the rate of EET, i.e., the transfer rate constant $k_{1\rightarrow 2}$ for this process, can be described according to Fermi's golden rule rate expression:

$$k_{1\rightarrow 2} = \frac{4\pi^2}{h}|V_{1,2}|^2\rho(E) \quad (1)$$

where $\rho(E)$ is related to the energy "matching" of the energy levels of the donor and acceptor molecules (i.e., Franck−Condon (FC) weighted density of states), h is Planck's constant, and $V_{1,2}$ is the coupling matrix element between the states 1 and 2 as schematically indicated in Figure 3, where the effect of interaction on energy levels (and spectra) of two identical molecules that have degenerate energy levels is illustrated (see also section 4.8, where modeling of HB spectra for various dimers and multichromophoric systems is discussed). Note that all parameters related to the vibrational states are combined in the integral $\rho(E)$ given by

$$\rho(E) = \int_{E=0}^{\infty} \mathrm{d}E\; G_D(E)\; G_A(E) \quad (2)$$

where $G_D(E)$ and $G_A(E)$ are normalized line shape functions that can be understood as densities of states that combine the respective ground and excited states. They are so-called Franck−Condon weighted and thermally averaged combined densities of states. Förster showed[109] that $G_D(E)$ and $G_A(E)$ can be related to the molar extinction coefficient $\varepsilon_A(\omega)$ and the fluorescence spectrum $f_D(\omega)$. $V_{1,2}$ is determined by coupling between donor and acceptor wave functions and strongly depends on the distance between chromophores. In practice, the Förster equation is often used in the form

$$k_{ij} = \frac{1}{\tau_D}\left(\frac{R_0}{R}\right)^6 \quad (3)$$

where R_0 is the characteristic distance (Förster radius, usually on the order of 4−10 nm) for the specific system and τ_D, as above, is the intrinsic lifetime of the excited donor. In essence, eq 1 can be used for both exciton migration and electron transfer (vide infra). Förster showed that $V_{1,2}$ and $\rho(E)$ can be related to the absorption $\varepsilon_A(\omega)$ of the acceptor and emission $f_D(\omega)$ of the donor via eq 4

$$k_{1\rightarrow 2} = \frac{9\kappa^2 c^4 \phi_D}{8\pi n^4 \tau_D R^6}\int_{\omega} \varepsilon_A(\omega)\, f_D(\omega)\, \frac{\mathrm{d}\omega}{\omega^4} \equiv \frac{3}{2}\frac{\kappa^2}{\tau_D}\left(\frac{\overline{R}_0}{R}\right)^6 \quad (4)$$

where κ is a factor dependent on angles of the dipole moments, n is the refractive index, τ_D is the fluorescence lifetime, and ϕ_D corresponds to the fluorescence quantum yield of the donor pigment.[108] Note that this approximation is valid if the interactions between pigments are smaller than the reorganization energy involved. If the coupling is larger than the limits set by the Förster theory, a group of pigments (e.g., Chls) should be treated as one

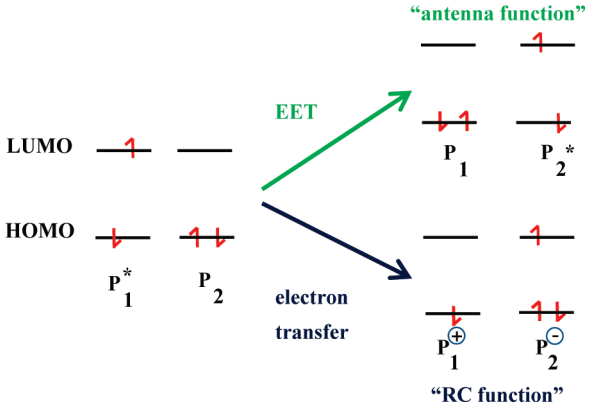

Figure 4. Simplified schematic representing the electronic coupling between two pigment molecules in the lowest excited state (P_1*) and ground state (P_2), respectively, giving rise either to EET (top right) or electron transfer (bottom) from P_1* to P_2. (Data taken from ref 108.)

system and optical spectra of such system must be calculated by quantum mechanical methods. As discussed in sections 4.8 and 5.1, the following factors need to be taken into account: (1) the strength of $V_{n,m}$ (where n and m label pigments), (2) the site energy of pigments before the excitonic interaction is turned on, and (3) the direction and magnitude of the transition dipole moment. For the case depicted in Figure 3B (upper spectrum) the exciton is delocalized over both pigments and the lowest-energy state possesses most of the oscillator strength. But depending on the structural arrangement in various antenna systems, the lowest state can be either weak or even forbidden, with the oscillator strength distributed over two or many pigments. Several examples of excitonically coupled systems are discussed in sections 4.8 and 5.1, where we explain the shape of complex antihole spectra observed in excitonically coupled systems. Here we only mention that identification of a system's "site-energies" is the major problem since, although several algorithms have been developed to find these parameters, it remains difficult to account for interaction with nearby protein.[85,86,111−113] In particular, as discussed below, interactions such as hydrogen bonding, coordination state of Chls, and protein-induced deviations of pigments from planarity are challenging to account for and if present may lead to changes in the electronic structures of PCs and RCs.

Finally, since in this review we discuss both EET ("antenna function") and electron transport ("RC" function), we note that these two functions (see Figure 4) depend on the mode of coupling.[44,105] The coupling depends on the nature of pigments P_1 and P_2 and on the electronic and vibronic interaction between these molecules, as well as interaction of molecules with their surrounding protein matrix. Often both exchange and Coulomb interactions need to be taken into account. Dexter theory[114] describes the exchange mechanism, while Förster[109] EET results from the dipole−dipole approximation of the Coulombic interactions. Both mechanisms have different distance dependence and different spin selection rules. Since the exchange mechanism depends strongly on the overlap of the electronic wave functions, the mechanism is restricted to rather short distances. In contrast, Förster (transfer between pigments of the same spin, i.e. the Coulomb type mechanism) permits EET over significantly longer distances.[44,105] On the other hand, the exchange mechanism (Dexter) does not have the spin restriction and permits EET from the triplet state to a pigment in the ground singlet state.

dx.doi.org/10.1021/cr100234j |Chem. Rev. 2011, 111, 4546–4598

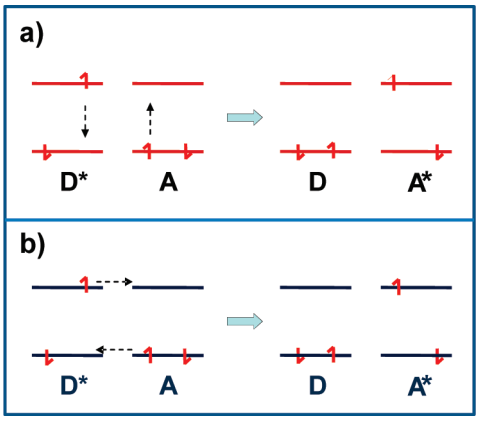

Figure 5. Mechanisms of EET: (a) Coulombic mechanism, as suggested by Förster,[109] and (b) electron exchange mechanism, as suggested by Dexter.[114]

Therefore, the protective carotenoid reaction for quenching chlorophyll triplets requires an exchange mechanism.[22,105,115] In short, in the Förster mechanism, multipole−multipole Coulomb interaction de-excites an initially excited electron on the donor molecule D (i.e., D*) and simultaneously excites an electron on the acceptor molecule A (leading to A*), as schematically shown in frame a of Figure 5. In the Dexter mechanism (frame b of Figure 5), excitation is transferred between a donor D and an acceptor A when an excited electron, initially belonging to D, is exchanged for a nonexcited electron initially belonging to A. For more details see refs 109 and 114.

Of course, EET treatment can be extended to transfer between a donor exciton state and an acceptor exciton state.[116−118] A detailed description is beyond the scope of this review; however, we hasten to mention that in the case when $\tau_{trans} \ll \tau_{rel}$, where τ_{trans} is the transfer time and τ_{rel} corresponds to the intramolecular vibrational relaxation time, the exciton (vide supra) can move freely from molecule to molecule according to the Schrödinger equation. Since this type of motion requires fixed phase relations between exciton wave functions of different molecules, it is called coherent transfer. If $\tau_{rel} \ll \tau_{trans}$, it is impossible to construct a wave function which involves different molecules. In this case, τ_{rel} introduces fast dephasing and this case is referred to as incoherent transfer regime. Of course, there is also the case where $\tau_{trans} \sim \tau_{rel}$; this is called partially coherent EET.[116,117]

These different regimes can also be described by the density matrix approach. When coupling between pigments is small (small $V_{n,m}$) the excitation can hop from Chl to Chl (i.e., there is no phase correlation between the excitation before and after the hop. For large $V_{n,m}$ (strong coupling), in a complex with many Chls, new eigenstates of the system need to be identified

$$\psi_k = \sum_{n=1}^{N} c_{nk}\varphi_n \qquad (5)$$

where φ_n are the locally excited states. In each eigenstate many local excited states participate, and the excitation can move coherently among them.[44,105] So in an excitonically coupled system, one has to deal with delocalized states. If the higher exciton state is occupied, the relaxation to the lower state can occur by exchanging energy with the bath; the latter coupling is represented by the spectral density of states, $\rho(\omega)$, which reflects the coupling between different exciton states and the bath. $\rho(\omega)$ defines which frequencies in the bath are available to relax. Thus, the relaxation process is associated with a net transfer of energy.

4. FUNDAMENTALS OF SPECTRAL HOLE-BURNING (SHB) AND FLUORESCENCE LINE-NARROWING SPECTROSCOPY (FLNS) AND SINGLE PHOTOSYNTHETIC COMPLEX SPECTROSCOPY (SPCS)

The successes of SHB spectroscopies (nonphotochemical, photochemical, triplet population bottleneck)[33,35,38] demonstrated over the years that these frequency domain techniques provide a lot of insight into the $S_1(Q_y)$-excited state electronic structure, EET, and electron transfer (ET) dynamics of protein−Chl complexes at low temperatures. A number of applications have been described in ref 48, while the basic principles of various high resolution spectroscopies have been explained in numerous books,[36,44] reviews,[27,33,35] and book chapters.[46,47] The advantages of SHB[33,36,38,119−121] in photosynthesis research stem from its ability to circumvent the inhomogeneous broadening—the static Γ_{inh} contribution to the widths of the $S_0 \rightarrow S_1$ absorption bands of Chl molecules and other cofactors. Γ_{inh} is a manifestation of the glasslike structural heterogeneity of proteins.[26,35,62,63] The parameters provided by SHB[32,33,35,36,38−41] are listed below and further discussed in subsequent sections. These parameters are essential for understanding EET, since they often determine the homogeneous spectral density in the nonadiabatic transfer rate expression (eq 2).[122] Several excellent descriptions of SHB and FLN spectroscopy (also called site-selection spectroscopy) can be found in recently published books[36,43,123−128] and reviews.[33,129−133] In this review, only the basic aspects of FLNS,[123,129−133] with an emphasis on the information it provides, are described. This method emerged from the works of Denisov and Kizel,[134] Szabo,[135] and Personov et al.[136] Recently, a combination of FLN with SHB, ΔFLN spectroscopy,[51−54] has been applied to photosynthetic complexes (PC), providing new insight into the el−ph coupling parameters.[55−61] FLNS also allows the measurement of ground-state vibrational frequencies, providing a selective tool for the identification of Chls with unique interactions within the surrounding protein.

Two additional remarks should be made with respect to differences in physics underlying SHB in PC embedded in glass and dispersed pigments in glasses. First, PC are networks of strongly interacting pigments in protein scaffolding, while in glasses one usually deals with a collection of noninteracting chromophores. Thus, in PC, structural heterogeneity (intracomplex and intercomplex) leads to diagonal and off-diagonal energy disorder associated with both Chl site excitation energies and couplings, respectively. Second, the dynamics of single molecules in photosynthetic complexes is typically explained in terms of protein "energy landscapes"[62,63] rather than just two-level systems (TLS). The high-dimensional energy surface of a protein is described in this picture by a hierarchy of conformational substates. Both SHB and FLNS can provide much needed quantitative data on these disorder-related parameters.

The information provided by SHB includes

(a) lifetimes of the *zero-point level* of $S_1(Q_y)$-states due to EET or ET, as determined by the widths of zero-phonon holes (ZPH);

(b) Γ_{inh} values, typically ∼50−200 cm^{-1} derived from the SHB action spectrum (also referred to as zero-phonon action (ZPA) spectrum in subsequent sections) and the

dx.doi.org/10.1021/cr100234j |*Chem. Rev.* 2011, 111, 4546–4598

profile of ZPHs burned at different wavelengths under constant irradiation dose conditions;

(c) the extent of correlation and excitonic interaction between the absorption bands of different Q_y-states, using satellite hole-burning [In this spectroscopy one burns into a higher energy state and records satellite holes associated with lower energy states that are populated by EET. The lack of strong correlation between the absorption bands of different states, usually observed for PC, results in formation of broad satellite holes. In the absence of correlation, there is a distribution of values for the electronic energy gap (ΔE_{DA}); energy transfer kinetics can be expected to be dispersive when the width of the ΔE_{DA} distribution is larger than that of the spectral density.[137] A limited degree of correlation is introduced, however, in the case of strong excitonic interactions (see section 4.8); this correlation can be observed, for example, via the correlation of absorption changes at various frequencies in nonresonant (satellite) HB spectra.];

(d) Franck−Condon factors and frequencies of Chl modes active in $S_0 \rightarrow Q_y$ transitions as determined by vibronic satellite HB spectroscopy [el−ph (protein) coupling parameters (Huang−Rhys factors, S, and phonon frequencies) can be also obtained];

(e) pure dephasing of Q_y-optical transitions due to coupling with the "bistable configurations" (TLS) of proteins.

Attributes a−e were already firmly established by the mid-90s.[33,35] The above types of information have had and continue to have very considerable impact on the field. However, as briefly eluded to earlier in this review, many new developments are possible (vide infra). A theory for the temperature dependence of HB spectra that is essential for interpretation of their dependence on the burn wavelength and temperature has been developed using the "mean-phonon approximation";[165] with modern computational capabilities, modeling using the more exact expression (no mean-phonon approximation) for the temperature dependence is also relatively straightforward.[138]

The linear pressure shift (usually to the red) rates (R_p) of Q_y-absorption bands and ZPH, as well as their broadening rates, provide new insights on the nature of excitonic coupling between neighboring Chl molecules; specifically, the contributions from electrostatic and electron-exchange interactions. The latter lead to charge transfer (CT) character for Q_y-states. In the absence of excitonic interactions, the shift rates reflect local compressibilities of the protein. Similarly, the permanent dipole moment changes ($\Delta\mu$) of the $S_0 \rightarrow S_1$ transitions can be used to identify states with significant CT character, as pointed out by Feher and Boxer in the 1990s.[139,140] They employed classical Stark modulation spectroscopy, though. Experimental results obtained over the years by our group indicated that there usually is positive correlation between R_p, $\Delta\mu$, and the linear el−ph coupling strength. Aside from detecting the CT states, the ability to resolve closely spaced states is also enhanced by high-pressure and Stark HB spectroscopies.[141,142]

Although significant progress has been achieved in the studies of single PC, we believe that much remains to be done (vide infra). It has to be stressed that so far the SPCS studies mainly focused on either LH2 antenna complexes of purple bacteria (particularly Aartsma's and Köhler's groups[69,143−148] at low temperatures and van Grondelle's group at room temperature;[77,78,80,149,150] we are going to consider the former ones in great detail as their results are more directly comparable with those of SHB studies) or cyanobacterial PSI.[73−76,151] Some SPCS results were reported also for LH1 complex of purple bacteria[143,152] and LHCII.[81,153] A detailed discussion of the properties of various PCs whenever studied by both SPCS and SHB will be presented in section 5.

For completeness, we note that inhomogeneous broadening may be also (partially) eliminated using photon echo (PE) techniques,[27,31,154] which also provide information on lifetimes and dephasing. Whereas FLNS and SHB provide a frequency selection by exciting the homogeneous ensemble of molecules, the PE experiments measure a temporal dependence of the dipolar moment of the molecular ensemble.[155−158] Therefore, in PE, in contrast to FLNS and SHB, the elimination of the inhomogeneous broadening has a different origin; it is the result of two carefully designed periods of evolution, where the optical inhomogeneous dephasing in the first period is exactly canceled by rephasing the process in the second period.[155−158] In SPCS, the effects of inhomogeneous broadening are removed by definition, and the complexes can be explored one by one. More details on SPCS are presented in section 4.9. 2D ES experiments, including photon echo, which also allow accessing the homogeneous line width, will be briefly discussed in section 4.10.

4.1. Zero-Phonon Lines, Homogeneous and Inhomogeneous Broadening

In solid molecular systems, all broadening mechanisms for absorption bands can be categorized as either homogeneous or inhomogeneous. Homogeneous broadening is that which is the same for each and every chemically identical molecule in the ensemble at given temperature (see below). Inhomogeneous broadening (Γ_{inh}) is the result of the chromophore in a disordered host (glasses, polymers, proteins, DNA) being able to adopt a very large number of energetically inequivalent sites (different individual microenvironments). Mechanisms leading to Γ_{inh} are strains, random electric fields, field gradients of charged defects, and interactions between centers/chromophores.[33,36,159] A simple way to illustrate such broadening (neglecting phonon contributions, i.e. the phonon sidebands) is shown in Figure 6. Consider an ensemble of chromophores in a rigid (low temperature) matrix, as shown schematically in the left frame; the immediate environments of the identical guest molecules (labeled as sites 1, 2, and 3) in the disordered matrix are different, and as a result, the molecules absorb at somewhat different energies, ω_1, ω_2, and ω_3, respectively. This is illustrated by the three narrow spectra (solid lines) shown to the right in Figure 6. In an absolutely perfect crystal all three transitions would have the same frequency, i.e. $\omega_1 = \omega_2 = \omega_3$, and the resulting narrow absorption band would be only homogeneously broadened.[160] An inhomogeneously broadened origin band [(0,0) band] has no apparent structure at low temperature (often being Gaussian with a typical width of up to several hundred wavenumbers), as shown by the dashed line in Figure 6. However, in reality it consists of many sharp bands (solid lines) that correspond to the absorption (ZPL; see below) of the "guest" molecules occupying inequivalent sites. These narrow spectra have a Lorentzian line shape with a homogeneous line width, Γ_{hom}, determined by excited-state dephasing interactions and lifetime effects, which are the same for all chromophores; the value of Γ_{hom} depends on the specific transition under consideration. Thus, the essential feature of SHB and FLNS is the use of a narrow laser source (with bandwidth smaller than Γ_{hom}) for excitation of chromophores,

dx.doi.org/10.1021/cr100234j |Chem. Rev. 2011, 111, 4546–4598

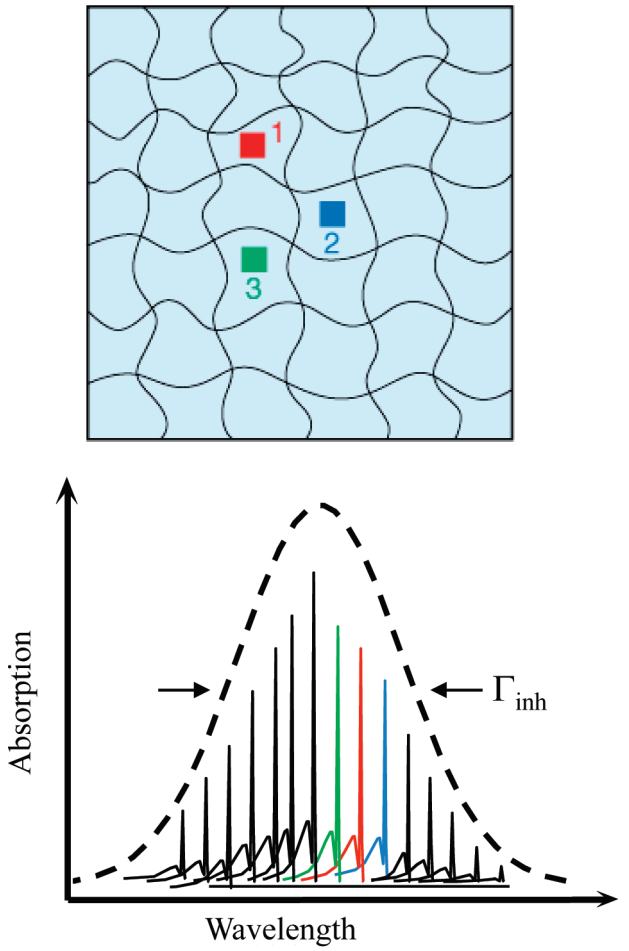

Figure 6. Schematic of absorbers dispersed in an amorphous solid matrix and the resulting low-temperature, inhomogeneously broadened absorption profile (dashed line); see the text.

either directly within the inhomogeneously broadened absorption profile [referred to below as (0,0) excitation] or into a vibronic region (called vibronic excitation). The Γ_{hom} is related to the T_2 relaxation time by the following relation

$$\frac{1}{T_2} = \pi c \Gamma_{hom} = \frac{1}{2T_1} + \frac{1}{T'_2} \quad (6)$$

where T_1 is the excited state lifetime and T'_2 is the pure dephasing time that depends on temperature. For the purpose of this chapter, it suffices to say that T'_2 is due to the modulation of the single site transition frequency, which results from the interaction of the excited state with bath phonons (and other low-energy excitations in amorphous solids[33,36,161]). This interaction does not lead to electronic relaxation of the excited state but rather to a decay of the phase coherence of the superposition state initially created by the photon. In units of cm^{-1}, Γ_{hom} can be expressed as

$$\Gamma_{hom} = (\pi T_2 c)^{-1} \quad (7)$$

where c is the speed of light in cm s^{-1} and T_2 is the total dephasing time in seconds.[34,37]

4.1.1. ZPLs and Phonon Sidebands (PSBs) . The main properties of narrow ZPLs in the spectra of crystal impurities were first discussed in detail by Kane.[162] Shortly thereafter, the principal analogy between the ZPL in the optical spectrum of

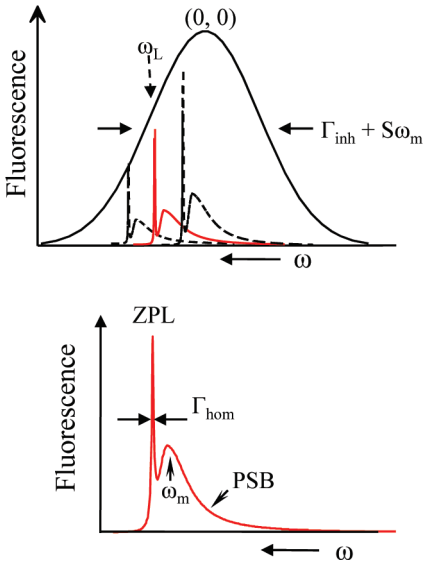

Figure 7. Top: Schematic of the inhomogeneously broadened fluorescence origin band; fwhm for low S values is given by $(\Gamma_{inh} + S\omega_m)$. ω_L is the laser excitation frequency. Bottom: Schematic view of the resulting ZPL and its PSB (or phonon wing, PW). The PSB has the intensity $(1 - \alpha)$ and is displaced to lower energies by ω_m, which corresponds to the mean phonon frequency. Γ_{hom} is the homogeneous line width.

an impurity center and the Mössbauer line in the spectrum of γ-quanta, absorbed or emitted by a radioactive nucleus in a crystal lattice, had been demonstrated.[163,164] A comprehensive theory of impurity spectra in solids can be found, for example, in an excellent book written by Rebane.[33] A zero-phonon transition is one for which no net change in the number of phonons accompanies the electronic transition. Building on each ZPL (of width Γ_{hom}) is a broad phonon (lattice vibrational) wing, referred to below as the phonon sideband (PSB). It is located to higher energies from ZPL in absorption and to lower energies from ZPL in emission. Summarizing, the band shape of the single site absorption or fluorescence profile, as shown in Figure 7, consists of two portions, i.e., ZPL and PSB, which can be written as

$$F(\omega, T) = \phi_{ZPL}(\omega, T) + \phi_{PSB}(\omega, T) \quad (8)$$

where the first term describes the ZPL and the second describes the PSB (i.e., phonon wing). The ZPL would have the form of a Lorentzian (vide infra), with a width at $T = 0$ defined by lifetime broadening only. However, due to the presence of el−ph coupling and interactions with the low-energy excitations (i.e., TLS), the width of the ZPL increases and becomes temperature-dependent.[123,124,165−167] Here one deals with quadratic el−ph coupling, as opposed to the linear one which leads only to PSB formation (with no effect on the ZPL width). The TLS in amorphous solids have a high spectral density at very low energies and are responsible for the observed anomalous temperature dependence of the ZPLs (as well as for anomalous nonoptical properties of amorphous solids, such as heat capacity and thermal conductivity). Typically, the homogeneous line width varies with temperature as $\sim T^{1+\mu}$ with $\mu \sim 0.3$ below 5 K.[34,36,168,169] The latter power law and time-dependence of the homogeneous line width, due to so-called spectral diffusion, are discussed in more detail in refs 157, 158, and 168−173.

Since the PSB contributes to the absorption and/or fluorescence origin bands, the width of the fluorescence spectrum shown in

dx.doi.org/10.1021/cr100234j |Chem. Rev. 2011, 111, 4546–4598

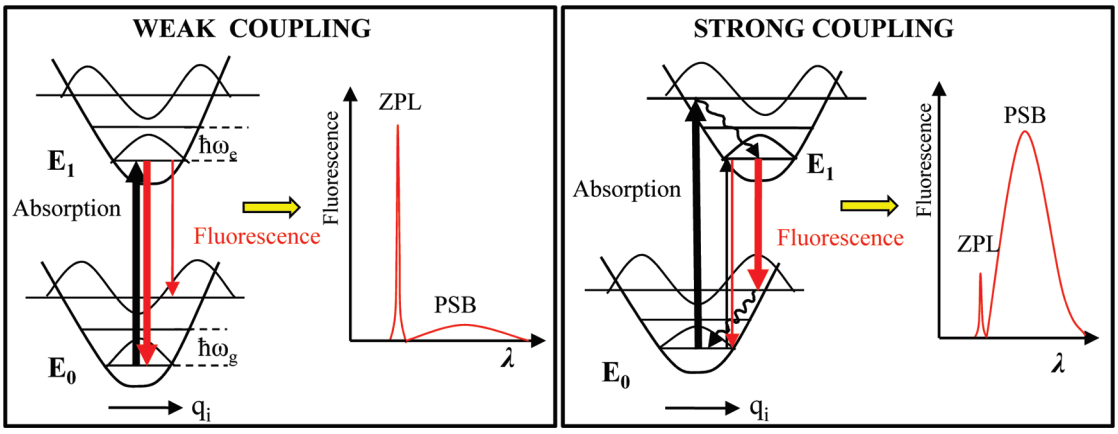

Figure 8. Diagram of potential curves in the case of linear el−ph coupling ($\hbar\omega_g = \hbar\omega_e$) and molecular lineshapes for a transition between two vibronic states of a guest molecule embedded in an amorphous host. Optical transitions are shown as vertical arrows, in accordance with the Franck−Condon principle. Both weak- and strong-coupling limits are illustrated. If $\hbar\omega_g \neq \hbar\omega_e$, then the transition energies are different and the (0−0) transition is accompanied by a change in the vibrational energy of the zero-point level.

Figure 7 (solid lines) is approximately given by[34,121,165] $\Gamma_{inh} + S\omega_m$, where ω_m is the mean phonon frequency (for organic molecules typically about 20−30 cm^{-1}) and S is a dimensionless parameter called the Huang−Rhys factor (S); see the next section. If excitation occurs at ω_L using a spectrally narrow laser, only those chromophores can be excited whose transition energies coincide with the frequency of the laser. If the concentration of chromophores is sufficiently low, no energy transfer to other chromophores occurs. While it is indeed the case for dopant centers in glasses, the situation is more complicated for PC (vide infra). Subsequently, resonant fluorescence occurs, providing a FLN spectrum, as shown at the bottom of Figure 7. Often one speaks of "selecting an isochromat".[33,123,124]

4.1.2. Electron−Phonon Coupling and Homogeneous Line Shapes. This section deals with the theory behind the phonon sidebands introduced in the previous subsection. In general, the coupling is strong for molecules which upon electronic excitation undergo large geometry changes and/or large changes of the electronic charge distribution. This is illustrated by Figure 8, where the configurational coordinate diagram of the ground- and excited-states of a hypothetical molecule is shown for a single phonon mode. The quantities that describe the FC and S factors (see below) are defined in Figure 8. The two parabolas represent the potential energy; the electronic ground state and the first excited state are labeled as E_0 and E_1, respectively. The energy levels of a guest molecule are depicted in the interaction with the local phonon with $\hbar\omega_g = \hbar\omega_e$. (A harmonic oscillator model could be used to describe multiple phonon quanta.) In general, the potential may be written in the following form:[174]

$$V = \sum_i A_i q_i + \sum_{ij} B_{ij} q_i q_j \qquad (9)$$

The linear coupling coefficients A_i (in eq 9) describe the change in energy of the excited state, due to shifts in the equilibrium positions of the normal oscillator that occurs during the optical transition. The quadratic coupling coefficients (B_{ij}), for $i = j$, describe the change in the energy of the excited state resulting from the change in the normal oscillator frequencies during an excitation. For $i \neq j$ they describe the change in the energy due to the mixing of normal coordinates. The quadratic el−ph coupling is responsible for an increase in the homogeneous line width,[46,124,158,175,176] as already mentioned above.

Within the linear el−ph coupling approximation, only the equilibrium position, but not the frequency ω_i, of the phonon mode i (with i = g, e) is changed between the two electronic states. For the remainder of this section, we restrict our attention to this situation. In this case q_i represents the lattice normal coordinate belonging to phonon mode i, and Δq_i corresponds to the change of the equilibrium position. The sensitivity to changes in the environment is characterized by the above-mentioned (dimensionless parameter) S, which in the low-temperature limit is defined as[123,124]

$$S(T = 0) = \sum_i \frac{M_i \omega_i}{2\hbar} (\Delta q_i)^2 \qquad (10)$$

where M_i and ω_i are the reduced mass and frequency of the mode i, respectively. Physically, weak interaction between the electronic transition and the delocalized phonon modes correspond to small equilibrium position changes Δq_i and a correspondingly small value of S. In the absorption/fluorescence spectrum, weak coupling ($S \ll 1$) is reflected in an intense ZPL (zero-phonon transitions) and a weak PSB (phonon-assisted transitions). Conversely, a large value of S ($S \gg 1$) corresponds to strong el−ph coupling, producing a weak ZPL and an intense PSB. Both cases are illustrated on the right side of Figure 8. For *very* strong coupling ($S \gtrsim 10$), no ZPL are observed; in this case, it is said that the transitions are FC-forbidden.

More quantitatively, the relative (integrated) intensities of the ZPL and PSB are often described in terms of the Debye−Waller factor,[33,123,124,177] α, where

$$\alpha = I_{ZPL}/(I_{ZPL} + I_{PSB}) = \sum \left| \left\langle \chi_{ph,1i}(0) \middle| \chi_{ph,0i}(0) \right\rangle \right|^2 \qquad (11)$$

$\langle \chi_{ph,1i} | \chi_{ph,0i} \rangle$ is the overlap integral, and $\chi_{ph,1i}$ and $\chi_{ph,0i}$ represent the phonon wave functions for mode i in the excited and ground-electronic state, respectively. It has been shown that α is a decreasing function of temperature. As shown in Figure 8, the relative intensities of these two contributions, i.e., ZPL and PSB, depend upon the strength of the el−ph coupling. In the low-temperature limit ($T \sim 0$ K) it can be shown that α is related to the Huang−Rhys factor by

$$\alpha = \exp(-S) \qquad (12)$$

Thus α, expressed in terms of S, measures the strength of the

dx.doi.org/10.1021/cr100234j |*Chem. Rev.* 2011, 111, 4546–4598

el−ph coupling.[123,124] Figure 8 shows that an excited state displacement suppresses the intensity of the ZPL, while eq 12 indicates that the decrease is exponential. The shape of the PSB is determined by the spectral density, $J(\omega)$, for the interaction, defined by[117]

$$J(\omega) = \sum_i \frac{M_i \omega_i}{2\hbar} (\Delta q_i)^2 \delta(\omega - \omega_i) \tag{13}$$

(Note that the coordinates q_i used here are not mass-weighted as in ref 117; this is the reason for the presence of the M_i factor.) The spectral density is determined by two factors: the density of states (DOS) and the FC factors for the individual modes. The DOS is a distribution function of phonon modes $\Sigma_i \delta(\omega - \omega_i)$ and is determined simply by the number and frequencies of the phonons in the system. The second term, the FC factor, $\frac{M_i \omega_i}{2\hbar}(\Delta q_i)^2$ for each phonon mode determines the strength of el−ph coupling, as discussed above. As per eq 10 above, it can be seen that at zero temperature the factor S is simply the integral of the spectral density over all frequencies; the spectral density thus determines both the *shape* and the *intensity* of the PSB in the molecular absorption/fluorescence line shape. The spectral density curve itself cannot usually be predicted a priori; it usually must be determined from experiment. It is generally found to be a broad, relatively featureless curve consisting of many individual phonon transitions (see below in this section and section 4.6).

Given the spectral density, the absorption and fluorescence line shape functions are usually expressed as[117]

$$L_{A/F}(\omega - \Omega_0) = e^{-S} \int_{-\infty}^{\infty} dt \exp(\pm i(\omega - \Omega_0)t + G(t,T)) \tag{14}$$

where $G(t;T) = \int_{-\infty}^{\infty} e^{-i\omega t}(1 + n(\omega;T))J(\omega) + n(-\omega;T)J(-\omega)\, d\omega$ and $n(\omega) = 1/(e^{-\hbar\omega/kT} - 1)$ is the thermal occupation number at temperature T. In the exponent of eq 14, "+" refers to absorption (L_A), while "−" refers to fluorescence (L_F). Note that by definition $L_A(\omega - \Omega_0) = L_F(\Omega_0 - \omega)$; i.e., the two functions are mirror images of each other around the ZPL frequency Ω_0.

Although convenient for computational purposes, eq 14 is not very physically transparent. A more intuitive formula is obtained by expanding the exponent inside the integral as an infinite sum. In the low-temperature limit, the equation then reads[121]

$$L_{A/F}(\omega - \Omega_0) = \underbrace{e^{-S} l_0(\omega - \Omega_0)}_{ZPL} + \underbrace{\sum_{R=1}^{\infty} S^R \frac{e^{-S}}{R!} l_R(\omega - \Omega_0 \mp R\omega_m)}_{PSB} \tag{15}$$

where $-R\omega_m$ and $+R\omega_m$ correspond to absorption $L_A(\omega)$ and fluorescence $L_F(\omega)$, respectively. The first term represents the Lorentzian ZPL $l_0(\omega - \Omega_0)$, which peaks at Ω_0 and possesses a homogeneous width Γ_{hom}. The second term is the PSB, consisting of a sum over all R-phonon transitions; the function $l_1(\omega) = J(\omega + \omega_m)/\int J(\omega)\, d\omega$ is the *one-phonon profile*, i.e., the normalized spectral density function, shifted by the mean phonon frequency ω_m so that its peak occurs at frequency zero. [For fluorescence $J(\omega + \omega_m)$ is replaced by its reflection $J(-\omega + \omega_m)$]. The constant ω_m is the peak (or mean) phonon frequency, i.e. the peak frequency of $J(\omega)$. For $R > 1$, $l_R(\omega)$ is the $(R-1)$-fold convolution of $l_1(\omega)$ with itself and represents absorption/fluorescence events involving R phonons. The shape of each $l_R(\omega)$ is thus completely determined by $l_1(\omega)$. In particular, for l_1 being a Gaussian (Lorentzian) with a full width at half-maximum (fwhm) Γ_G (Γ_L), the profile l_R becomes a Gaussian (Lorentzian) with fwhm $(R)^{1/2}\Gamma_G$ (or $R\Gamma_L$, respectively).[121]

As stated above, the one-phonon profile $l_1(\omega)$ represents the product of DOS of the phonon modes and of the el−ph coupling term. The latter two terms cannot be separated by the site selective optical spectroscopic techniques discussed in this review. However, the density of phonon states can be obtained separately using the complementary method of inelastic neutron scattering.[178] Although on the basis of neutron work the density of phonon states appears to be relatively similar for many different proteins (see refs 119, 178−181), its spectral form was shown to vary with protein size (see, for example, refs 120, 122) and due to interaction with the solvent (see, for example, ref 121). Guided by the experimental work of ref 165 and the references given therein, the one-phonon profile l_1 can often be assumed to be asymmetric with a Gaussian shape at its low-energy wing and a Lorentzian shape at its high-energy wing. The full profile then has a peak frequency of ω_m and a width of $\Gamma = \Gamma_G/2 + \Gamma_L/2$. It should be noted, however, that the analytical expressions for the shape of the R-phonon profile provided by ref 165 (eqs 15a and 15b of that work) and commonly used in later works is an approximation that relies strongly on the similarity of the shapes of the Gaussian and Lorentzian components of the PSB. Application of this formula to systems with very different widths of the Gaussian and Lorentzian components can produce significant deviations in the apparent mean-phonon frequency in a calculated single-site spectrum. Fortunately, for most applications, modern computational capabilities make the direct calculation of the convoluted l_R terms almost trivial for arbitrary PSB shapes, and the direct approach should be used in modeling studies.

At higher temperature creation (and annihilation) of phonons takes place. Therefore, for $T > 0$ K, a thermal population of phonon levels, according to Bose−Einstein statistics, has to be taken into account.[33] As noted above, while eq 14 is valid for arbitrary temperatures, eq 15 has been expressed in the limit as $T \to 0$ K. A similar expansion can be performed for arbitrary temperatures to produce[138]

$$L_{A/F}(\omega - \Omega_0, T) = \underbrace{e^{-S(T)} l_0(\omega - \Omega_0, T)}_{ZPL} + \underbrace{\sum_{R=1}^{\infty} S(T)^R \frac{e^{-S(T)}}{R!} l_R(\omega - \Omega_0 \mp R\omega_m, T)}_{PSB} \tag{16}$$

where $S(T) = \int_{-\infty}^{\infty} p(\omega;T)\, d\omega$, $p(\omega;T) = (1 + n(\omega;T))J(\omega) + n(-\omega;T)J(-\omega)$, $l_0(\omega;T)$ represents the ZPL, $l_1(\omega;T) = S(T)^{-1} p(\omega + \omega_m;T)$ for absorption or $l_1(\omega;T) = S(T)^{-1} p(-\omega + \omega_m;T)$ for fluorescence, and for $R > 1$, $l_R(\omega;T)$ is as above the convolution of $l_1(\omega;T)$ with itself $R - 1$ times. Comparison of this equation with eq 15 reveals that the spectral density $J(\omega)$ has simply been replaced by the temperature-dependent function $p(\omega;T)$; the Huang−Rhys factor S has then likewise been replaced by the temperature-dependent function $S(T)$, which can be considered a "temperature dependent" $S(T)$ factor. Indeed, using this definition of $S(T)$, eq 12 becomes valid at all temperatures, not only in the low-temperature limit. An alternative form for the temperature-dependent line shape function was presented by Hayes et al.[165] In that work it was observed that in the mean-phonon approximation the expression

reduces to

$$L_{A/F}(\omega - \Omega_0) = e^{-S(2\overline{n}+1)} \sum_{R=0}^{\infty} \sum_{r=0}^{R} \frac{[S(\overline{n}+1)]^{R-r}[S\overline{n}]^r}{(R-r)!r!} \times l_{R,r}[\omega - \Omega_0 \mp (R-2r)\omega_m] \quad (17)$$

In this equation, $\overline{n}$ is the phonon occupation number of a phonon with frequency ω_m; the factors $S(\overline{n}+1)$ and $S\overline{n}$ represent phonon creation and annihilation, respectively. Again, the value of R corresponds to the zero-, one-, ..., R-phonon transition, while the second sum over r leads to a redistribution of intensity within the PSB according to the number of created or annihilated phonons. An increase of temperature not only leads to more intense PSBs at the expense of the ZPL, but also gives rise to the anti-Stokes part of the PSB. As for eq 15 above, the multiphonon profiles $l_{R,r}$ are obtained from the one-phonon profile by folding $l_{1,0}$ with itself $|R-2r| - 1$ times. The advantage of this equation is that it is both physically transparent and easily computed. On the other hand, it is strictly valid only for a relatively narrow one-phonon profile, when the mean-phonon approximation is reasonable.

4.2. Nonphotochemical, Photochemical, and Transient SHB Spectroscopy

Three types of SHB can be distinguished on the basis of the mechanism of the process on a molecular level. In the case where pigment molecule in resonance with narrow band laser excitation experiences photochemical reaction, one speaks of photochemical hole-burning (PHB). Examples of PHB include permanent photobleaching and tautomerization, as in the case of free-base chlorin.[182] The product of the reaction usually absorbs far from the original excitation wavelength. This HB mechanism is relatively unimportant in the case of Chls in PC. In the case of nonphotochemical spectral hole-burning (NPHB), the pigment molecule does not experience a chemical reaction. Instead, excitation of the molecule triggers the rearrangement of the local environment of the pigment, which results in the change in the interactions between the pigment and its surroundings. If the barriers between the environment configurations are higher in the ground electronic state than in the excited electronic state of the pigment molecule, the system gets permanently trapped in the new configuration, where the pigment experiences a different solvent shift. Obviously, for such a mechanism to be effective, the host has to possess some freedom to rearrange. Thus, NPHB is effective only in amorphous solids.[33,37] In glasses the mechanism responsible for NPHB involves the TLS, similar to that mentioned above in relation to pure dephasing at low temperatures.[37,183,184] In proteins there is switching between nearly identical substates on the protein energy landscape containing significantly more than two wells per pigment.[26,62,70] For FLN, no phototransformation is required; fluorescence is measured while the exciting light is on, and as a result, the ZPL contribution to the spectrum is obscured by the excitation; the latter, however can be circumvented by ΔFLN approach.[61] See also section 4.6.

Both PHB and NPHB result in the formation of persistent holes, meaning that the holes are preserved long after the initial excitation is turned off. Transient HB requires the presence of the third, relatively long-lived state (usually a triplet state; thus, this technique is especially sensitive to the RC states), directly or indirectly populated from the excited singlet state. Then, the pigment's ground state will be depopulated for the lifetime of the triplet state (in the μs to ms range) and the spectral hole will be observable only for the duration of this lifetime. Technically, transient spectral holes can be acquired using CW laser as the difference between the absorption spectra measured while the excitation is on and while the excitation is off. Transient SHB experiments are also possible using pulsed lasers.[185]

In pigment−protein complexes, the NPHB mechanism is by far the most dominant and widespread. In the absence of the antihole or photoproduct (see next sections), the hole-burned absorption spectrum (the postburn spectrum) is a convolution of the postburn SDF $N(\omega)e^{-P\sigma\phi L_A(\omega_B-\omega)t}$ with the single site absorption spectrum

$$A(\Omega,t) = \int d\omega\, L_A(\omega-\Omega)N(\omega)e^{-P\sigma\phi L_A(\omega_B-\omega)t} \quad (18)$$

Here ω_B is the burn/excitation frequency, P is the photon flux, t is the burn time, and $N(\omega)$ is the preburn SDF, describing the probabilities of encountering different zero-phonon transition frequencies. $L_A(\omega)$ is the single site absorption profile as defined above (section 4.1). Multiphonon processes are taken into account during calculation of $L_A(\omega)$. σ and ϕ are the integrated absorption cross-section of the molecule aligned with transition dipole parallel to laser polarization and HB quantum yield, respectively. (Equation 18 does not include any factors that result in the dispersive HB kinetics; these will be described in the next sections.) The FLN spectrum may be similarly expressed as

$$FLN(\Omega) = \int d\omega\, L_F(\omega-\Omega)L_A(\omega_B-\omega)N(\omega) \quad (19)$$

Note that the SDF $N(\omega)$ in eq 19 is not modified by HB; the selectivity of FLN measurements originates rather from the selective excitation term $L_A(\omega_B-\omega)$. In contrast, as discussed in more detail in section 4.6, for a ΔFLN spectrum the $N(\omega)$ in eq 19 has to be substituted by $N(\omega)(1-e^{-P\sigma\phi L_A(\omega_B-\omega)t})$, i.e.

$$\Delta FLN(\Omega,t) = \int d\omega\, L_F(\omega-\Omega)L_A(\omega_B-\omega)N(\omega)(1-e^{-P\sigma\phi L_A(\omega_B-\omega)t}) \quad (20)$$

In this expression, excitation is doubly selective—first via selective burning [as reflected in the modified SDF, $N(\omega)(1-e^{-P\sigma\phi L_A(\omega_B-\omega)t})$] and second by the selective excitation for postburn fluorescence, $L_A(\omega_B-\omega)$.[186]

Returning to the absorption HB expression, eq 18, it is useful to note that in the shallow hole limit $1-e^x \approx x$. If one further assumes that the SDF width Γ_{inh} is much larger than Γ_{hom} and ignores the el−ph coupling, the only remaining contribution to the hole spectrum will be a ZPH, a convolution of ZPL with itself. For a Lorentzian ZPL line shape, the width of the ZPH, in the shallow hole limit, will be twice the width of the ZPL:

$$\Gamma_{hole} = 2\Gamma_{hom} \quad (21)$$

As discussed above, the absorption and emission spectra of chromophores in amorphous solids consist of ZPLs and broad PSBs (see the previous section). As a result, hole spectra in absorption contain additional features as well. To higher energy with respect to the ZPH the ("real") PSB is located. This is the true PSB of the ZPH, due to the loss of PSB absorption from resonantly burned pigments (i.e., pigments excited through their ZPL). In addition, to the lower energy with respect to the ZPH one can observe the

contribution of the molecules whose ZPLs were at $\omega < \omega_B$ but which burned due to excitation via their real sidebands at ω_B. The shape of the "pseudo-PSB" feature depends not only on the actual shape of the phonon sideband but also on the shape of the SDF. In the case of the FLN and ΔFLN spectra, both real and pseudo-PSB are located at lower energies with respect to the excitation wavelength (though the pseudo-PSB in ΔFLN spectra is generally suppressed). More details, including modeling data, will be presented in section 4.6.

4.3. Mechanism of Nonphotochemical Hole-Burning (NPHB)

The detailed treatment of NPHB has been first developed for glasses.[34,37,183,184,187] Although NPHB has been applied to studies of PC for more than 20 years, the details and peculiarities of that process in the PC have not been studied until recently. Thus, in this section we first follow the treatment developed for glasses and then discuss the differences expected in the case of proteins. In glasses, NPHB is a manifestation of configurational tunneling between bistable configurations (two level systems, TLS) of the guest−host system.[34,37,183,184] Two types of TLS are distinguished in the classical case of guest−host systems. The intrinsic TLS (TLS_{int}) of the host are associated with the *excess free volume* of glasses.[183] The chromophore (impurity) introduces extrinsic TLS (TLS_{ext}) in glasses that are associated with the chromophore and its inner shell of solvent molecules. (In PC, where Chl molecules are introduced into protein by nature, the distinction between TLS_{int} and TLS_{ext} fades.) Regarding dynamics (e.g., long-range interaction) and the nature of TLSs in glasses, many important questions remain unanswered. The nature of the low-energy excitations (i.e., TLSs) of chromophores (e.g., Chls) residing in proteins is even less understood. Proper treatment of proteins most likely requires consideration of the whole multidimensional multitier energy landscape. Nevertheless, the TLS model still can be applied to proteins in some approximation, and it is widely accepted in the SHB community that optical excitation of the chromophore triggers the phonon-assisted tunneling processes, which lead to hole formation. In the SPCS community, the light-induced character of observed spectral diffusion behavior seems to remain a matter of debate.[26,62,70,188] In the Shu−Small mechanism[183] for NPHB, a sequence of tunneling events begins in the outer shell and involves the TLS_{int} and terminates in the inner shell. This outside-in chain of events can result in diffusion of excess free volume to the inner shell, setting the stage for the final (and rate-determining) step of NPHB that involves the TLS_{ext}^{e}, where e indicates the chromophore in its excited state. This final step is depicted in Figure 9. In case the double-well potential exhibits different asymmetry in the ground and excited electronic states, the chromophore will be found at different frequency after burning. The absorption spectrum of such shifted molecules is referred to as antihole (sometimes it is also called a photoproduct, which may be somewhat erroneous, as no chemical reaction occurs in the case of NPHB). The Shu−Small mechanism[183] was developed to explain the preferential blue shift of the burned absorption; however, it is not clear if this preference for the blue shift cannot be explained, at least in PC, with their multiwell energy landscapes, just by blue-shifted molecules becoming unexcitable at ω_B while red-shifted molecules still can be excited via their PSBs (that is, until they finally shift to the blue of ω_B as a result of a multistep process). There are indications that at least in the initial stages of burning the molecules in protein environment experience both blue and red shifts.[10,70,85] As is clear from SPCS data,[62,188−190] at least in the case of proteins, the chromophore−environment system can be found in more than two states, making the multistep burning even more feasible.[70] There are also multiple indications that even in glasses and polymers the one-TLS-per-chromophore model is too crude, and one has to consider either multiple TLS interacting with the same chromophore or multilevel systems, MLS.[41] Finally we note that the molecules that experienced the light-induced absorption frequency shifts can return to their original wavelengths via thermal- or light-induced hole filling.[41]

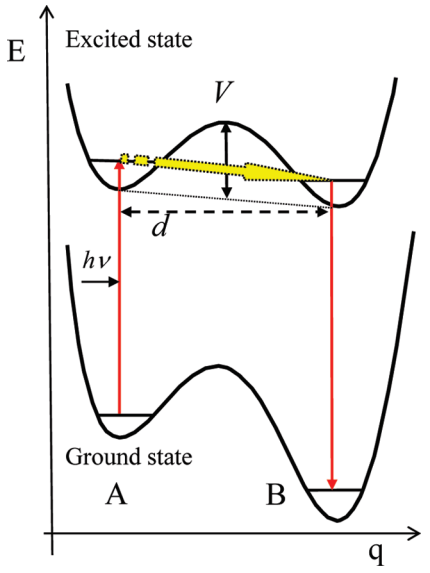

Figure 9. TLS with ground and excited electronic states of the pigment. The barrier between conformations A and B is lower in the excited state. System starts in conformation A and with the pigment in the ground state and absorbs a resonant photon. After tunneling (block arrow), the pigment returns to the ground state and due to different asymmetry of the potentials the absorption frequency of the pigment in conformation B is shifted (to the blue in this case). If the barrier in the ground state is high enough, the pigment/host system is trapped in the new conformation.

One additional effect complicating the discussion on NPHB in PC is excitonic interactions between pigments. Effects due to NPHB into delocalized excitonic states are readily recognized in recent data obtained for CP43[10,12,85,191] and CP47 complexes.[9,86] Sharp antiholes evenly distributed (i.e., ±20 cm^{-1}) about the resonant hole are accompanied by much broader features in the higher energy region (i.e., hundreds of cm^{-1}, far outside the preburn SDF). Different mechanisms were proposed to account for origin of these broad, strongly blue-shifted antiholes, one based on the redistribution of oscillator strength due to excitonic interactions and the traditional NPHB process[39,40,85,86] and one based on a proposed "photoconversion" mechanism that in the case of the CP43 complex was suggested to involve changes in pigment−protein hydrogen bonds.[12,191] The key difference between these two mechanisms is that the first[39,40,85,86] accounts for the extreme blue-shifted antihole based purely on modified excitonic interactions after NPHB [while leaving the site energies of burned pigments within their original (0,0) SDF], while the photoconversion mechanism relies on the shift of some pigment site energies far outside their site distribution function due to a photochemical/photophysical modifications.[12,191] Support for the former mechanism is discussed in section 5.1.2 and in refs 39, 40, 85, and 86.

It should be emphasized that in all mechanisms the hierarchical character of the protein/glass energy landscape strongly

dx.doi.org/10.1021/cr100234j |*Chem. Rev.* 2011, 111, 4546–4598

affects the observed burn efficiency and shapes of both holes and antihole distributions within the original SDF. This effect is clearly observed in light-induced spectral diffusion SPCS experiments, where small and moderate shifts (on the order of ± 1 or ± 10 cm^{-1}, respectively) of electronic transitions are very likely (typical for resonant HB), whereas larger shifts (although still within the original pigment SDF, on the order of ± 100 cm^{-1}) during the HB process are significantly less likely.[26,62,70] Smaller shifts with no preferential direction tend to cancel/average out in nonline narrowed HB spectra, as revealed by our modeling studies (data not shown), although they may be important in determining the shapes of resonantly burned holes; see also the discussion of LH2 system by SPCS and SHB in section 5.1.3. In summary, the shapes of nonresonant holes and antiholes can be adequately described even for excitonically coupled pigments,[39,40,85,86] but more work is required to provide more insight into the various contributions to *resonant* NPHB holes, in particular for excitonically coupled chromophores embedded in proteins. Resonant NPHB is more difficult to describe, as several different photoproduct distributions can be formed due to the complex energy landscape of proteins in glasses (research in progress), while these effects tend to average out in nonresonant HB spectra; in photosynthetic complexes, the presence of energy transfer and multiple pigment distributions adds an additional layer of complexity to the problem.

Summarizing, although the mechanism of NPHB process based on the simple TLS model (Figure 9) is most likely oversimplified (for details, see refs 26, 62, 70), in general, however, the model established over the years by Small and his co-workers provides a simple and quite adequate description of the light-induced spectral shifts in PCs. Thus, it is important to continue generating experimental data that will take us beyond the TLS model, e.g. data that firmly establish the existence of MLS, which definitely play a significant role in photosynthetic antenna protein complexes. The detailed discussion on such a model, including dispersion of the hole growth kinetics (HGK), i.e., dispersion of the line shift rates, is presented in the next section.

4.4. Kinetics of NPHB

It has been recognized long ago that attempts to model the spectral hole evolution using simple eq 18 result in errors even in the simplest glasses, where one-TLS-per-chromophore approximation is most likely valid. Significant dispersion of hole growth kinetics (HGK) has been observed.[192−197] Whether or not this dispersion stems mainly from structural disorder has been subject to debate for several years. Nevertheless, by now it is widely accepted that it is indeed the disorder which gives rise to a distribution of values for the tunnel parameter λ of the TLS involved in the rate-determining step of NPHB (λ-distribution).[192,193] Parameter λ describes the "strength" of the energy barrier to be overcome during the tunneling event in the excited state; see Figure 9, where $\lambda = d(2mV)^{1/2}/\hbar$ and d is the displacement along generalized coordinate, m is the effective mass of entity rearranging during the conformational change, and V is the barrier height. Dispersive kinetics also arises from the intrinsic α- and ω-distributions, where α is the angle between the laser polarization and the chromophore's transition.[194−196] The ω-distribution is due to off-resonant absorption; it is responsible, for example, for pseudo-PSB formation. It has been determined that λ-distribution is the main factor affecting the dispersive character of the HGKs.[194] Equation 18 can be modified to include the above distributions;[194] the modified equation is written as

$$A(\Omega,t) = 1.5\int d\omega\, L(\Omega-\omega)N(\omega) \int d\lambda\, f(\lambda)\int d\alpha \sin\alpha\cos^2\alpha e^{-P\sigma\phi(\lambda)L(\omega_B-\omega)t\cos^2\alpha} \quad (22)$$

Most parameters are the same as in the eq 18. λ and $f(\lambda)$ are the tunneling parameter and (Gaussian) distribution thereof, with mean λ_0 and standard deviation σ_λ. α is the angle between laser polarization and transition dipole. The NPHB yield can be expressed as[193,194]

$$\phi(\lambda) = \frac{\Omega_0 \exp(-2\lambda)}{\Omega_0 \exp(-2\lambda) + {T_1}^{-1}} \quad (23)$$

where T_1 is, in the absence of energy transfer, fluorescence lifetime. $\Omega_0 = 7.6 \times 10^{12}$ s^{-1} is a constant prefactor (change of this prefactor results in the shift of the maximum of the λ-distribution). Remember that the width of the Lorentzian homogeneous ZPL contributing to $L(\omega)$ is determined not by T_1, but by the total dephasing time T_2. The HGK curve describes the evolution of absorption in resonance with the burning laser, i.e., at ω_B. The standard deviation, σ_λ, of the λ-distribution can be used to compare the extent of structural disorder in different amorphous systems. In order to determine the relative contributions of these three distributions, it is necessary to measure the HGK over five or more decades of burn fluence. Recently, we have modified the master equation for HGK by taking into account both the T-dependent absorption profile and static thermal hole filling.[197] However, this particular model has not been applied to photosynthetic complexes yet.

In case energy transfer from the burnable state takes place, EET time, T_{EET}, should be used in eq 23 as T_1. Note that tunneling (NPHB) and EET are competing processes. Thus, EET reduces the HB efficiency. This effect can be observed, for example, in case of the B800 band of LH2 antenna complex.[70,198] HB yield is indeed reduced at the blue side of the B800 band where B800→B800 EET is present in addition to B800→B850 EET. On the other hand, in the RCs, such as PSII or bacterial RCs, the T_1 is determined by charge separation, with triplet formation following the primary charge separation. The triplet HB yield is then

$$\phi(\tau_{CS}) = \frac{{\tau_{CS}}^{-1}}{{\tau_{fl}}^{-1} + {\tau_{CS}}^{-1}} \quad (24)$$

Here τ_{fl} and τ_{CS} are fluorescence lifetime and charge separation time, respectively. As in HB experiments, one usually saturates the persistently burnable holes before exploring triplet bottleneck ones, and one can usually assume that ${\tau_{fl}}^{-1} \ll {\tau_{CS}}^{-1}$ and $\phi(\tau_{CS}) \approx 1$. Triplet bottleneck holes are not affected by the tunneling parameter distribution, as tunneling between the wells on the energy landscape does not remove the molecule from the electronically excited state. (This is not the case for persistent holes, as charge separation will reduce the NPHB yield. In this case, charge separation time will have to be used in the eq 23 for NPHB yield as T_1.) Several additional distributions have been observed or predicted which are specific to PC. As mentioned above, the absence of correlation between the SDF of donors and acceptors in EET results in distributions of EET rates. Recently we demonstrated that the distribution of B800→B850 EET rates resulting from refs 199−201 is indeed in agreement with the HB

data.[70] However, the detailed exploration of the effects of various EET rate distributions on hole parameters (HGK, width dependence on depth, etc.) has not yet been undertaken (research in progress). In addition, oscillator strength distributions could be present if one is burning into the excitonic state delocalized over several chlorophylls. Recent SPCS results[202] as well as ΔFLN work[57] obtained for LH2 indicate that the strength of the el−ph coupling could be subject to distribution as well. However, as briefly discussed in ref 70, the latter two distributions had negligible effect on the dispersive HGKs and could be ignored to speed up the simulations.

The above eqs 22 and 23 adequately describe the HB process at a broad range of irradiation doses (not just in the shallow hole limit) only in the case where NPHB antihole can be ignored. Two different approaches have been proposed[70,203] where the effects of antihole have been taking into consideration. In ref 203, it was assumed that the chromophore interacts with one and only one TLS of the amorphous solid, and therefore the system has perfect spectral memory (upon light- or thermal-induced hole filling the chromophore always returns to its original preburn absorption frequency). However, recent SPCS results[144−148,188,202] suggest that a protein containing chromophores can assume more than two slightly different conformations (different wells on the protein energy landscape[62,146,204,205]), and the NPHB modeling procedure has been modified accordingly in ref 70. Namely, it was assumed that molecules starting at ω_{init} (which is not equivalent to ω_B; it can be any frequency where burning occurs either via ZPL or via PSB) before burning are redistributed around ω_{init} according to a certain distribution, called the antihole function, as a result of burning. Technically, the following sequence is repeated in a loop: the SDF of the burnt molecules, $N(\omega)[1 - \exp(-Pt\sigma\phi L(\omega - \omega_B)\cos^2\alpha)]$, is convoluted with the properly normalized antihole function and added to the burnt SDF, $N(\omega)\exp[-Pt\sigma\phi L(\omega - \omega_B)\cos^2\alpha]$. This results in a modified shape of the SDF $N(\omega)$, without change in its normalization. (One starts with $N(\omega)$ being Gaussian). Unlike in ref 203, there is no spectral memory (i.e., it is assumed that the single molecule line can be found at significantly more than two frequencies) and no correlation was implied between the shifts of the absorption of a molecule in the consecutive steps. The probability of burning at each step of the sequence is still determined by the standard SHB yield formula (eq 23). It is obvious that the above two approaches represent two opposite limiting cases with respect to spectral memory. Developing a realistic intermediate model, based on protein energy landscapes or MLS, is one possible future direction of utilizing SHB in studying photosynthetic complexes (and proteins in general).

4.5. Zero-Phonon Action (ZPA) Spectroscopy: Site Distribution Function (SDF)

In addition to providing single site information, such as el−ph coupling strength and homogeneous broadening, SHB spectroscopy can be used to reveal inhomogenous broadening parameters, i.e., the shape and width of the SDF. One of the primary tools for this task is ZPA spectroscopy.[9,10,17,60,206] In this technique, applied for the first time to the LH1 antenna complex of *R. sphaeroides*,[206] HB spectra are measured for fixed low irradiation doses at many excitation wavelengths (λ_{ex}) across the inhomogeneously broadened absorption profile. The ZPA spectrum is then obtained as a plot of resonant hole depth versus λ_{ex}. The key concept behind this technique is that because the ZPL is generally orders of magnitude narrower than the broad PSB, the contribution of nonresonant pigments to the low-fluence hole is negligible. As a result, the shape of the ZPA spectrum is largely determined by the probability of burning a pigment at λ_{ex}, which for a system of noninteracting pigments is directly proportional to the value of the SDF at λ_{ex}. The ZPA spectrum thus provides a convenient means of directly measuring the extent of inhomogeneous broadening. An example of a ZPA spectrum is shown in Figure 10 (unpublished results); in the figure, the triangular data points represent resonant hole depth (the ZPA spectrum), while the solid line shows the bulk absorption spectrum for comparison. Whereas the absorption spectrum is additionally broadened by PSB absorption, the ZPA spectrum reflects the shape of the SDF (inhomogeneous broadening) alone.

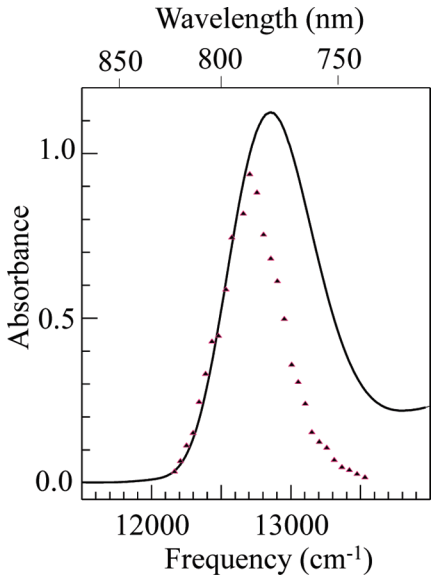

Figure 10. Zero-phonon action spectrum (triangles) obtained for Bchl *a* in 1:2 buffer−glycerol glass. The Q_y absorption spectrum is presented for comparison (solid curve) (unpublished data).

In the systems of interacting pigments, the situation is somewhat more complex, since pigments that are able to transfer energy rapidly are unlikely to burn (having very short lifetimes; see eq 23) and so will not contribute to the ZPA spectrum. In the first approximation, then, one can consider the ZPA spectrum to reflect the SDF of so-called "trap state" pigments, i.e., pigments which are the lowest energy pigment in their complex and thus *unable to transfer energy*.[207] In the case of multiple quasidegenerate low-energy pigment SDFs, the measured ZPA spectrum (trap state distribution) can be related back to the SDF for the individual pigments contributing to the lowest energy state, as recently demonstrated for the CP43 antenna complex of PSII.[207] The basic assumption in the "trap state" analysis of ref 207 is that coupling between pigments is sufficiently strong as to allow for fast and efficient energy transfer (e.g., by a Förster mechanism), thereby reducing the HB yield (see eq 23), but sufficiently weak that excitations can be considered essentially localized on individual pigments. For any frequency, then, the probability of finding a trap state localized on a given pigment m (out of a complex of say N pigments) is simply proportional to the probability that (1) a pigment of type m is located at the selected frequency and (2) this pigment is the lowest-energy pigment in its complex. The first term is proportional to the SDF (as for noninteracting pigments), while the second is given by the

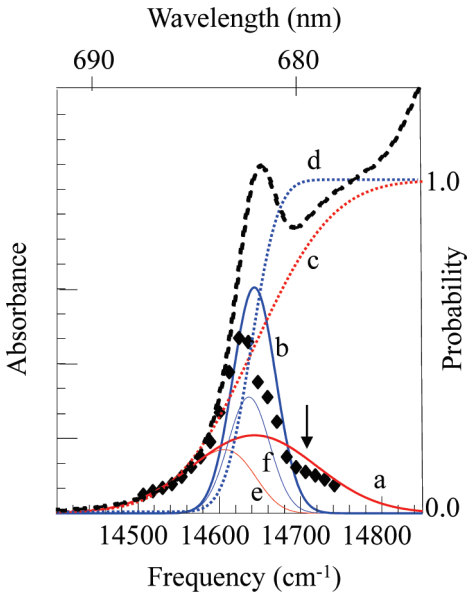

Figure 11. Components of the absorption and ZPA spectra of CP43 complex: Curves a and b are true SDF of two lowest-energy states of CP43 complex, A and B, respectively. Curves c and d are integrals of curves a and b, respectively, reflecting the probability of finding pigment A (or B) at wavelength lower than a certain wavelength. Curves e and f are actual contributions of pigments A and B to the ZPA spectrum (diamonds). The absorption spectrum is shown for comparison (dashed line). An arrow points at the discrepancy region. Reprinted with permission from ref 10. Copyright 2008 American Chemical Society.

product of the probabilities that all other pigments have a higher excitation energy than pigment m. More explicitly, if $f_m(\varepsilon_m)$ is the SDF for the site energy ε_m of pigment m, the SDF for pigments m which can undergo HB is given by

$$L_m(\varepsilon_m) = f_m(\varepsilon_m) \prod_{\substack{i=1 \\ i \neq m}}^{N} \left(1 - \int_{-\infty}^{\varepsilon_m} f_i(\varepsilon_i) d\varepsilon_i\right) \qquad (25)$$

In this model, the ZPA spectrum is then given by the sum of the distributions $L_m(\omega)$ for all pigments m. A similar approach has been used recently to examine nonresonant HB spectra in dimers and multipigment assemblies.[39] Of course, this "trap-state" model is itself only an approximation, but for relatively weak electrostatic interactions (such as in the CP43 complex[207]), it has been shown to match rather well with experimental data, as depicted in Figure 11 As discussed in ref 207 in the case of CP43, only the two lowest-energy pigments (denoted as pigments A and B) appear to be important for determining the lowest-energy state and thus the HB characteristics. The ZPA spectrum is thus obtained from eq 25 as the sum $L_A(\omega) + L_B(\omega)$, reflecting the distributions of A and B type trap-state pigments, i.e.,

$$\mathrm{ZPA}(\omega) = L_A(\omega) + L_B(\omega) = f_A(\omega)\left(1 - \int_{-\infty}^{\varepsilon_m} f_B(\varepsilon_B)\, d\varepsilon_B\right) + f_B(\omega)\left(1 - \int_{-\infty}^{\varepsilon_m} f_A(\varepsilon_A)\, d\varepsilon_A\right) \qquad (26)$$

In Figure 11, curves a and b are the SDFs $f_A(\varepsilon_A)$ and $f_B(\varepsilon_B)$ for pigments A and B, respectively.[207] Curves c and d are integrals of curves a and b (the two integrals in eq 26), respectively, reflecting the probability of findig pigment A (or B) at some energy lower than the corresponding energy of the x-axis. Curves e and f are the actual contributions, $L_A(\omega)$ and $L_B(\omega)$, of pigments A and B to the ZPA spectrum (diamonds). These represent the distribution of A and B pigments which, due to disorder, are the lowest-energy pigments in their individual complexes. We stress that in every individual complex *either* the A or B pigment contributes to the ZPA spectrum; in every individual complex there is only one lowest-energy state. For comparison, the dashed line shows the experimental absorption spectrum for CP43. While the ZPA spectrum (data points denoted by diamonds) is the sum of the curves e and f, the absorption spectrum, in the low-energy region, is a sum of the curves a and b. The arrow indicates a discrepancy between the model and experimental ZPA spectrum at higher energies.

In contrast to such weak-coupling calculations, the more general strong-coupling case is substantially more complicated and has yet to be investigated in detail for ZPA spectroscopy (a brief description of strong-coupling excitonic effects in HB is presented in section 4.8 in reference to nonresonant HB spectra). Qualitatively, however, one can imagine that the most important effect of strong excitonic interactions on ZPA spectra should be that, while HB is still expected to occur in the lowest excitonic state, it may influence the absorption transitions of higher excitonic states as well. It might be concluded, then, that excitonic interactions could allow higher excitonic states to contribute to the ZPA spectrum. At the same time, however, it should be remembered that excitonic interactions also tend to broaden the ZPLs of higher energy transitions (due to shortened EET lifetimes), limiting the influence of higher excitonic states on the narrow resonant hole depth. While these basic considerations can provide some insight into the shapes that can be expected for the ZPA spectra of strongly coupled systems, more precise conclusions must await further study.

4.6. Hole Shapes and FLN Line Shapes—Electron Phonon Coupling and ΔFLNS

In photosynthetic pigment−protein complexes, purely electronic (or excitonic) transitions as described in section 4.1 are accompanied by a large number of vibrational replicas due to el−ph and electron−vibrational (el−vibr) coupling. Here, the energetic difference between the purely electronic transition and a given vibrational line reflects the corresponding vibrational frequency. This is illustrated in Figure 12, which shows a ΔFLN spectrum excited within the lowest electronic state of the CP29 antenna complex,[60] which is assumed to be largely localized on a relatively isolated Chl *a* molecule. In this spectrum, the purely electronic line at 0 cm^{-1} appears along with a broad and asymmetric "phonon" wing peaking roughly at ∼20 cm^{-1} as well as with almost 50 distinct vibrational lines in the frequency range between ∼200 and 1700 cm^{-1}. The "phonon" wing at about 20 cm^{-1} is typically identified with a broad and almost continuous distribution of widely delocalized low-frequency protein vibrations, while the vibrational lines at frequencies higher than ∼200 cm^{-1} (see Table 1)[208,209] can be attributed to localized Chl vibrations (see, for example, Kühn et al.[210] for a review). Here, the term "phonon" is often used in analogy to vibrations in perfectly periodic lattices to distinguish low-frequency protein vibrations in pigment−protein complexes (and amorphous lattices in general) from the localized higher-frequency vibrations of the Chl (and other pigment) molecules bound to photosynthetic

dx.doi.org/10.1021/cr100234j |*Chem. Rev.* 2011, 111, 4546–4598

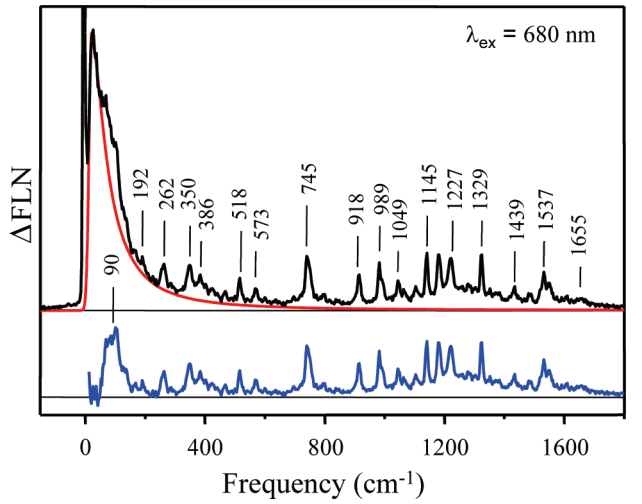

Figure 12. The vibronic region of the CP29 ΔFLN spectrum obtained with λ_{ex} = 680 nm. The ZPL is cut off at ~2% of its peak intensity. The modeled ΔFLN spectrum is shown by a smooth red curve. The lower blue curve is the difference between the above curves and offset for clarity. The numbers indicate the vibrational frequencies in wavenumbers. Reprinted with permission from ref 60. Copyright 2008 American Chemical Society.

pigment−protein complexes. The intensity distribution between the ZPL and the phonon wing is governed by the so-called Huang−Rhys factor S (see section 4.1).

In summary, it is apparent from Figure 12 that even the spectrum of one pigment molecule embedded into a protein matrix is complex and extends over a range of almost 2000 cm^{-1}. This underlines that detailed knowledge of parameters of el−ph and el−vibr coupling is essential for proper theoretical simulations of optical spectra as well as for the calculation of energy transfer rates of PC (see section 3). El−ph coupling in various PC has already been characterized by SHB[9,10,121,191,211−216] as well as by FLN[217−221] and in particular via the ΔFLN techniques.[55−61,222] Examples of Huang−Rhys factors S obtained in these studies are compiled in Table 2. Recently, the first results from single molecule spectroscopy on this topic have begun to emerge.[144,223] This section will provide an overview on the analysis of phonon structure illustrated by model calculations using the single-site absorption and fluorescence spectra of eq 13 (el−vibr coupling will be addressed separately in section 4.7).

In general, the SHB spectrum is obtained as the difference between the absorption spectrum at a particular time τ and the absorption at the start of the experiment, i.e.,

$$\Delta A(\omega) = A(\tau,\omega) - A(\tau = 0,\omega) \tag{27}$$

For simplicity, we begin our discussion here with the shallow hole burn limit; in this case, by expressing the exponential in eq 18 by a Taylor series and neglecting second- and higher-order terms (and again neglecting photoproduct) one obtains the following expression for the HB spectrum

$$\Delta A(\omega) = \sum_{R,P=0}^{\infty} \left(S^R \frac{e^{-S}}{R!}\right)\left(S^P \frac{e^{-S}}{P!}\right) \int d\Omega_0\, N(\Omega_0 - \omega_C) l_P(\omega_B - \Omega_0 - P\omega_m) l_R(\omega - \Omega_0 - R\omega_m) \tag{28}$$

Table 1. Vibrational Mode Frequencies, ν_j ($\pm$2 cm^{-1}), and Coupling Strengths, S_j, ($\pm$0.001), of Chl *a* in Selectively Excited Q_y Vibronic Spectra at 4.5 K

	ν_j			
S_j: Rätsep et al.[60]	Rätsep et al.[60]	Avarmaa and Rebane[208]	Gillie et al.[209]	Peterman et al.[217]
0.048	90			97
				138
0.004	192			213
0.010	262	260	262	260
0.001	287		283	
				298
0.015	350	350	350	342
0.009	386	390	390	388
0.003	425		425	425
0.002	443			
0.002	467	470	469	
			501	
0.006	518	520	521	518
0.0004	545		541	546
0.005	573	570	574	573
			588	585
0.001	607		607	604
0.001	638			
0.001	701			
			714	722
0.027	745	745	746	742
		755		752
			771	
0.002	800		791	
			805/819	
0.002	842		855	
			864/674	
			896	
0.013	918	915		916
0.019	989	987		986
				995
0.010	1049			1052
0.005	1070			1069
0.009	1109		1114	1110
0.018	1145	1145		1143
0.021	1186	1185	1178	1181/1190
			1203	1208
0.032	1227			1216/1235
0.001	1262		1259	1252/1260
0.003	1286		1285	1286
0.002	1307			1304
0.020	1329	1325	1340	1322
0.001	1353		1364	
0.002	1387	1385	1390/1411	1382
0.002	1439	1430	1433/1455	1439
0.007	1490	1485	1465/1504	1487
0.008	1525	1525	1524	1524
0.014	1537			1537
0.013	1556	1545		1553

dx.doi.org/10.1021/cr100234j |Chem. Rev. 2011, 111, 4546–4598

Table 1. Continued

	ν_j			
S_j: Rätsep et al.[60]	Rätsep et al.[60]	Avarmaa and Rebane[208]	Gillie et al.[209]	Peterman et al.[217]
				1573/1580
0.001	1610			1612
0.004	1665			1645/1673
$S_{vib} = \Sigma S_j$	0.34	not available	0.57	0.019

where l_P represents the electronic transitions bleached during the burn process. For simplicity, the prefactor $\sigma P \phi \tau$ was set to unity here (in the low-fluence limit, this has no effect on the shape of the spectrum). Likewise (though without the need for any series expansion), eqs 15 and 19 give the FLN spectrum as

$$\mathrm{FLN}(\omega) \propto \sum_{R,P=0}^{\infty} \left(S^R \frac{e^{-S}}{R!}\right)\left(S^P \frac{e^{-S}}{P!}\right) \int_{-\infty}^{\infty} d\Omega_0\, N(\Omega_0 - \omega_C) l_P(\omega_E - \Omega_0 - P\omega_m) l_R(\omega - \Omega_0 + R\omega_m) \quad (29)$$

which resembles the expressions of McColgin[224] and Personov.[123] However, eqs 28 and 29 use the line shape functions of Hayes et al.,[121] allowing an analysis of phonon structure in HB and FLN spectra on the basis of a consistent theoretical model. For illustration of the abstract expressions given above, Figure 13 (taken from ref 225) shows line-narrowed spectra calculated for the model system defined in Table 3. The results are directly comparable to the homogeneously broadened absorption and non-line-narrowed (NLN) spectra shown in Figure 14.

The full line in the lower part of Figure 13 is a HB spectrum calculated according to eq 22 for $\omega_B = 0\ \mathrm{cm}^{-1}$, i.e. in the center of the SDF. The full line in the upper part of Figure 13 is a line-narrowed fluorescence spectrum calculated according to eq 29 for $\omega_E = 0\ \mathrm{cm}^{-1}$. For comparison, the central part of Figure 13 shows corresponding homogeneously broadened absorption spectra (full and dashed lines) and the Gaussian SDF (dashed-dotted line).

The SHB spectrum exhibits a sharp ZPH coincident with the burn frequency ω_B and PSB holes (PSBH) on both sides of the ZPH. The ZPH is due to electronic transitions, which are resonantly bleached; i.e., their ZPL overlap the burn frequency ω_B. As discussed above, the resulting ZPH width is $2\Gamma_{hom}$. The theory discussed in the present chapter does not account for finite laser line width or spectral resolution. If either of these two parameters is of the same magnitude as the homogeneous width Γ_{hom}, the ZPH width is given by $\Gamma_{ZPH} = 2\Gamma_{hom} + \delta$, where δ accounts for an additional contribution. The feature at the high-energy side of the ZPH is the real-PSBH, which is due to the phonon wings that build on the ZPH. ZPH and real-PSBH correspond to ZPL and PSB of the homogeneously broadened absorption spectrum, respectively. In addition, there are electronic transitions at lower energy than ω_B, which are excited through their phonon wings. These transitions form the pseudo-PSBH, which is the mirror image of the real-PSB for the parameters employed here; see below for a more detailed discussion. The selection of homogeneously broadened absorption spectra by SHB is further illustrated in the central part of Figure 13. The spectrum represented by the full line is resonantly burned and leads to formation of ZPH and real-PSBH. The spectra given by dashed lines are nonresonantly burned via their PSB and contribute to the pseudo-PSBH. Electronic transitions at higher energy than ω_B do not contribute to the hole-burned spectrum. At the first glance, the composition of the FLN spectrum is quite similar to that of the SHB spectrum discussed above. The only difference is that the real-PSB lies on the low-energy side of the ZPL and is, therefore, superimposed on the pseudo-PSB. At first glance, one may thus tend to believe that the FLN spectrum exhibits less structure than the SHB spectrum. In practice, however, the different composition of FLN and SHB spectra can be effectively used to reliably determine the shape of the one-phonon profile in independent experiments (see below). Unfortunately, in conventional FLN experiments the ZPL possessing a width of $2\Gamma_{hom}$ is usually contaminated with scattered laser light because it is coincident with ω_E. This shortcoming precludes a thorough determination of the Huang−Rhys factor S. The corresponding homogeneously broadened and NLN absorption and fluorescence spectra are shown in Figure 14. It is apparent that the NLN spectra are widely featureless due to inhomogeneous broadening and thus provide less information on el−ph coupling than the line-narrowed spectra discussed above. The only remnants of el−ph coupling still visible are the Stokes shift of $\sim 2S\omega_m$ between the maxima of the absorption and fluorescence spectra and a slightly asymmetric shape with a full width of roughly $\Gamma_{inh} + S\omega_m$.[121]

In what follows we will extend the model presented above to the case of arbitrary burn fluence and concentrate on the PSB due to delocalized phonons. Substituting the line shape function of eq 15 into eq 18 produces for the entire absorption spectrum after a burn time τ

$$A(\tau,\omega) = \sum_{R=0}^{\infty} \left(S^R \frac{e^{-S}}{R!}\right) \int d\Omega_0\, N(\Omega_0 - \omega_C) \exp[-\sigma I \Phi \tau L(\omega - \Omega_0)] l_R(\omega - \Omega_0 - R\omega_m) \quad (30)$$

The hole-burned spectrum $\Delta A(\omega)$ is then obtained per eq 27 above. It is apparent from eq 30 that the HB spectrum may also depend on photon flux (P) or on burn time (t). Because the effect of variation of either parameter is similar, we will consider a variation of burn fluence (Pt) here. According to Hayes et al.,[121] the saturated fractional hole depth of the ZPH is given by

$$\Delta A_{saturated}(\omega_B)/A(\tau = 0, \omega_B) = \exp(-S) \quad (31)$$

As outlined by Lee et al.,[226] a number of further conclusions can be drawn from the eq 30. In the short burn time limit, the ZPH width is $2\Gamma_{hom}$, so that determination of ZPL line width Γ_{hom} should be based on shallow holes with a fractional hole depth <10%. Furthermore, for lower burn fluences the intensities of real- and pseudo-PSBH are almost comparable. With increasing burn fluence, however, there is a considerable gain in intensity for the pseudo-PSBH. This effect may lead to some uncertainty when determining the Huang−Rhys factor S from PSBH intensity of HB spectra, especially, because PSBH may not be discernible in the short burn time limit for weak coupling. Nevertheless, S can be obtained from the saturated hole-depth and/or from a thorough theoretical analysis of the burn fluence dependence of the HB spectra. HB and FLN spectra, as described

Table 2. Huang−Rhys Factor *S* Obtained by HB, FLN, and ΔFLN for the Lowest Energy States of Different Photosynthetic Pigment−Protein Complexes

complex	HB	FLN	ΔFLN	ref
FMO from green sulfur bacteria	0.3			Zazubovich et al.[216]
		0.3		Wendling et al.[218]
			0.28−0.70	Rätsep and Freiberg[61]
CP43	0.25 (A and B band)			Hughes et al.[12]
	0.30 (A band) 0.25 (B band)			Dang et al.[10]
CP47	0.7			den Hartog et al.[212]
	1.0			Neupane et al.[9]
CP29 from green plants	0.5			Pieper et al.[214]
			0.41−0.66	Rätsep et al.[60]
LHCII from green plants	0.8			Pieper et al.[213]
		0.6		Peterman et al.[217]
		0.9		Pieper et al.[214]
			0.85	Pieper et al.[222]
LH1 from purple bacteria			0.85	Timpmann et al.[56]
LH2 from purple bacteria			1.05	Timpmann et al.[56]
			0.1−0.9[a]	Hoffmann et al.[144]
PSI core from cyanobacteria	2.0			Hayes et al.[215]
LHCI from green plants		2.9		Ihalainen et al.[221]
P680 from PSII RC	1.9			Chang et al.[211]

[a] Determined in SPCS experiments.

by model calculations above, have been routinely employed to investigate el−ph coupling in photosynthetic antenna pigment−protein complexes[9,10,191,212−221] and RCs.[121,211] A more detailed discussion of phonon structure in site selective spectra is beyond the scope of this review.

More recently, FLN experiments on the trimeric LHCII antenna complex of green plants[227] established that the width of the PSB of ∼100 cm^{-1} may compete with the inhomogeneous width of only ∼80 cm^{-1} as determined by ZPA spectroscopy. At the same time, apparent discrepancies were observed in the PSB structures obtained by SHB[228] and FLN,[217] respectively. The model calculations of line-narrowed spectra presented above assumed that $\Gamma_{inh} > \Gamma$, where Γ is the width of the one-phonon profile. Therefore, we will now consider the different PSB contributions in the $\Gamma_{inh} \approx \Gamma$ regime. The discussion of the individual PSB contributions to line-narrowed spectra in the low-temperature limit will be based on eqs 28 and 29. However, following the approach of ref 227 for FLN spectra, four contributions to line-narrowed spectra are defined (see Figure 15): First, the ZPH (ZPL) located at ω_B (ω_E) is obtained for $R, P = 0$ in eqs 28 and 29 (contribution a). Second, the $P = 0, R \geq 1$ terms (contribution b) represent phonon transitions that build on the ZPH (ZPL) and form the real-PSB. Third, the $R = 0, P \geq 1$ terms (contribution c) correspond to electronic transitions that are nonresonantly burned (excited) at ω_B (ω_E) via multiphonon transitions and constitute the pseudo-PSB. Finally, the $R, P \neq 0$ multiphonon terms, i.e., the (integrated) phonon wing(s) of contribution c, are sometimes referred to as multi-PSB (contribution d) but can also be considered as a part of the pseudo-PSB.

The simulated FLN and HB spectra for the $\Gamma \approx \Gamma_{inh}$ regime are shown as dashed curves in frames A and B of Figure 15, respectively. The calculations were performed with the parameter values of Table 4, but especially using Γ = 57.5 cm^{-1} (Γ_G = 15 cm^{-1}, Γ_L = 100 cm^{-1}); i.e., the Lorentzian tailing of the one-phonon profile does now exceed Γ_{inh}. As outlined in ref 227, it is obvious from Figure 15 that the general composition of the line-narrowed spectra is the same as above. Most striking, however, is that the real- (contribution b) and pseudo-PSB (contribution c) exhibit apparently different shapes. The numbers in Figure 15 correspond to the displacements of PSB features (in cm^{-1}) measured relative to the ZPL (ZPH) at 0 cm^{-1}. The PSB of the dashed FLN spectrum and the real-PSB of the dashed HB spectrum show features at 15 and 26 cm^{-1} that correspond to one- and two quantum transitions of phonons with ω_m = 15 cm^{-1}. The two-quantum transition and the slight tailing toward higher phonon frequencies, however, are not observed in the pseudo-PSB of the dashed spectrum in frame B. This is most easily understood by separately analyzing contributions b and c to the FLN spectrum (eq 27). Recalling that $P = 0, R \geq 1$ and $R = 0, P \geq 1$ define contributions b and c, respectively, and using a delta function for the ZPL of the homogeneously broadened spectrum, it follows easily that they are given by

$$F_b(\omega) = \sum_{R=1}^{\infty} \left(S^R \frac{e^{-2S}}{R!} \right) N(\omega_E) l_R(\omega - \omega_E + R\omega_m) \quad (32)$$

and

$$F_c(\omega) = \sum_{P=1}^{\infty} \left(S^P \frac{e^{-2S}}{P!} \right) N(\omega) l_P(\omega - \omega_E + P\omega_m) \quad (33)$$

The apparent difference between the two equations is that $F_b(\omega)$ depends on the fixed value of the SDF ($N(\omega)$) at ω_E while $F_c(\omega)$ depends on $N(\omega)$, i.e., on the shape of the SDF function. The latter point is nicely illustrated in frame A of Figure 15, where it is obvious that the SDF determines the shape of the pseudo-PSB (c) on its low-energy side; i.e., the mirror symmetry

dx.doi.org/10.1021/cr100234j |*Chem. Rev.* 2011, 111, 4546–4598

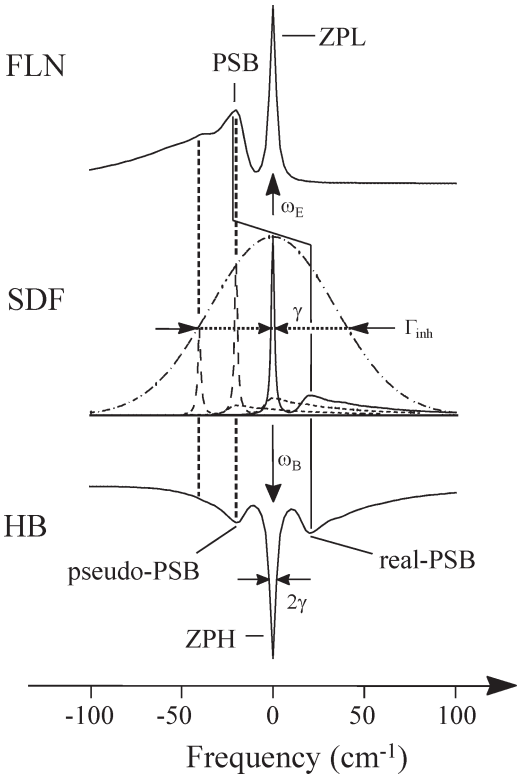

Figure 13. Low-temperature line-narrowed spectra for an excitation/burn frequency of $\omega_E/\omega_B = 0$ cm^{-1} (see arrows) and the model system defined in Table 3. Central part: homogeneously broadened absorption spectra calculated according to eq 15 and distributed according to the SDF (dashed-dotted line). Absorption spectra of resonantly and non-resonantly excited pigments are shown as full and dashed lines, respectively. Absorption spectra of pigments that are not excited were omitted for ease of inspection. Upper part: resulting line-narrowed fluorescence spectrum calculated according to eq 29. Lower part: resulting hole-burned spectrum calculated in the short burn time limit according to eq 28. Provided by J.P.

Table 3. Parameters of the Model Calculations Shown in Figures 13 and 14[a]

temperature	T (K)	5
position of SDF	ω_C (cm^{-1})	0
homogeneous width	γ (cm^{-1})	2.0
inhomogeneous width	Γ_{inh} (cm^{-1})	80
Huang–Rhys factor	S	1.0
peak phonon frequency	ω_m (cm^{-1})	20
fwhm of Gaussian wing	Γ_G (cm^{-1})	10
fwhm of Lorentzian wing	Γ_L (cm^{-1})	30
fwhm of one-phonon profile	Γ (cm^{-1})	20

[a] Data taken from ref 225.

between real- and pseudo-PSB breaks down in the $\Gamma \approx \Gamma_{inh}$ regime. This effect is directly observed for the pseudo-PSB of the dashed HB spectrum. As a consequence, the low-energy wing of the pseudo-PSB in HB spectra is determined by the quickly tailing Gaussian SDF rather than by the slowly tailing Lorentzian wing of the one-phonon profile. This finding readily explains the discrepancies in the shapes of the line-narrowed spectra of LHCII.[227] More recently, similar effects were reported for the

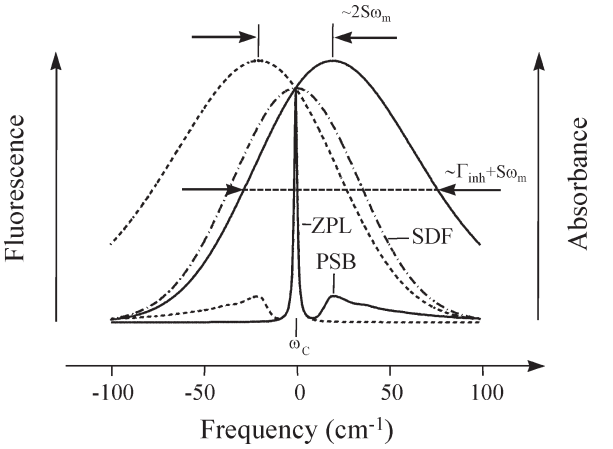

Figure 14. Low-temperature homogeneously broadened and non-line-narrowed spectra for the model system defined in Table 3. Non-line-narrowed absorption (full line) and fluorescence spectra (dashed line) calculated according to eq 18 for $t = 0$. The corresponding homogeneously broadened spectra and SDF are given for comparison. Provided by J.P.

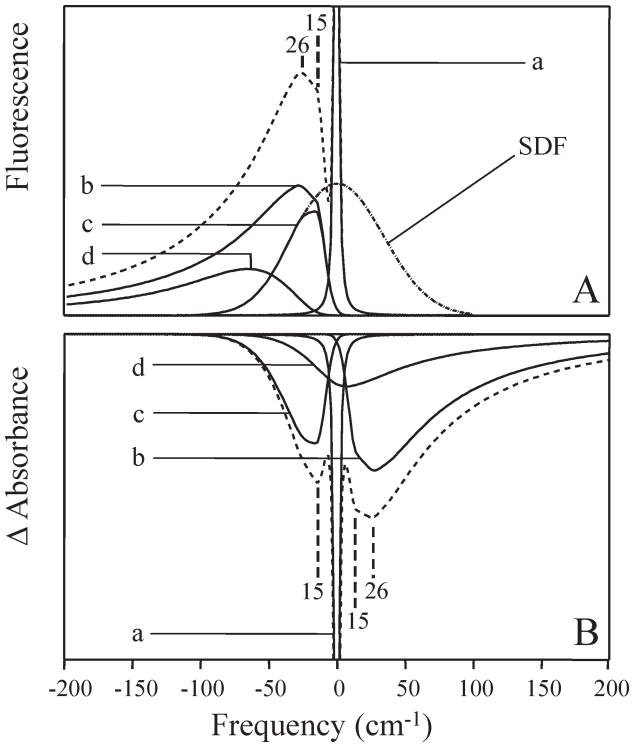

Figure 15. Low-temperature HB (frame B) and line-narrowed fluorescence (frame A) spectra (dashed lines) calculated according to eqs 28 and 29, respectively, for illustration of the $\Gamma_{inh} \cong \Gamma$ regime. The model system is defined in Table 4. In frames A and B, the full lines represent the ZPH (a) and multiphonon contributions (b–d). The ZPLs are cut off at 4% of their peak intensity value. The dashed-dotted line represents the profile of the SDF. Reprinted with permission from ref 227. Copyright 1999 Elsevier B.V.

bacterial antenna complex LH2[55] and for the minor antenna complex CP29 of green plants.[60] These findings suggest that accurate extraction of Huang–Rhys factors from HB spectra requires a much more careful analysis than has often been done in

dx.doi.org/10.1021/cr100234j |*Chem. Rev.* 2011, 111, 4546–4598

Table 4. Parameters of the Model Calculations Shown in Figure 15[a]

temperature	T (K)	5
position of SDF	ω_C (cm^{-1})	0
burn/excitation frequency	$\omega_{B/E}$ (cm^{-1})	0
homogeneous width	γ (cm^{-1})	0.4
inhomogeneous width	Γ_{inh} (cm^{-1})	80
Huang−Rhys factor	S	1.0
peak phonon frequency	ω_m (cm^{-1})	15
fwhm of Gaussian wing	Γ_G (cm^{-1})	15
fwhm of Lorentzian wing	Γ_L (cm^{-1})	100
fwhm of one-phonon profile	Γ (cm^{-1})	57.5

[a] Data taken from ref 227.

the past, especially for systems in which the width of the PSB is similar to or larger than that of the SDF. Although HB in principle provides real- and pseudo-PSBs as separate features (see above), the real-PSB is often interfered with by the antihole, so that the one-phonon profile is routinely obtained from the more intense pseudo-PSB. In the limit of an infinitely wide SDF, this approximation would be rigorously justified, since in the low-fluence limit, the real- and pseudo-PSB terms must in this case be mirror symmetric. On the basis of the argumentation above, however, it can be expected that in real systems, the one-phonon profile determined this way will not reflect the correct tailing at its high-energy side, particularly for systems in which the SDF is narrow relative to the PSB. As a result, Huang−Rhys factors calculated from the areas of ZPL and PSB only would be artificially lowered, with the extent of lowering depending on the burn wavelength and the relative widths of the SDF and PSB.

Fortunately, these shortcomings of HB spectroscopy can be avoided by using a combination of HB and FLN spectroscopy. Very recently[55−61] Rätsep and Freiberg established a new method for obtaining el−ph coupling strengths using ΔFLN spectroscopy,[46,51−54] as already mentioned above. In this approach, a ΔFLN spectrum is obtained as the difference between FLN spectra recorded before and after an intermediate HB step. This technique provides two important advantages over traditional HB and FLN spectroscopy: first, the scattered laser light which otherwise obscures the ZPL in FLN spectra can be effectively eliminated in the difference spectrum, allowing direct measurement of ZPL fluorescence; second, the "double selection" via both HB and FLN suppresses the pseudo-PSB term in the measured signal, greatly simplifying the analysis of experimental data. Similar subtraction techniques have been applied before[51−54,229−232] to enhance the spectral selectivity of FLN spectra. Nevertheless, the approach of Rätsep and Freiberg appears to be the first application to PC that readily yields the ZPL together with the phonon and vibrational structure building on it so that el−ph and el−vibr coupling strengths can be determined directly. An example of a ΔFLN spectrum is shown in Figure 16 for the case of trimeric LHCII.[222] A FLN spectrum selectively excited within the fluorescence origin band of LHCII is shown in Figure 16 (black curve) for a representative excitation wavelength of 682 nm. As expected, the spectrum is composed of a sharp ZPL located at the excitation wavelength and the broad phonon wing peaking about 22 cm^{-1} to the red of the ZPL. In this spectrum the ZPL is still contaminated with scattered light originating from the excitation laser. Additional FLN spectra were recorded after hole-

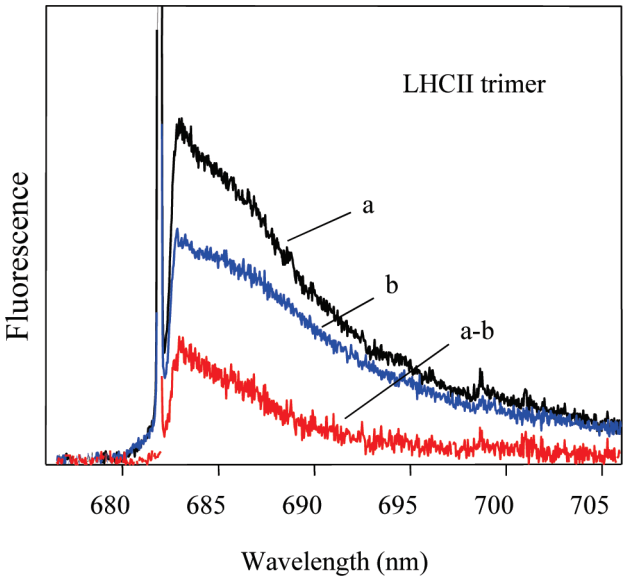

Figure 16. Experimental and simulated 4.5 K ΔFLN spectra of trimeric LHCII. ΔFLN spectrum excited and burned at 682.0 nm (lower red curve) with the ZPL cut off at 3.7% of its full intensity. The black (a) and blue curves (b) show the corresponding pre- and postburn FLN spectra, respectively. FLN spectra were recorded with a fluence of 0.4 mJ/cm^2, while the fluence applied for hole-burning was 32 mJ/cm^2. Reprinted with permission from ref 222. Copyright 2009 American Chemical Society.

burning at the excitation wavelength with different burn fluences ranging from 1.8 to 32 mJ/cm^2 (blue curve in Figure 16). ΔFLN spectra are readily obtained after subtracting the postburn from the preburn FLN spectra. The ΔFLN spectrum is shown as the red curve in Figure 16. Under these conditions the intensity ratio between ZPL and PSB reflects the Huang−Rhys factor S, because subtraction of the postburn from the preburn FLN spectra widely eliminates the scattering contribution and thus provides a reliable measure of the ZPL intensity.

It goes without saying that accurate determination of Huang−Rhys factors from ΔFLN spectra requires an accurate model for the experimentally measured spectra. In many recent papers,[55−61,222] the ΔFLN signal has been modeled using eq 29, i.e., the traditional FLN line shape function. In contrast, the early theoretical descriptions of Jaaniso[52] and Fünfschilling[54] imply that, in contrast to traditional FLN spectra, ΔFLN spectra in the low-fluence limit should be essentially free of pseudo-PSB contributions. Instead, these works indicate that experimental ΔFLN spectra should be essentially proportional to the single-site fluorescence spectrum. As discussed recently,[186] improper application of eq 29 to measured ΔFLN spectra incorrectly lowers the apparent Huang−Rhys factors (especially for excitation frequencies on the high-energy side of the SDF) due to an artificial subtraction of an (experimentally nonexistent) pseudo-PSB term. As a result, while the experimental data of refs 55−61 and 222 are unaffected, the obtained Huang−Rhys factors in most cases are somewhat underestimated. In this regard, it should be added that the ΔFLN signal is truly proportional to the single-site fluorescence spectrum only in the limit of an infinitely narrow excitation laser line width. For larger excitation bandwidths, selectivity is decreased, allowing in principle for the reappearing of some pseudo-PSB contributions. In practice, the narrow-line width assumption is an excellent approximation

when experimental data is obtained with high-resolution lasers; however, the experimental data presented in refs 55−61 and 222 were obtained with a laser with a much larger excitation laser line width (~0.5 cm^{-1}). While model calculations in ref 186 indicate that in this range the effects of the finite excitation line width on the ΔFLN signal are quite negligible (aside from a slight distortion of the line shape), an accurate reanalysis of the data in refs 55−61 and 222 will require consideration of the finite linewidths employed; equations for this purpose are also described in ref 186.

4.7. Ground and Excited State Vibrational Frequencies

FLN spectroscopy can also provide vibrationally resolved spectra of cofactors in photosynthetic complexes for both ground (origin band excitation) and excited state (excitation through vibronic replicas in absorption). As mentioned above, (0,0) band excitation can also provide insight into the electron−phonon coupling strength and Franck−Condon factors that define the intensity of the vibronic transitions. The ZPLs, i.e., pure electronic transitions, have to be excited in order to achieve the highest selectivity and sensitivity in FLN spectroscopy, since typically there is no correlation between different excited states. As a result, S_2 excitation of isolated molecules in glasses (or high energy excitation of Chls in PC) leads to population of all sites (within the inhomogeneously broadened band) and a disappointingly broad fluorescence spectra. The measurements of excited- and ground-state vibrational frequencies have been well described in refs 46, 123, 124, 132, and 233. In general, the origin band excited FLN spectrum may provide ground state (S_0) vibrational frequencies and relative vibronic intensities which, in combination, may serve as a fingerprint of studied chromophores, e.g., Chl *a*. To probe the S_1-state vibrational structure, one employs vibronically excited FLN.[132,233] An example of an experimental FLN spectrum is shown in Figure 12.

4.8. SHB in Excitonically Coupled Systems

As mentioned above in reference to ZPA spectroscopy, the presence of excitonic interactions in a system significantly complicates the analysis of HB spectra. While excitonic effects in HB spectra have been discussed qualitatively for many years, only recently efforts have been made to quantitatively investigate these effects in real[85,86] and model[39,40] systems. These quantitative analyses have so far been limited to nonresonant HB spectra due to computational constraints, although the theories developed can be fairly easily adapted to deal with resonant HB spectra as well. In this section, we provide a brief overview of the effects that interpigment interactions can have on the HB spectra of photosynthetic complexes and other multichromophoric molecular assemblies (dimers, trimers, etc.), for interaction regimes ranging from weak (Förster EET) to very strong (Frenkel exciton).

The simplest case is that of weakly interacting pigments (the Förster regime), as discussed in section 4.6 regarding ZPA spectroscopy; in this case, excitations are assumed to be completely localized on individual pigments but are nonetheless capable of being transferred from pigment to pigment. Under these conditions, so long as EET is reasonably fast (much faster than the rate of fluorescence, for example, which is generally much faster than the rate of HB), one can expect HB to occur only for "trap" pigments, i.e., those pigments which are the lowest energy pigment in their complex and are thus *unable to transfer energy further*. These processes typically have a fairly intuitive effect on the HB spectrum: when the system is excited nonresonantly (i.e., either at high enough energy that all pigments are excited or using a broad band excitation source such as white light), the resulting HB spectrum appears flat (or positive) at high energy with negative features only within the SDF of the lowest-energy pigments.

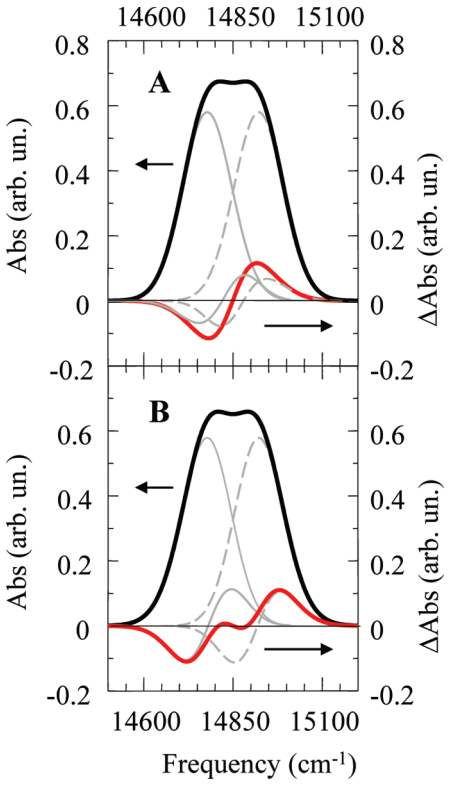

Figure 17. Simulated nonresonant HB spectra for model dimers coupled by (A) Förster energy transfer and (B) an electronic coupling constant of 50 cm^{-1} (parallel transition dipole moments). In both frames, the thick red curve represents the net HB spectrum, while the thick black curve represents total preburn absorption. In frame A, the positive gray curves (solid and dashed) show the SDF for each pigment (chosen to approximately match the excitonic state absorption curves in frame B), while the gray HB curves show the corresponding HB contributions of each pigment to the total HB spectrum. In frame B, both pigments are assigned identical Gaussian site energy SDFs with a width of 90 and 14 850 cm^{-1} expectation value. See the text for details (unpublished data).

As explored recently,[39] such systems can easily be modeled using equations similar to eqs 25 and 26 (see section 4.5 on ZPA spectroscopy), after making simple modifications to account for photoproduct absorption. As an example, frame A of Figure 17 shows the calculated HB spectrum (thick red curve) for a dimer of pigments connected by Förster energy transfer. The SDFs and component HB curves for each pigment are shown in gray for comparison; the Gaussian SDFs are shifted by 144 cm^{-1} with respect to each other and chosen to mimic the excitonic absorption spectrum shown in frame B (discussed below). In these calculations, photoproduct is assumed to fall within the original SDF of the burned pigment. The component HB curves show the contribution of each pigment to the net HB spectrum: the solid gray HB curve is due to HB on the pigment with the red-shifted SDF, while the dashed gray curve represents HB on the pigment with blue-shifted SDF. (Note that, regardless of how far the shift is between the SDFs of the two pigments, there is always some probability due to disorder that HB will occur on either pigment.) An important feature to notice from these calculations

dx.doi.org/10.1021/cr100234j |*Chem. Rev.* 2011, 111, 4546–4598

is that, although HB involves only the lowest-energy pigment (in any given realization of disorder), the contribution of each pigment to the net HB spectrum is approximately equal. As discussed in more detail in ref 39, this somewhat counterintuitive observation is a result of hole-refilling: although the pigment with red-shifted SDF is more likely to be burned in any given realization of disorder, it is also more likely to have its hole refilled by photoproduct, since the distribution of burn frequencies is spread out over a much wider portion of the preburn SDF than for its more blue-shifted counterpart (where pigments are burned only from the red-most portion of the SDF). As a result, the increased rate of burning of the low-energy distribution is almost exactly balanced by the increased rate of hole-refilling, so that the net spectrum has the appearance of an average between the two pigment HB spectra. This effect becomes even more pronounced as the shift between the pigment SDFs increases, although for large SDF shifts, the shape of the spectrum is strongly dependent on the placement of photoproduct.

In the more general case of strong excitonic interactions (the regime of delocalized excitons), several additional effects come into play. First, one must consider that even after EET to the lowest excitonic state, delocalization implies that *any given pigment in the complex can be burned*, with burn probabilities weighted by the contribution of the given pigment to the lowest excitonic state. More precisely, the distribution of *m*-type pigments which *can* be burned is in this case obtained as[40]

$$L_m(\varepsilon_m) = \int_{-\infty}^{\infty} {c_{1,m}}^2(\varepsilon_1,\ldots,\varepsilon_N) f(\varepsilon_1,\ldots,\varepsilon_N)\, d\varepsilon_1\, d\varepsilon_2 \ldots d\varepsilon_{m-1}\, d\varepsilon_{m+1} \ldots d\varepsilon_N \quad (34)$$

where $\varepsilon_1, \ldots, \varepsilon_N$ are the site energies of the N excitonically coupled pigments in the complex, ${c_{1,m}}^2(\varepsilon_1,\ldots,\varepsilon_N)$ is the probability that the lowest excitonic state is localized on pigment m, and $f(\varepsilon_1,\ldots,\varepsilon_N)$ is the N-dimensional SDF for pigment site energies. Note that for uncorrelated site energies, $f(\varepsilon_1,\ldots,\varepsilon_N) = f_1(\varepsilon_1)f_2(\varepsilon_2)\ldots f_N(\varepsilon_N)$, where $f_i(\varepsilon_i)$ is the SDF for the site energy of the ith pigment; in the weak coupling limit, we have

$${c_{1,m}}^2(\varepsilon_1,\ldots,\varepsilon_N) = \begin{cases} 1 & \varepsilon_m < \varepsilon_i, \quad \forall_{i\neq m} \\ 0 & \text{otherwise} \end{cases} \quad (35)$$

in which case eq 34 reduces to eq 25.

A second—and perhaps even more significant—effect of excitonic interactions on HB spectra is that since any given pigment contributes to multiple transitions, HB of *any* pigment can in principle alter the transition energies of *all* excitonic states. For example, in the case of the excitonically coupled dimer, the transition energies of the upper and lower excitonic components are given by the average of the two pigment site energies plus or minus a constant determined by the strength of interpigment coupling and the shift between the pigment site energies; as a result, when HB occurs in the lower-energy excitonic state, the transition frequencies of *both* excitonic states shift, even though only one of the two pigment site energies has changed. This can have a dramatic effect on HB spectra, producing split holes, broad antiholes, and in general significant HB signal at all excitation wavelengths across the absorption spectrum.

As an example, frame B of Figure 17 shows the calculated absorption and HB spectra for an excitonically coupled dimer of two pigments with perpendicular transition dipole moments and an electronic coupling constant of 50 cm^{-1}. In contrast, with the spectra shown in frame A of Figure 20, frame B is calculated for a system in which the SDFs of the two pigments are identical Gaussian functions centered at 14 850 cm^{-1} with fwhm of 90 cm^{-1} (i.e., there is no shift between the SDFs of the two pigments). The double peak in both absorption and HB spectra is instead caused by excitonic interactions. Instead of representing pigment distribution curves, the gray curves in frame B thus represent absorption and component HB curves of the two different *excitonic states* of the system. It is easily seen that the contributions of both excitonic states to the net HB spectrum are similar; as discussed above, this is because, regardless of which pigment in the system burns, the transition frequencies of both excitonic states are shifted in the postburn spectrum. In the example shown, the photoproduct of the lower excitonic state largely fills the hole created by the upper excitonic state; for more strongly coupled systems (where the excitonic absorption peaks are further separated) and in cases where the transition dipole moments of the pigments are not perpendicular, a variety of complex hole shapes can be produced, including double holes and holes that appear to be blue-shifted from the lowest-energy component.[40] It has recently been demonstrated that such excitonic effects can quantitatively account for the complex antihole structure of the PSII core antenna subunits CP43[85] and CP47[86] (see also section 5.1.2) given suitably chosen site energies. Indeed, the strong dependence of antihole shapes on the site energies of individual pigments in excitonically coupled systems opens the door to the use of HB spectra as a sensitive test for extracted pigment site energies for photosynthetic complexes.

4.9. Basic Principles of SPCS

The key advantage of SPCS is that this approach entirely eliminates the problem of automatic subensemble averaging and allows one to investigate the properties of individual complexes, thereby completely removing effects due to inhomogeneous broadening.[62,65] From the methodological viewpoint, the vast majority of SPCS experiments are based on the commercial or, especially at low temperature, home-built confocal fluorescence microscopes. The small amount of fairly diluted sample is spin-coated onto a substrate, ensuring that only one complex at a time is present in the diffraction-limited volume selected by the microscope objective. After such selection has been achieved, fluorescence or fluorescence excitation spectra of PC are measured. The excited state lifetimes can be extracted directly from the homogeneous ZPL widths at low temperatures.[234] A word of caution is in order, though, as sometimes the ZPL widths in SPCS experiments are affected by light- and thermal-induced spectral diffusion and as a result become larger than granted by SHB or time-domain data.[70,146] In fact, most of SPCS studies currently focus on the spectral diffusion, essentially utilizing PC as model systems in the studies of the low-temperature protein dynamics in general.[62] It also appears useful to ensure that other properties of the single complex spectra, averaged over a large enough number of single complexes, are in agreement with the ensemble averages. SHB, probing these averages, could be used to verify if light-induced spectral diffusion behavior observed in SPCS experiments represents behavior *typical* for the protein under study and independent of sample preparation details (e.g., nature of the amorphous host surrounding the protein) and/or other experimental procedures. In other words, the property widely considered to be a deficiency of the SHB with respect to

SPCS may be treated as beneficial, since it provides independent benchmarks for SPCS results.

4.10. Basic Principles of Two-Dimensional Electronic Spectroscopy (2D ES)

A large fraction of information obtainable via SHB (as well as some additional information) can also be obtained by a new class of techniques collectively known as 2D electronic spectroscopies (2D ES).[27,235−237] In this review, which focuses on SHB, these powerful techniques will be only briefly addressed, concentrating on the information these techniques provide and on the comparison of these techniques with SHB and FLN methodologies viewed as 2D techniques.[236] The details on the physics behind 2D ES and the experimental arrangements can be found in recent excellent papers.[27,235−241] Whenever possible, 2D ES results will be discussed along with SHB results in the sections devoted to particular PCs.[241−243]

2D optical signals[235,239−242] represent the response of the system to three ultrashort chronologically ordered laser pulses with wave vectors $\mathbf{k}_1$, $\mathbf{k}_2$, and $\mathbf{k}_3$, respectively. The time intervals between pulses are t_1 (or coherence time, τ) and t_2 (waiting or population time, T); t_3 (rephasing time, t) is the time between the third pulse and the third-order signal. The 2D spectrum is usually obtained by performing 2D Fourier transform with respect to the first and third intervals $t_1 \rightarrow \Omega_1$ and $t_3 \rightarrow \Omega_3$; all time delays between pulses are positive and the second time interval, t_2, is varied as a parameter, which allows one to obtain various information on the dynamics of the system. Various contributions to the third-order response function may be observed by exploring signals in different directions. The photon echo is observed in the $\mathbf{k}_{PE} = -\mathbf{k}_1 + \mathbf{k}_2 + \mathbf{k}_3$ direction. This *rephasing* 2D signal shows correlations between absorbed, Ω_1, and emitted, Ω_3, energies; excitation energy transport takes place during t_2. A different *nonrephasing* signal is obtained along the $\mathbf{k}_{TG} = \mathbf{k}_1 - \mathbf{k}_2 + \mathbf{k}_3$ direction, where TG stands for transient grating. This is the wave-vector matching condition for TG, pump−probe, and hole-burning experiments.[236] In the TG experiment the signal direction is kept the same as in $\mathbf{k}_I$, but pulses 1 and 2 are interchanged. The *double-quantum coherence* signal is in the $\mathbf{k}_{III} = \mathbf{k}_1 + \mathbf{k}_2 - \mathbf{k}_3$ direction. Here, the Fourier transform can be made in two ways: either $t_1 \rightarrow \Omega_1$, $t_2 \rightarrow \Omega_2$, holding t_3 as a parameter, or $t_2 \rightarrow \Omega_2$, $t_3 \rightarrow \Omega_3$, holding t_1 as a parameter. In this signal the Ω_2 axis shows double-exciton resonances and their distribution between single excitons on Ω_1 or Ω_3 axes.

Figure 18 (from ref 240) depicts the main features of the 2D spectra of a coupled chlorophyll dimer, a fundamental constituent of the molecular aggregates involved in photosynthetic light-harvesting systems. The cut along the diagonal reflects the dimer's linear absorption. Both higher and lower excitonic components are inhomogeneously broadened. While inhomogeneous broadening affects the width of the diagonal cut, the cut in the perpendicular, or antidiagonal direction, characterizes homogeneous broadening. Thus, 2D ES allows one to obtain information on both inhomogeneous and homogeneous broadening. The off-diagonal contributions to the 2D spectrum, or cross-peaks, indicate correlations between excitons, and their evolution (with changing t_2) can be used to characterize the energy transfer processes. Cross-peaks due to excitonic coupling are best visualized at $t_2 = 0$. The cross-peak sign is an indicator of mutual orientations of the interacting dipoles. Obviously, this logic can be extended to the case of a larger number of interacting chlorophylls.[239−241,243] Experimental

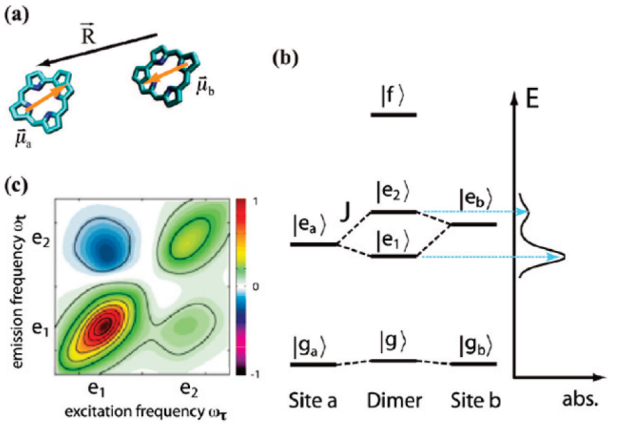

Figure 18. A coupled dimer of chlorophyll pigments and its 2D spectra: (a) chromophores are approximated as two-level electronic systems; (b) excitons e_1 and e_2 (ψ_+ and ψ_- in section 3) are superpositions of original states e_a and e_b, and are split due to coupling J ($V_{1,2}$ in section 3 and Figure 3), while f corresponds to doubly excited $\psi_1^e\psi_2^e$. The coupling also redistributes transition strength, shown in the absorption spectrum at right and also in the dimer 2D spectrum at $T = 0$ (c). Figure reprinted by permission from ref 240. Copyright 2009 American Chemical Society.

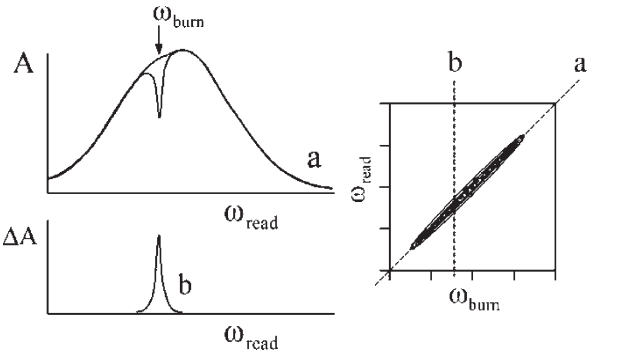

Figure 19. Schematic of a two-dimensional experiment based on hole-burning (see the text for details). Figure reprinted by permission from ref 236. Copyright 2000 American Chemical Society.

observation of cross-peaks and their transient behaviors in time also provides invaluable information about the exciton−exciton coherence and population transfers.[235] The capability to explore the phase and coherence information in the time evolution of the optical polarization induced by the optical pulses is used to study protein structure and dynamics.[244] For example, a remarkably long-lived electronic quantum coherence, which most likely plays an important role in the efficient energy transfer process in photosynthetic complexes, was observed in *Chlorobium tepidum* FMO complex at 77 K.[245] Coherences were also observed in bacterial RC[246] and marine algae antenna complexes.[247,248]

Figure 19 from ref 236 illustrates the connection between 2D spectroscopies and SHB. In SHB a subset of the ensemble can be photobleached by an intense monochromatic field with a frequency ω_{burn}. The induced change in the absorption line shape is measured by a weak read-out beam at frequency ω_{read}, as discussed. For a distribution of homogeneous line shapes masked by inhomogeneous broadening, the difference spectrum is representative of the homogeneous line shape of the subensemble absorbing at ω_{burn}. This experiment is a function of two

dx.doi.org/10.1021/cr100234j |*Chem. Rev.* 2011, 111, 4546–4598

independent frequency variables and can similarly be regarded as two-dimensional. If we now allow both ω_{burn} and ω_{read} to be tuned through the inhomogeneous line shape, we can construct a 2D line shape as a function of these two variables. This line shape will have an elliptical line shape whose profile (see Figure 19) along the diagonal frequency axis ($\omega_{burn} = \omega_{read}$) reproduces the site distribution function, i.e., corresponds to ZPA spectrum discussed in section 4.5. The width perpendicular to the diagonal represents the homogeneous line width. The ellipticity of the line tells about the extent of inhomogeneous vs homogeneous broadening. These observations suggest that the 2D line shape, in addition to giving a quantitative description of multiple time scales, allows tremendous intuitive insight into the nature of spectral broadening and the makeup of the ensemble.

Interestingly, the 2D analog of the FLN spectroscopies has been known for quite a while, under the name total luminescence spectroscopy. Initially developed for detection of pollutants in the air, it was employed by Wild, one of the pioneers of SHB and single molecule spectroscopy, for investigating impurity spectra in crystals and glasses. The best description of the method can be found in ref 249. Considering total luminescence spectroscopy is particularly instructive, as it allows one to recognize how phonons and vibrations are expected to affect the 2D spectra. Note that the vast majority of 2D ES data on PC has been obtained at 77 K and higher temperatures, where ZPL and PSB are not well-resolved. Briefly, localized chlorophyll modes should manifest as weak peaks vertically (emission) and horizontally (excitation) shifted from the origin bands by respective vibration frequencies. The 1150 cm^{-1} C−C vibration mode of β-carotene was indeed observed by means of 2D spectroscopy.[250] The phonon sideband would appear as off-diagonal elongation of the origin peak. At 77 K the PSB and ZPL are not resolved and low-frequency vibrations manifest as pronounced beating of the antidiagonal absorptive peak width.[251]

5. EXAMPLES OF APPLICATIONS OF NPHB, FLNS, SPCS, AND 2D ES TO PHOTOSYNTHESIS

5.1. Light-Harvesting and EET in Antenna Complexes

5.1.1. Peripheral Antenna Systems of Photosystem II (LHCI, LHCII, CP29) . The antenna system of PSII from green algae and higher plants consists of a core antenna of two Chl *a*/carotenoid binding proteins, CP47 and CP43 (see section 5.1.2), located close to the RC complex, and a number of peripherally situated light-harvesting complexes that bind Chl *a*, Chl *b*, and various xanthophylls.[252−255] The latter antenna complexes encoded by a multigene family are referred to as Lhcb1−6 (for a recent review see, for example, van Amerongen and Croce[256]). Here, Lhcb1−3 are constituents of the major light-harvesting complex LHCII, which binds approximately 65% of the chlorophyll associated with PSII. Lhcb4−6 (or CP29, CP26, and CP24, respectively) are referred to as minor Chl *a*/*b* binding pigment protein complexes. These complexes contain approximately 15% of the Chl molecules of PSII.[252] On the basis of their high sequence homology to Lhcb1−3, they were predicted to form similar secondary structure elements as those of the major LHCII. In contrast to the LHCII trimer, however, they occur in monomeric form. Although the transmembrane folding pattern of the polypeptides Lhcb1−6 is similar, their pigment compositions and stoichiometries differ significantly.[252−254,257,258]

Of the peripheral antenna systems, a high-resolution X-ray structure is so far available only for the trimeric major light-harvesting complex LHCII, while structural models for CP29 are based on the sequence homology to LHCII (see below). The structure of LHCII was first analyzed by electron crystallography with a resolution of 3.4 Å,[259] which did not permit an unambiguous identification of Chl *a* and Chl *b* molecules. A tentative assignment identified seven Chl molecules in close contact with carotenoids as Chl *a* based on the criterion of efficient triplet quenching. The remaining five Chl molecules were assumed to be Chl *b*. This assignment led to closest center to center distances of ∼9−14 Å for Chl *a*−Chl *b* heterodimers, suggesting relatively weak excitonic interactions and concomitantly weak delocalization of excitonic states of LHCII.[260] The identities of several Chl molecules (Chls a1, a2, a4, a5, b5, and b6 according to the nomenclature of ref 259) were later confirmed by spectroscopic studies of LHCII mutants lacking single pigments,[261−263] while different identities were observed in the case of Chl b3[262] as well as Chls a7, b1, and b3.[261] Also mixed occupancies were reported for several binding sites by Remelli et al.[261] It has to be kept in mind that several SHB studies discussed below (e.g. refs 213, 214, 217, 219) were originally interpreted in terms of the structural assignments of ref 259.

More recently, X-ray diffraction studies revealed the structures of trimeric LHCII from spinach[90] and pea[264] at nearly atomic

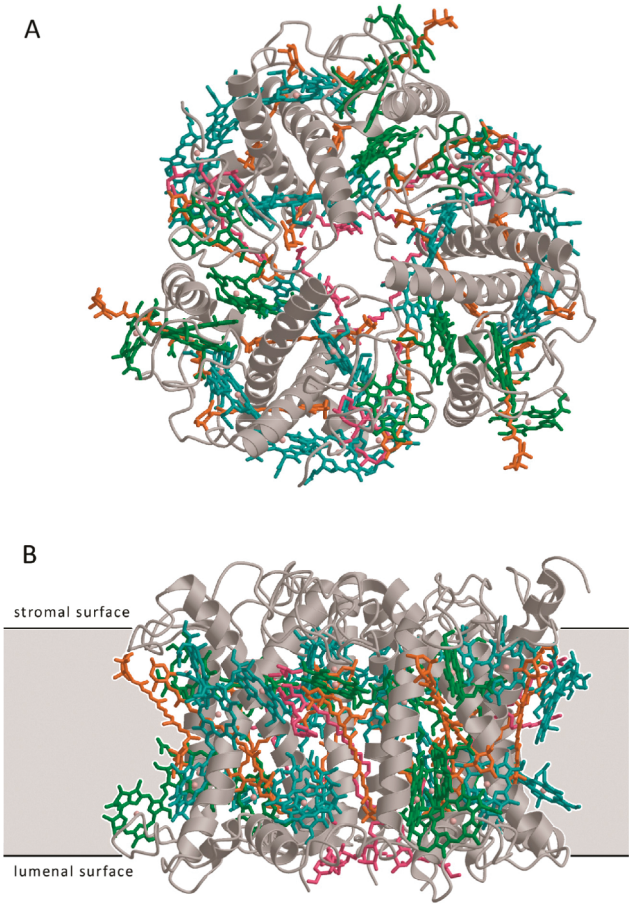

Figure 20. The X-ray structure of the LHCII trimer according to Standfuss et al.:[264] (A) top view from the stromal side and (B) side view. LHCII protrudes from a 35 Å lipid bilayer (black lines) by 13 Å on the stromal side and by 8 Å on the lumenal side. Gray, polypeptide; cyan, Chl *a*; green, Chl *b*; orange, carotenoids; pink, lipids. Figure reprinted with permission from ref 264. Copyright 2005 Nature Publishing Group.

Table 5. Nomenclature of Chl Molecules in LHCII According to Refs 90, 259, and 264

Chl type	Kühlbrandt et al.[259]	Liu et al.[90]	Standfuss et al.[264]
A	a1	610	Chl 1
A	a2	612	Chl 2
A	a3	613	Chl 3
A	a4	602	Chl 4
A	a5	603	Chl 5
A	a6	604	Chl 6
A	b2	611	Chl 7
A	b3	614	Chl 8
B	–	601	Chl 9
B	a7	607	Chl 10
B	b1	608	Chl 11
B	b5	609	Chl 12
B	b6	606	Chl 13
B	–	605	Chl 14

resolution. According to these studies, each monomeric subunit binds 14 Chl molecules arranged in two layers close to the stromal and lumenal surfaces of the thylakoid membrane, respectively, and four carotenoid molecules. The structure of an LHCII trimer from pea is shown in Figure 20.[264] The identities of eight Chl *a* and six Chl *b* molecules as well as the orientation of their transition dipole moments can now be unambiguously assigned, while mixed occupancy was excluded. New nomenclatures for the Chl molecules were introduced in refs 90 and 264 (see Table 5 for a comparison) to account for new assignments of Chl identities and so far unresolved pigments. In what follows, we will generally apply the nomenclature of Liu et al.[90] Short center-to-center distances on the order of ~8−10 Å are now reported for Chl *a*−Chl *a* and Chl *b*−Chl *b* homodimers as well as for Chl *a*−Chl *b* heterodimers. In addition, close center-to-center distances of up to ~12 Å are also observed between Chl *b* molecules of adjacent monomeric subunits. The Chls are preferentially bound via ligation and hydrogen bonding to the protein backbone formed by three membrane-spanning and two amphipathic α-helices. However, there is also coordination of Chls via water molecules and in one exceptional case to the lipid phosphatidyl glycerol (PG) located in the core of the LHCII trimer. It adds to the complexity that the LHCII trimer may contain three different Lhcb1−3 proteins (see above) in different combinations, which exhibit slightly different spectroscopic properties.[265] The functional role of the different Lhcb1−3 proteins is so far unknown, although the extent of their expression appears to depend on illumination conditions.[266] The largest of the minor Chl *a*/*b* binding pigment protein complexes, CP29, has been shown to bind six Chl *a*, two Chl *b*, and two to three carotenoid molecules.[267−269] As mentioned above, the transmembrane folding pattern of CP29 is expected to be similar to that of LHCII, with three membrane-spanning α-helices and a fourth amphipathic helix. Despite the lack of direct information, a structural model for CP29 has been proposed on the basis of the high sequence homology among the LHCII proteins and the finding that most of the Chls present in CP29 adopt binding sites similar to those in LHCII.[257]

The major light-harvesting complex LHCII has been intensively studied using HB,[213,222,228] SPCS,[153] and complementary site selective methods like FLN[217,219] and fluorescence hole-burning.[270] Similar information is available for CP29.[60,214] As

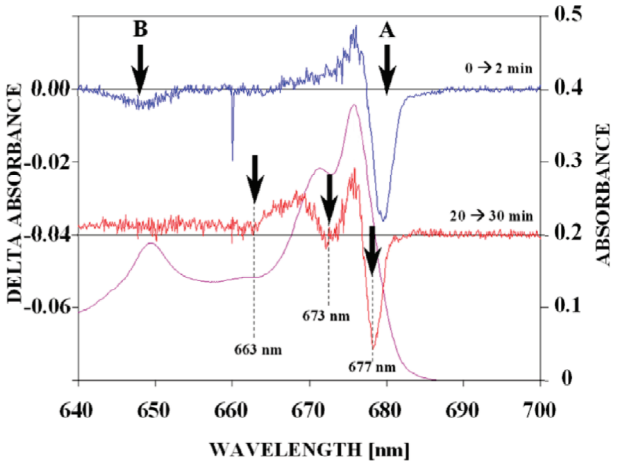

Figure 21. The 4.2 K absorption spectrum (black curve) and SHB spectra of trimeric LHCII obtained with a burn wavelength of 660 nm. The burn intensity was 130 mW/cm^2; the blue curve is the hole spectrum after the first 2 min of illumination; the red curve is the difference between the postburn spectra obtained with 30 and 20 min of illumination. Satellite holes are labeled by arrows. A 4.2 K Q_y-absorption spectrum of trimeric LHCII is shown as a black line for comparison. Reprinted with permission from ref 274. Copyright 2005 American Chemical Society.

discussed below, these studies contributed valuable information on the excited state positions and homogeneous and inhomogeneous broadening, as well as el−ph coupling, to the overall understanding of EET in this antenna complex. The 4.2 K Q_y-absorption spectrum of trimeric LHCII is shown as a black line in Figure 21 (taken from ref 274) and exhibits only three prominent bands located at ~649.5, 671.0, and 676.0 nm (see, for example, ref 213). This spectrum is similar to those reported in refs 213, 217, 219, 222, and 270 for nonaggregated trimeric LHCII. The main effect of monomerization appears to be a broadening of the Q_y-absorption bands along with a slight red-shift of the lowest energy Q_y-state,[222] while aggregation leads to the appearance of red-shifted long-wavelength states hardly visible in absorption but producing intense red-shifted peaks or shoulders in fluorescence, depending on preparation protocol.[271,272] In contrast to the relatively structureless Q_y-absorption spectrum, the persistent NPHB spectrum shown in Figure 21 for trimeric LHCII (see blue line) reveals remarkable substructures and is composed of three main features: (i) a narrow zero-phonon hole coincident with the burn wavelength, (ii) an intense hole in the vicinity of 680 nm, which appears as a result of efficient EET to low-energy trap state(s) (see below), and (iii) a weak satellite hole at about 649 nm which builds on the low-energy 680 nm-hole.[213]

Detailed HB studies of trimeric LHCII[213,228] have established on the basis of the broad low-energy hole that the lowest excitonic energy level lies at ~680 nm at 4.2 K. Thus, the lowest energy state of trimeric LHCII is located about 4 nm to the red of the main absorption band at ~676 nm. This was first reported by Reddy et al.[228] using partly aggregated samples and was later confirmed by Pieper et al.[213] for nonaggregated LHCII. Very recently, fluorescence hole-burning studies were used to verify the assignment of the lowest Q_y-state.[270] Employing a combination of SHB[213] and FLN[219] (see Figure 22 for a compilation of these data) it was shown that the 680 nm state is characterized by moderate el−ph coupling with a Huang−Rhys factor $S \sim 0.9$ as well as by a strongly asymmetric one-phonon profile with a mean

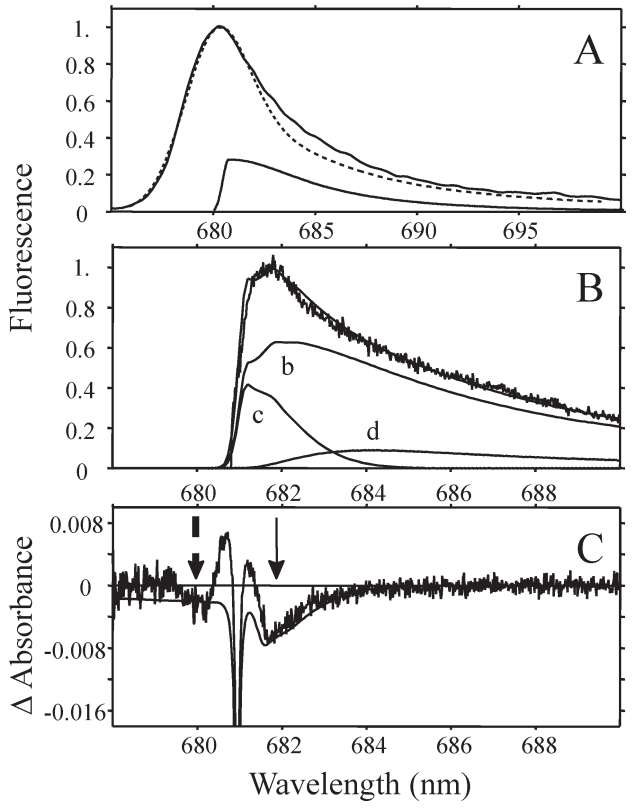

Figure 22. Analysis of phonon structure in HB, FLN, and NLN fluorescence spectra of trimeric LHCII at 4.2 K. (A) Experimental (full line) and calculated (dashed line) nonline-narrowed fluorescence spectra, respectively. The one-phonon profile is shown as a full line on the bottom. (B) Experimental FLN spectrum (noisy line) obtained with λ_E = 680.5 nm. The scattered laser light has been subtracted. The fit was calculated according to eq 29 (smooth line). As in Figures 17 and 18, contributions (b, c, and d) label real-, pseudo-, and multi-PSB, respectively. (C) Experimental HB spectrum (noisy line) obtained with λ_B = 681.0 nm and a burn fluence of 15 J/cm.[2] The real- and pseudo-PSBH are indicated by full and broken arrows, respectively. The fit was calculated according to eq 27 with γ = 0.2 cm^{-1} and $\sigma I\Phi\tau$ = 0.003 (smooth line). Reprinted with permission from ref 227. Copyright 1999 Elsevier B.V.

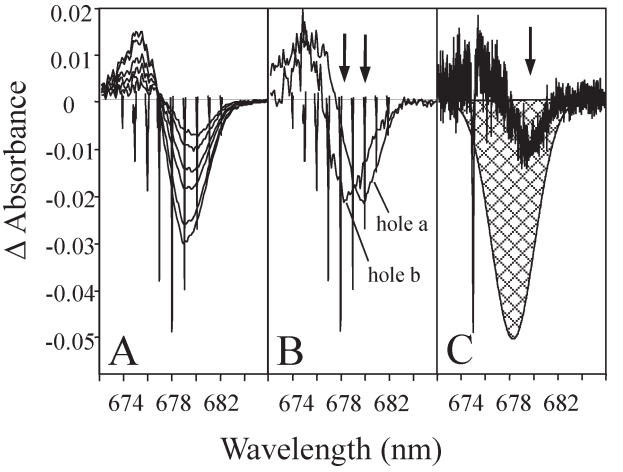

Figure 23. (A) Burn fluence dependence of the 680 nm hole (cf. Figure 21) obtained for λ_B = 660 nm, a burn intensity of 130 mW/cm^2, and burn times (top to bottom) of 1, 2, 5, 10, 20, and 30 min. Read resolution = 4.0 cm^{-1}. The ZPH action spectrum is shown for comparison. (B) Further illustration of blue-shift of the 680 nm hole. Hole a was obtained for the shortest burn time of 30 s, while hole b is the difference between the low two hole spectra of frame A. Holes a and b peak at 679.6 ± 0.2 and 678.4 ± 0.2 nm (see arrows). (C) HB spectrum obtained with λ_B = 675.0 nm (coincident with the sharp ZPH), burn intensity = 100 mW/cm^2, and burn time = 60 s. The broad hole indicated by the arrow at 679.6 nm carries a width of 70 cm^{-1}; see the text. The ZPA spectrum is shown for easy comparison. Reprinted with permission from ref 213. Copyright 1999 Americian Chemical Society.

phonon frequency ω_m of ~18 cm^{-1} and a width of ~105 cm^{-1}.[219,227] The spectral position of the 680 nm state and the latter parameters of el−ph coupling have been shown to perfectly account for the position and line shape of the NLN fluorescence spectrum of LHCII (see frame A of Figure 22).[219,227]

Fluence-dependent HB experiments on nonaggregated trimeric LHCII[213] revealed a remarkable blue-shift of the low-energy hole at ~680 nm with increasing fluence (see Figure 23). The fluence-dependence of the low-energy 680 nm hole was significantly smaller in monomeric LHCII.[222] This has been interpreted in terms of the presence of three energetically inequivalent low-energy states in trimeric LHCII located at 677.1 ± 0.2, 678.4 ± 0.2, and 679.8 ± 0.2 nm each possessing an inhomogeneous width of 80 ± 10 cm^{-1}. The absorption intensity of each of these low-energy states was estimated to be equivalent to that of about one Chl *a* molecule per LHCII trimer.[213] Indeed, it was shown later that the spectral position of the lowest energy states of the individual Lhcb1−3 proteins varies on the same order of magnitude.[265] Thus, the three closely spaced low-energy states may probably be identified with the lowest states of the Lhcb1−3 proteins constituting the LHCII trimer.[265] In addition, SPCS experiments on LHCII frequently showed three fluorescence lines for trimeric LHCII, confirming the existence of—on average—three emitting Q_y-states, while mostly one fluorescence line was observed for monomeric LHCII.[153] More recently, there is emerging evidence from hole-growth kinetics experiments[273] and from reconsideration of satellite hole structure[274] that second- and third-lowest excitonic states (of the monomeric subunit) may also contribute to the action spectrum and, thus, to the fluence-dependence of the nonresonantly burned low-energy 680 nm hole of LHCII trimers (see below). These findings indicate that the composition of the low-energy level structure of LHCII is highly complex.

In addition to assignment of spectral positions, SHB can also contribute valuable information on the nature of the low-energy states of LHCII. A high degree of localization and concomitant weak coupling of the 680 nm state to other Chls has been concluded on the basis of the following arguments:[213] (i) its oscillator strength of roughly one Chl *a* per monomeric subunit, (ii) the weak satellite hole structure produced by both resonant and nonresonant hole-burning within the ~680 nm state, and (iii) the small pressure shift rates observed for resonantly burned holes in this spectral region. When ref 213 was published, the observation of a highly localized low-energy state at ~680 nm appeared to be consistent, because the above results were still interpreted in terms of the 3.4 Å structure of LHCII,[259] suggesting closest center-to-center distances and concomitantly strongest excitonic couplings for Chl *a*/*b* heterodimers (see above). As discussed already in ref 222, however, the nature of the 680 nm state as being highly localized appears quite unusual in the light of

the more recent high-resolution structures,[90,264] which predict more significant excitonic interactions for most Chl *a* molecules of LHCII. Therefore, it is instructive to compare the characteristics of the 680 nm state established by SHB to the results of recent excitonic calculations for LHCII based on the high-resolution crystal structures.

The availability of high-resolution structural models with an unambiguous assignment of pigment identities has been followed by a number of theoretical simulations.[275−277] Low-temperature (77 K) time-resolved and frequency domain spectroscopic data were simulated using a modified Redfield approach, which accounted reasonably well for many features of 77 K time-domain, CD, absorption, and fluorescence data.[276] In this study, the femtosecond kinetics is attributed to fast EET within excitonically coupled clusters of Chl *b* and Chl *a* molecules, respectively, while the slower picosecond components are ascribed to relatively long-lived monomeric electronic states that are mainly found in the intermediate wavelength region of 660−670 nm. A bottleneck state characterized by relatively slow downward EET observed in the latter spectral region has been attributed to Chl *a*604, because it is weakly coupled to other Chl molecules. The terminal (fluorescent) excitonic state was found on a cluster of strongly coupled Chl *a* molecules *a*610−*a*611−*a*612 in this model. At first glance, this appears to be in line with a site-directed mutagenesis study, which found the lowest excitonic state of LHCII to be located on Chl *a*612 at room temperature.[263]

More recently, 2D ES has evolved as a powerful and versatile tool to study excitonic interactions and EET in photosynthetic pigment−protein complexes (see section 4.10 for an introduction). This approach has established that quantum coherence plays an important role in EET in several photosynthetic antenna complexes, but also specifically in LHCII (for a review see ref 278). The 2D ES spectra of LHCII were described by a theoretical model based on exciton energies determined from the coherent beating signal in ref 279, while the EET dynamics and participation of pigments in energy flow were monitored via 2D relaxation and nonrephasing spectra in ref 280. More recently, polarized 2D ES has been used to elucidate uncoupled transitions mainly in the Chl *b* region of LHCII.[281] The 2D ES data of ref 280 reveal sub-100 fs excitonic relaxation within clusters of strongly coupled Chl molecules, EET with several 100 fs between neighboring Chls, and picosecond EET between different pigment layers. The results of refs 279 and 280 have confirmed the basic features of the spectral assignments of site energies of ref 276 but especially the location of the lowest energy state at the strongly coupled trimer of Chl *a* molecules *a*610−*a*611−*a*612.

However, comparison with the SHB results discussed above reveals that the assignment of the lowest energy state of LHCII to the Chl *a* heterotrimer *a*610−*a*611−*a*612 is in contradiction to the characteristics of the 680 nm state that was found to be widely localized on one Chl molecule and weakly coupled to other Chl molecules. As discussed in ref 222, a delocalized lowest energy state should result in the observation of a corresponding satellite hole structure upon burning within the lowest energy level (see also section 4.8). Instead, the satellite hole structure produced by both resonant and nonresonant hole-burning at low fluence within the ~680 nm state is weak with only one satellite hole located at ~649 nm (see the blue line in Figure 21), which is almost coincident with the major Chl *b* absorption band of trimeric LHCII. Consequently, it appears that the lowest energy state should be weakly coupled to others. On the basis of these

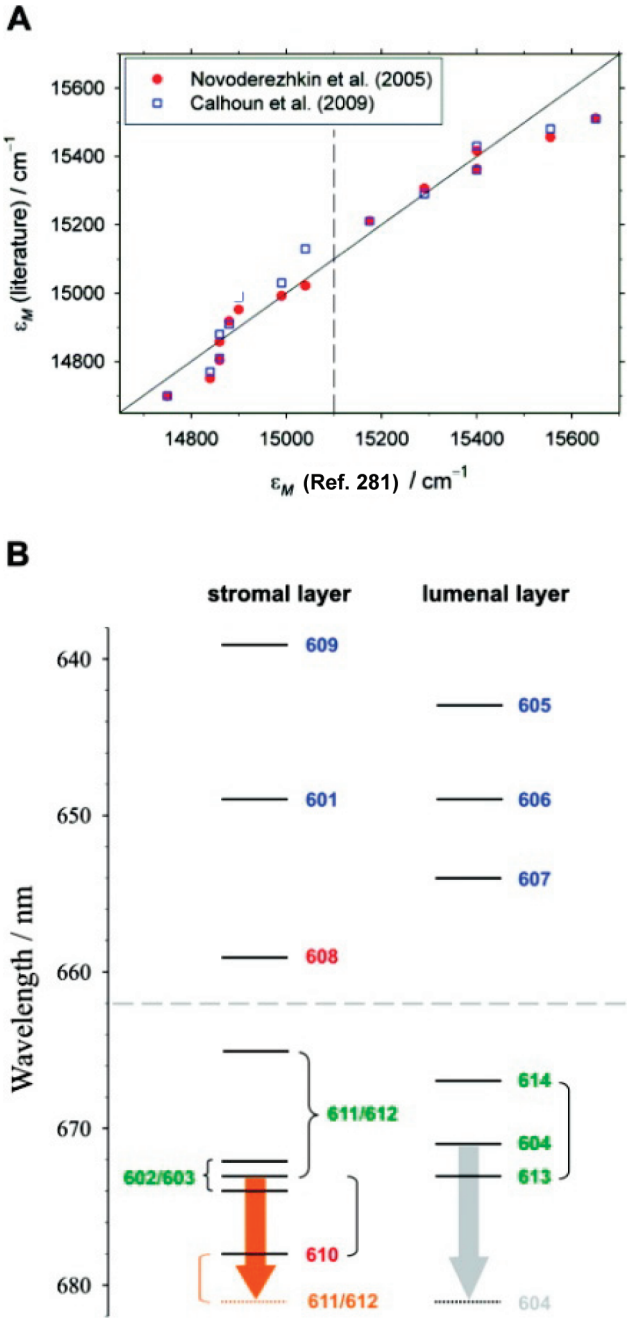

Figure 24. (A) Correlation of exciton state energies ε_M of trimeric LHCII calculated by Müh et al.[282] with exciton state energies reported by Novoderezhkin et al.[276] and Calhoun et al.[279] (B) Exciton energy level scheme for the stromal and lumenal layer of pigments in trimeric LHCII based on the values of ε_M from this work. Dominant pigment contributions are indicated by numbers following the numbering scheme of Liu et al.[90] Curly brackets connect exciton states that are significantly delocalized between two pigments, whereas round brackets connect exciton states that are delocalized but still dominated by the indicated pigments. The orange arrow represents a possible temperature-dependent shift of an exciton state with a large contribution from Chl *a*612, as suggested by the data of Rogl et al.[263] The gray arrow represents the hypothetical red-shift of the site energy of Chl *a*604 due to a conformational change of neighboring hydroxyl groups (cf. Figure 25). The dashed lines in frames A and B indicate the borderline between the Chl *a* and Chl *b* regions. Reprinted with permission from ref 282. Copyright 2010 Americian Chemical Society.

dx.doi.org/10.1021/cr100234j |*Chem. Rev.* 2011, 111, 4546–4598

arguments, Chl *a*604 has been proposed to carry the lowest energy state of LHCII as an alternative possibility in ref 222.

A solution of this apparent contradiction was recently proposed by Müh et al.[282] using a combined quantum chemical/electrostatic approach to calculate site energies directly on the basis of the high-resolution crystal structures of LHCII.[90,264] The excitonic energy level scheme emerging from these calculations is shown in Figure 24 (taken from ref 282). A comparison of the latter site energies with those of Novoderezhkin et al.[276] and Calhoun et al.[279] is shown in Frame A of Figure 24. While the individual site energies differ, the different energy level structures agree in finding the lowest energy state of LHCII on the strongly coupled trimer of Chl *a* molecules *a*610−*a*611−*a*612. In addition, however, Müh et al.[282] discussed the possibility that the site energy of Chl *a*604 can be affected by a conformational change in its vicinity involving hydroxyl groups of tyrosine 112 and neoxanthin. This would result in a red-shift of the site energy of Chl *a*604 by 212 cm^{-1}. The two different conformations are shown in Figure 25 (taken from ref 282). As a consequence, the energy sink of LHCII would be located on Chl *a*604, which is indicated by a dotted line in Figure 24.

As discussed in ref 274, the latter assignment appears to be in better agreement with the fluence dependence of SHB. At low fluence, the satellite hole structure produced by both resonant and nonresonant hole-burning within the ∼680 nm state is weak (see the blue line in Figure 21) as already reported in ref 213. At higher fluence, however, the low-energy 680 nm hole shifts blue to ∼677 nm and is accompanied by two more satellite holes at ∼673 and 663 nm, respectively (see the red line in Figure 21 that represents the difference between the postburn spectra resulting from 30 and 20 min of illumination). The latter satellite hole structure is in agreement with a Chl *a* homotrimer, so that the second-lowest state of LHCII may be located on the *a*610−*a*611−*a*612 cluster at 4.2 K. In short, further work is required to identify a set of site energies that can account for hole-burning,[213] time-resolved,[276] and 2D[279,280] spectroscopic data in a unified assignment.

A number of time-resolved spectroscopic studies revealed that Chl *b*→Chl *a* EET in trimeric LHCII is ultrafast with kinetic components of ∼150 fs, 600 fs, and 10 ps at room temperature[283−288] and exhibits only a weak dependence on temperature.[287−289] More recently, 2D ES revealed previously unresolved sub-100 fs relaxation components.[280] The kinetics of Chl *b*→Chl *a* EET are phenomenologically quite similar in trimeric and monomeric LHCII, suggesting that the determining EET steps occur within the monomeric subunit of LHCII.[286] The spectral characteristics of EET were shown to be slightly different for the Lhcb1−3 proteins.[288] As discussed in refs 213, 222, and 228, short excited state lifetimes due to efficient downward EET are qualitatively consistent with the low burn efficiency at wavelengths shorter than 676 nm. Excited state lifetimes of higher-energy Q_y-states can be gathered directly from shallow ZPH coincident with the burn wavelengths (see Figure 21). The lifetimes T_1 obtained at λ_B = 649, 660, and 670 nm are 1.1 ± 1.0, 2.8 ± 1.0, and 3.5 ± 1.0 ps, respectively, which are in reasonable agreement with the slower EET components observed in time-resolved experiments (see above). Especially, assuming a weak temperature dependence, the 1.1 ps lifetime determined at 649 nm may be similar to the intermediate 600 fs component reported for Chl *b*→Chl *a* EET in LHCII at room temperature (see, for example, ref 289). The equivalent of the faster ∼150 fs EET component—which slows down to ∼310 fs at 12 K[287]—is not directly observed by SHB, because it is most probably hidden by the broad hole B.

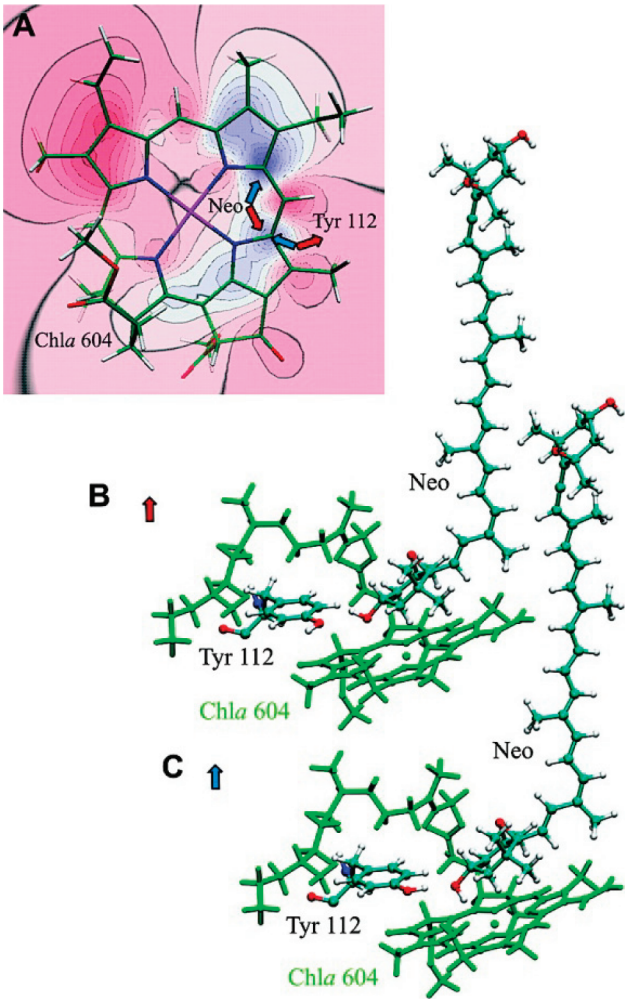

Figure 25. (A) Location of the hydroxyl dipoles of Tyr112 and Neo in the $\Delta\varphi(r)$ potential (in the plane of the tetrapyrrole macrocycle) of Chl *a*604 corresponding to the two conformations shown in frames B and C. (B) "Red" conformation, in which the 3′-hydroxyl group of Neo points away from the macrocycle and donates a hydrogen bond to Tyr112. (C) "Blue" conformation, in which the 3′-hydroxyl group of Neo points toward the macrocycle and accepts a hydrogen bond from Tyr112. The hydroxyl group of Tyr112 is oriented parallel to the π-plane of Chl *a*604 in both conformations. Reprinted with permission from ref 282. Copyright 2010 Americian Chemical Society.

In summary, SHB and other site-selective methods contribute invaluable information on excited state positions and their Γ_{hom} and Γ_{inh}, as well as electron−phonon coupling of LHCII, which is complementary to results from SPCS and time domain experiments. These results can serve as important benchmarks to verify the validity of excitonic simulations for photosynthetic pigment−protein complexes.

5.1.2. Core Antenna Complexes. *5.1.2.1. CP43 Antenna Complex.* It is well-known that the CP43 complex of PSII (with 13 Chl *a* molecules) possesses two quasidegenerate lowest-energy states (A and B in the notation of ref 207), one of which, namely state B, is characterized by an unusually narrow inhomogeneous bandwidth.[10,207,290] Early Gaussian fitting of the absorption spectra indicated that the red absorption region can be fitted only using one narrow and one broad band,[290] thus suggesting the presence of two different sets of red absorbing

dx.doi.org/10.1021/cr100234j |*Chem. Rev.* 2011, 111, 4546–4598

pigments. This two-state model is consistent with FLN experiments, which showed[290] (upon excitation below 680 nm) emission from two different pools of Chls. The presence of two different pools of Chl was later confirmed by HB experiments.[12,15,291] We have recently demonstrated that the CP43′ complex of PSI isolated from cyanobacteria grown under iron-stress conditions, which is homologous to the CP43 complex of PSII, also possesses A and B states (see section 5.3.1) and that the results for both CP43 and CP43′ can better be explained if one allows for EET between these two states on a ∼10 ps time scale.[292]

Early excitonic calculations for CP43 complex[15] were performed assuming that transition dipoles of all Chl molecules are oriented in the membrane plane (detailed structural orientations of Chls in the CP43 antenna complex were unknown at that time). In ref 15 it was suggested that broader band A might be due to an ensemble of strongly coupled Chls. In turn, in ref 291 evidence was presented, based on the results of time domain room-temperature experiments, that the chlorophyll responsible for the B band is weakly coupled to the rest of the pigments in the CP43, i.e., the pigment contributing to the B band is monomeric. On the other hand, the CD spectra[12] indicated that narrow band B has significant rotational strength, which appears to be inconsistent with the assignment of the B state to a monomeric Chl *a*. Hughes et al[12] suggested that band B is the lowest excitonic state of a relatively strongly coupled chlorophyll ensemble, with two other states of the same ensemble peaking at ∼680 and 676.5 nm. Their conclusion was based on the analysis of the changes in the CD spectra upon nonresonant higher-energy illumination at 4 K (i.e., nonresonant HB detected via CD spectra). They also suggested that band A is due to a state well-localized on a single Chl *a*. However, Hughes et al.[12] in their analysis did not account for NPHB photoproduct contributions in the ΔCD spectra; see refs 10 and 85 for discussion. We hasten to add that several candidates for Chls contributing to the lowest-energy states of CP43 have been considered so far. For example, Chls 34, 37, 41, 47, and 49 were mentioned by Di Donato et al.[291] in the analysis of femtosecond visible/visible and visible/mid-infrared pump/probe spectroscopic data, although no specific assignments were proposed. (Throughout this section, the numbering of Loll et al.[4] is used; for comparison with that of Vasil'ev et al., see Table 6). Chl 41 was also suggested to contribute to the low-energy state(s) by Hughes et al,[12] Vasil'ev et al.,[293] and Saito et al.,[294] where it was proposed that Chl 41 plays the most important role in transferring energy to the RC of PSII. This assignment, however, as briefly discussed below, seems to be inconsistent with the simultaneous fitting of various optical spectra obtained in our laboratories.[85]

Recently, the excitonic structure of CP43 complex was probed by Monte Carlo simulations using fitting algorithms.[85,112] An example of experimental and calculated CP43 absorption and HB spectra from our laboratories[10,85] is shown in Figure 26. The calculated spectra were obtained for an optimized set of parameters based on fits to absorption, emission, and nonresonant transient and persistent HB spectra using a fitting algorithm; see ref 85 for details. Frame A of Figure 26 shows the experimental CP43 absorption spectrum (smooth, solid curve) and transient hole spectrum (noisy, gray curve) along with the calculated absorption (long-dashed curve) and triplet bottleneck holes (black solid and dotted hole spectra). The dotted black curve in frame A corresponds to the calculated triplet bottleneck hole under the assumption that Chl 44 contributes to the transient hole with twice the efficiency of other pigments; this assumption increases the depth of the satellite transient bleach near 671 nm, highlighting the fact that this high energy bleach is due to the strong excitonic interactions of Chl 44 with other pigments in the stromal domain. Frame B of Figure 26 shows the experimental (solid curve) and calculated (dashed curve) low-fluence persistent HB spectra. Notice the "anti-hole" feature near 671 nm (comparable to the transient bleach in this region in the triplet bottleneck hole). Just as for the triplet bottleneck holes in frame A, detailed analysis reveals that the strong excitonic interactions of Chl 44 with other stromal layer pigments are critical in forming this high-energy feature. It is significant to note that of the many likely A/B candidate pairs tested only the A44/B37 combination was capable of simultaneously fitting the transient and persistent HB spectra, absorption spectrum, as well as the emission spectrum; in particular, no combinations that did not involve Chl 44 were capable of fitting either the triplet bottleneck or persistent HB data.[85] Thus, in refs 10 and 85 it was concluded that the best Chl candidates to contribute to the low-energy A and B states are most likely Chl 44 and Chl 37, respectively. (Recall that Chl 44 and Chl 37 in the Loll et al.[4] notation correspond to Chl 481 and Chl 477 using the nomenclature of Guskov et al.[7]). It should be emphasized that the site energies provided in ref 85 should be interpreted as a first approximation only; while the HB simulations of that work are quite sensitive to the site energies of the lowest-energy pigments of the complex, they are much less sensitive to the site energies of the blue-shifted pigments. Together with the need for more advanced theory (including coupling to phonons and vibrational modes and the refined treatment of HB simulations discussed in sections 4.8 and 5.1.2.2), these considerations imply that more advanced calculations are needed to refine the site energies and parameters presented in ref 85 before final assignments are made. Indeed, a somewhat different assignment has been proposed by Raszewski and Renger[112] (based on fits to absorption, LD, and fluorescence data), where it was argued that the three lowest site

Table 6. Numbering of Pigments in CP43, CP47, and RC of PSII in the Nomenclature of Loll et al.[4] (Protein Data Bank ID 2AXT) and Guskov et al.[7] (ID 3BZ1)

CP47		CP43		RC		
Loll et al.[4]	Guskov et al.[7]	Loll et al.[4]	Guskov et al.[7]	Loll et al.[4]	Guskov et al.[7]	pigment name
11	511	33	474	1	362	$P680_1$
12	512	34	475	2	354	$P680_2$
13	513	35	476	3	363	Chl_{Acc1}
14	514	37	477	4	364	Chl_{Acc2}
15	515	41	478	5	365	$Pheo_{D1}$
16	516	42	479	6	355	$Pheo_{D2}$
17	517	43	480	7	366	Chl_{Z1}
21	518	44	481	8	356	Chl_{Z2}
22	519	45	482			
23	520	46	483			
24	521	47	484			
25	522	48	485			
26	523	49	486			
27	524					
28	525					
29	526					

dx.doi.org/10.1021/cr100234j |*Chem. Rev.* 2011, 111, 4546–4598

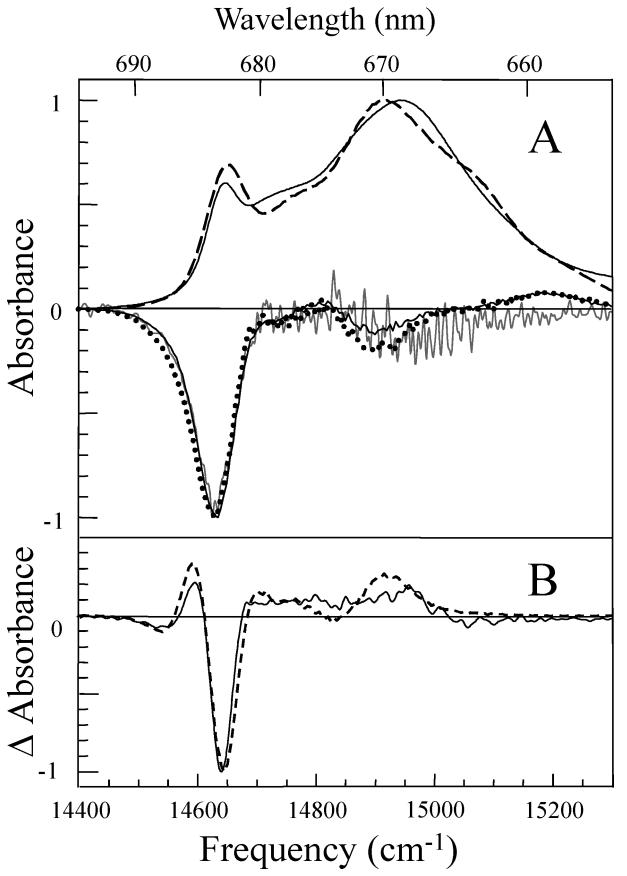

Figure 26. Experimental CP43 spectra and spectra calculated using best-fit parameters for the A44/B37 pair. (A) Experimental (smooth, solid curve) and calculated (long-dashed curve) absorption spectra of CP43 together with experimental (noisy, solid hole) and calculated (solid and dotted holes) triplet bottleneck hole spectra of CP43. The dotted transient hole-burned curve corresponds to the calculated transient hole-burned spectrum. (B) Experimental (solid curve) and calculated (dashed curve) persistent hole-burning spectra of CP43. Reprinted with permission from ref 85. Copyright 2008 American Chemical Society.

energies in CP43 belong to Chls 37, 43, and 45 using notation of ref 4. Only the combination of more advanced theoretical methods (including both time and frequency domain measurements) together with new experimental work (possibly including mutational studies) can provide a final refinement of these various assignments.

Figure 27 (from ref 85) shows the location of these pigments in CP43 (structure of ref 4). Chls on the stromal side (frame A) of the membrane are colored red, Chl 46 (which lies in the middle of the membrane) is colored pink, and lumenal Chls are colored blue. CP43 Chls separated into stromal and lumenal groups (Chl 46 is shown twice for clarity) are shown in frame B. Chls 44 and 37 are shown in red in frame B. In summary, we proposed in ref 85 that both the transient and persistent HB spectra have significant contribution from an A-state localized primarily on Chl 44. These calculations are in excellent agreement with the model of uncorrelated EET between quasidegenerated state A and B, as presented in ref 207, where it was argued that Chls in lumenal and stromal layers might be connected by efficient (~10 ps) EET.

Finally, regarding the nature (and shape) of nonresonant HB spectra in CP43, it was suggested recently[12,191] that a novel "photoconversion" process (aside from the traditional NPHB mechanism) involving tunneling between alternate configurations of a C═O···H−protein hydrogen bond might be necessary to account for the strongly blue-shifted antihole peak in the NPHB spectrum of CP43. However, the excitonic calculations[85] discussed above demonstrate that this suggestion, while it cannot be definitively excluded, is not required to account for the strong positive absorption increase in the saturated HB spectra. Instead we suggested that persistent holes originate from the regular NPHB process accompanied by the statistical reshuffling of site energies contributing to the lowest-energy trap state and by altered excitonic transition energies of various excitonic states (see section 4.8 and refs 39 and 40 for a discussion of the origin of nonresonant NPHB spectral shapes in various model systems). As discussed in the next section, similar results have been obtained from excitonic fitting of the NPHB spectra of the CP47 complex.[9,86]

5.1.2.2. CP47 Antenna Complex. The CP47 complex is the second (besides CP43) antenna complex of the oxygen-evolving PSII core (see also section 5.3.2). CP47 contains 16 Chl *a* molecules divided largely between two pools located on opposite sides of the thylakoid membrane in an arrangement quite similar to that of CP43.[7] There have been many attempts in recent years to unravel the electronic structure and EET dynamics of this antenna protein via both time[15,295−298] and frequency domain studies,[299,300] including SHB.[9,212,301−303] Data obtained at low temperatures showed significant differences between optical spectra of the same type for different sample preparations.[15,212,302,304] For example, low temperature (4.2 K) fluorescence spectra of the isolated CP47 complex obtained by various groups appeared to be contributed to by at least three different emission bands, resulting in fluorescence maxima in the range of 690−693 nm.[212,295,298,299,302,304] Huyer et al.[298] suggested that the isolated CP47 complex contains two subpopulations having lowest energy states with distinctly different lifetimes (~1.6 ns and ~6.2 ns for "fast"- and "slow"-state subpopulations, respectively). den Hartog et al.[212] determined via HB spectroscopy that the CP47 trap lies near 690 nm and found an *S* value of ~0.7, in agreement with the observed 690−691 nm fluorescence origin band.[212,295] Polivka et al.[302] suggested that fluorescence of the wild type CP47−D_1D_2−Cyt_{b559} complex could be ascribed to fluorescence of two Chl *a* clusters of CP47 with fluorescence maxima at ~688 and ~695 nm. In addition, CP47 studies by de Weerd et al.[15] including pump−probe (magic-angle) data (T = 77 K) and global analysis fit for CP47 after 670.0 nm excitation showed that one of the species-associated difference spectra (SADS) was linked with only a partial relaxation from the Chls that were bleached at 677 and 683/684 nm to a Chl absorbing at even lower energy. Though not commented on by the authors, this could mean that in this particular CP47 sample the EET was not very efficient from the 683/684 nm state. The SADS spectra obtained at 17 ps and a few nanoseconds showed the bleach with a peak near 684−685 nm, respectively. It appears that the 685 nm peak (asymmetric and very broad, with full width at half-maximum (fwhm) of ~11 nm) contained a contribution from the 684 nm pigments along with bleaches from 690/695 nm bands. A significant contribution to the above-discussed SADS spectra from the 684 nm state is consistent with ref 301, where it was observed that the extent of the triplet-bottleneck hole near 684 nm varied from preparation to preparation and as a result might be contributed to by destabilized complexes; for more detailed discussion of intact and destabilized CP47 complexes, see refs 9 and 86.

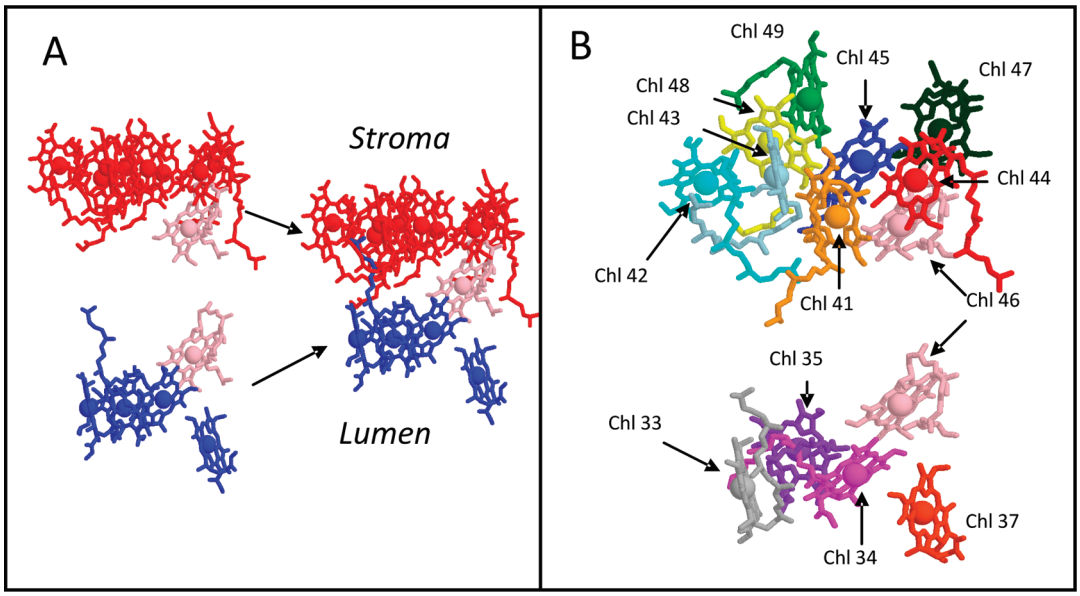

Figure 27. The Chls of the CP43 antenna protein according to the structure of Loll et al.[4] (A) Chls on the stromal side of the membrane are colored red, Chl 46 (which lies in the middle of the membrane) is colored pink, and lumenal Chls are colored blue. (B) CP43 chlorophylls separated into stromal and lumenal groupings (Chl 46 is shown twice for clarity). Reprinted with permission from ref 85. Copyright 2008 American Chemical Society.

Very recently, to provide more insight into the electronic structure and the extent to which the Q_y-states are excitonically correlated in CP47, various optical spectra, including the HB spectra, were obtained for intact and partly destabilized CP47 complexes.[9] Calculated optical spectra (including absorption, emission, and persistent HB spectra) were compared with the experimental results obtained for the native CP47.[86] It was shown that the isolated (*intact*) CP47 antenna from PSII has a low-*T* fluorescence emission maximum near 695 nm (F1) and not, as previously reported,[212,295,299,301,303] at 690−693 nm. The observation of the 695 nm emission is in excellent agreement with the 695 nm emission observed at 77 K in intact PSII cores and thylakoid membranes.[300,305−307] It was also demonstrated that varying contributions from the intact and partly destabilized complexes could explain different maxima of fluorescence spectra reported in the literature. The emission spectra were consistent with the ZPH action spectra obtained in absorption mode, the profiles of the nonresonantly burned holes as a function of fluence, as well as the FLN spectra obtained for the Q_y-band. In addition, in contrast to previous observations,[301] it was observed that intact isolated CP47 has negligible contribution from the triplet-bottleneck hole at ~684 nm, suggesting that respective Chls in intact CP47 are likely connected via efficient EET to the lowest-energy trap near 693 nm (A1). It was also shown that the position of the fluorescence maximum depends on the irradiation dose;[138] that is, the 695 nm fluorescence maximum shifts blue with increasing dose (i.e., when HB takes place), in agreement with nonresonant HB spectra. If permanent damage does not occur, the shift is reversible by cycling the temperature. In contrast, the emission peaks previously observed near 685 nm and ~691 nm could not be eliminated by temperature cycling and most likely represent emissions from destabilized complexes.[9] (Note that the 685 nm emission band observed in some CP47 complexes is apparently unrelated to the ~685 nm band observed in the PSII core, which most likely originates from CP43 complexes[306,307] (see section 5.3.2 for more details).

To characterize a spectral distribution of the low-energy trap(s) of CP47, a series of FLN experiments (T = 4.5 K) was performed at different λ_{ex}. The results for samples 1A (partly destabilized complexes) and 1B (intact sample) from ref 9 are shown in Figure 28, frames A and B, respectively. Note that λ_{ex} of 680.0 nm also gives a fluorescence maximum near 695 nm (see frame B). However, the same λ_{ex} for sample 1A (frame A) provides a spectrum that is only slightly red-shifted (i.e., 692 nm) with respect to the 691 nm band observed for the 496.5 nm excitation.[9] These data demonstrate that when λ_{ex} reaches the low-energy trap(s), resonant FLN spectra are observed. Although low excitation intensity was used, due to multiple spectra consecutively obtained for the same sample, a small contribution from the $F1_{mod}$ emission (due to partly modified low-energy state via continuous HB process) cannot be excluded (Figure 28B,D).

FLN spectra shown in Figure 28A are in agreement with the data reported previously,[212] but results shown in Figure 28B, as argued in ref 9, correspond to more intact CP47 sample with a majority of complexes exhibiting efficient "downhill" EET from higher lying states to the lowest energy trap (A1) near 693 nm. Frame B clearly shows that the EET in intact CP47 complexes is significantly less disturbed than that observed in frame A for sample 1A. Frames C (sample 1A) and D (sample 1B) show the positions of the maxima λ_{em} of the fluorescence spectra at 4.5 K as function of λ_{ex}. In both frames (C and D) three types of maxima λ_{em} are plotted (see figure caption for details). The intactness of sample 1B is apparent when the data obtained for samples 1A and 1B (see black data points in Figures 28C and 28D) are compared with data obtained for CP47 in ref 212 (gray data points in frame C). In agreement with previous data,[212] the 20 cm^{-1} phonon sideband and a broader weak shoulder near 80 cm^{-1} from the excitation frequency are resolved.

The experimental and simulated steady-state absorption, emission, and nonresonant HB spectra for the CP47 antenna complex of PSII based on fits to the recently refined experimental data are shown in Figure 29.[9,86] Excitonic simulations were based on the 2.9 Å resolution structure of the PSII core from cyanobacteria[7]

dx.doi.org/10.1021/cr100234j |*Chem. Rev.* 2011, 111, 4546–4598

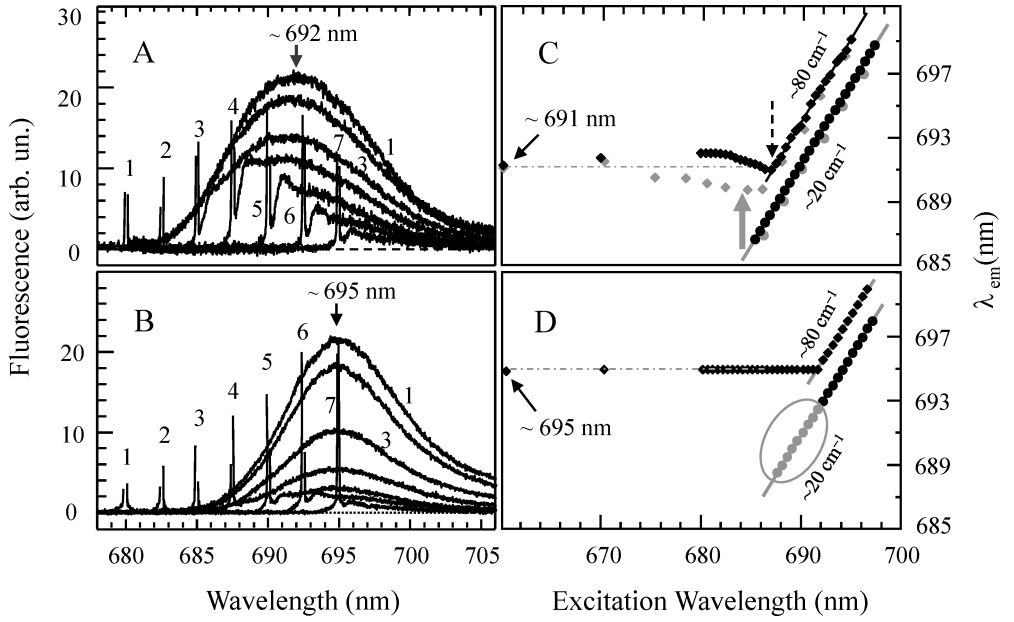

Figure 28. Frames A and B show non-line-narrowed and line-narrowed fluorescence spectra obtained for samples 1A and 1B, respectively. Fluorescence spectra labeled 1−7 were obtained using λ_{ex} of 680.0, 682.5, 685.0, 687.5, 690.0, 692.5, and 695.0 nm, respectively. The sharp lines are in part contaminated by a laser scatter and are arbitrarily cut to reveal the nonresonant fluorescence contributions. ΔFLN spectra, however, had negligible contribution from the laser scatter. Frames C (sample 1A) and D (sample 1B) show the positions of the maxima λ_{em} of the fluorescence spectra at 4.5 K as function of λ_{ex}. In both frames (C and D) three types of maxima λ_{em} are plotted. The solid black circle symbols represent the sharp maxima near the 20 cm^{-1} feature from the laser excitation wavelength; in frames C and D, the 20 cm^{-1} phonon sidebands are observed for λ_{ex} > 685 and 687 nm, respectively. The solid black diamond symbols represent the position of the broad fluorescence maximum (i.e., nonresonant fluorescence). In the spectral region where the 20 cm^{-1} mode is observed in addition to the broad fluorescence band, a weak mode near 80 cm^{-1} is also observed, as indicated by the solid black diamond symbols (extended spectra and hole shape analyses are not shown for brevity). The curves traced through the data are guides for the eye. In frame C, for comparison, the gray diamonds and circles represent similar data from ref 212. Note the different depth and width of the "dip" in frame C (see thick gray and dashed arrows in frame C) and its absence in frame D. Reprinted with permission from ref 9. Copyright 2010 American Chemical Society.

and allowed for preliminary assignment of the Chls contributing to the lowest excitonic states of CP47 complex.[86] The search for realistic site energies of Chls in CP47 was guided by the following experimental constraints: (i) the oscillator strength of the lowest-energy state should be approximately ≤0.5 Chl equivalents (to match the very low experimentally observed oscillator strength of the lowest state), (ii) the excitonic structure must explain the experimentally observed red-shifted (∼695 nm) emission maximum, and (iii) the excitonic interactions of *all states* must properly describe the broad (non-line-narrowed, NLN) HB spectrum (including its *anti*hole) whose shape is extremely sensitive to the excitonic structure of the complex, especially the lowest excitonic states. The calculated absorption, fluorescence, and non-line-narrowed HB spectra for *intact* CP47 (dashed blue curves) are shown in Figure 29 along with the experimental data (black curves). The shape of the persistent (nonresonant) HB spectrum was found to be extremely sensitive to the relative site energies of the various pigments in the complex; its shape was largely determined by a combination of the mutually strong excitonic interactions within the Chl 521/523/524 group of pigments and the relatively weak interactions of Chl 526 (the second-most red-shifted pigment; the numbering of Guskov et al.[7] is used throughout this section; for comparison with that of Loll et al. see Table 6) with the rest of the complex. The strong interactions of the Chl 521/523/524 group produce the strong double-peak feature of the spectrum (especially the ∼14 730 cm^{-1} hole and corresponding 14 800 cm^{-1} antihole), while the presence of a weakly interacting second excitonic state produced much of the lower energy ∼14 630 cm^{-1} antihole peak (see Figure 29).[40,86] This finding provided more credibility for site energies (not listed here for brevity) of other Chls.

Regarding the calculated nonresonant HB spectra, we note that in the simulations discussed earlier for the CP43 complex[85] in each iteration of the Monte Carlo procedure, HB was assumed to occur on the pigment which most strongly contributed to the lowest-energy excitonic state. The spectra calculated for the CP47 complex represent a refinement of this approach, i.e., as discussed in section 4.8 the burned pigment was selected randomly using the excitonic eigenvector coefficients $c_{1,n}^2$ (the probability that the lowest excitonic state resides on pigment n) as the probability that the nth pigment is burned.[86] Although the differences between the above two approaches are relatively small, we believe that the latter model should be used in future modeling studies, as it reflects more accurately the true quantum mechanical nature of the NPHB process. In addition, we note that in calculating the persistent nonresonant HB spectra for CP47, the photoproduct from all pigments is placed randomly within the original SDF for the corresponding pigment (i.e., no SDF shift or broadening was required to explain HB features).[86]

The calculated emission spectrum of CP47 shown in Figure 29 (obtained by convolution of the lowest state with the single site fluorescence spectrum) is also in very good agreement with the experimental data. Extensive calculations suggest that the lowest energy state (A1) in native CP47 is *not* localized exclusively on Chl 526 (Chl 29^4) as proposed in ref 112, although this pigment does partially contribute (∼11%); it appears instead that Chl 523

dx.doi.org/10.1021/cr100234j |*Chem. Rev.* 2011, 111, 4546–4598

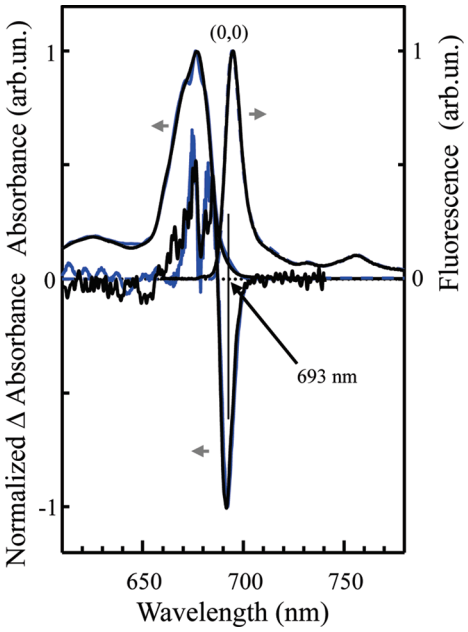

Figure 29. Best fits (blue dashed curves) to the experimental absorption, emission, and nonline-narrowed hole burned spectra for intact CP47 complex (black curves). In the fit shown, the lowest state resides mainly on Chl 523, while Chl 526 contributes strongly to the second lowest state. Taken with permission from ref 86. Copyright 2010 American Chemical Society.

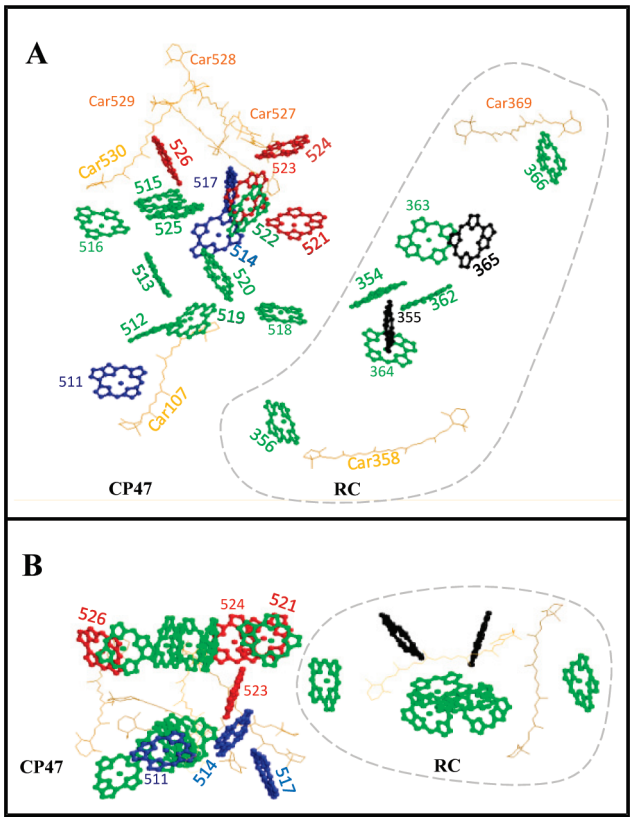

Figure 30. (A) The arrangement of CP47 Chls and carotenes (in orange) on the stromal and lumenal side of the membrane along with pigments that belong to the RC. The pigments of CP47 are numbered by the nomenclature of Guskov et al.[7] Chls 521, 523, 524, and 526 are shown in red. Chls 511, 514, and 517 are in blue. Pheophytins ($Pheo_{D1}$ and $Pheo_{D2}$) are shown in black and the remaining Chls are in green. See Table 6 for the correspondence between the numbering systems of Loll et al.[4] and Guskov et al.[7] Frame B shows the same structure in a different orientation. Reprinted with permission from ref 86. Copyright 2010 American Chemical Society.

(Chl 26[4]) provides the largest contribution (~77%) to this state.[86] The arrangement of pigments in CP47 is shown in Figure 30 (from ref 86). We hasten to add that although the above-discussed model provides a reasonable explanation of the recently obtained data, we do not insist that the site energies are perfect. These parameters, especially for the Chls contributing to the high-energy edge of the absorption spectrum, have to be further tested and optimized to provide a good description of both static and dynamic spectra/data.

In summary, the lowest-energy state of CP47 (A1 band) appears to be located near 693 nm,[9] i.e., energetically below the primary electron-donor state of the PSII RC that until recently was expected to lie near 685 nm.[185,308,309] (see section 5.3.2 on PSII core for more details). Still, even if it is located near 685 nm, at room temperature the energy of the primary electron-donor state is within reach of thermal energy kT. The lowest Q_y-state is characterized by weak el−ph coupling with a Huang−Rhys factor $S \sim 1 \pm 0.2$ and an Γ_{inh} of 180 cm^{-1}. The mean phonon frequency of the lowest-energy trap A1 is 20 cm^{-1}. HB and absorption data[9] indicate that the A1 state has small oscillator strength, i.e., it is much smaller than the oscillator strength corresponding to one Chl, in contrast to earlier assignments.[15] On the basis of data shown in refs 9 and 86, one can conclude the following (in order of increasing strength of argument): (1) it is very likely that Chl 523 contributes strongly to the lowest-energy state in order to provide the proper oscillator strength for the first excitonic band; (2) if Chl 526 contributes to the lowest-energy region (as suggested previously[112] in conjunction with mutation data), then it most likely contributes to the second excitonic state, which has a much higher oscillator strength than the lowest state; in any case, it is unlikely that Chl 526 contributes solely to the lowest energy state, since it is too weakly coupled to other pigments to produce either the low oscillator strength needed to fit the absorption and red-shifted emission spectra or the excitonic features of the persistent HB spectrum; (3) regardless of these specific assignments, the Chls contributing to the lowest state must be strongly coupled to pigments absorbing near the absorption maximum in order to explain the HB spectrum (not to mention its low oscillator strength), suggesting that the lowest state belongs to the "stromal" domain of strongly coupled pigments. These assignments should be further refined and tested by a combination of more advanced theory with new CD, LD, and time-resolved spectra, along with mutation studies and further biochemical characterization of intact isolated CP47 complexes. Finally, we note in passing that the above-discussed absorption spectra of *intact* CP43 and CP47 should allow extraction the absorption spectrum of the intact RC residing in the PSII core and possibly shed more light on charge-transfer (CT) emission in PSII core (see also section 5.2.1.).

5.1.3. LH2 Antenna Complexes of Purple Bacteria. Since the high-resolution structure of LH2 from *R. acidophila* was determined in 1995 by X-ray crystallography,[97] this system continues to be one of the most widely studied systems in photosynthesis research, including by means of SHB, related spectroscopies, and SPCS. As mentioned in section 2.2., LH2 is a cyclic structure possessing approximate C_n symmetry (with $n = 8$

dx.doi.org/10.1021/cr100234j |*Chem. Rev.* 2011, 111, 4546–4598

or 9 depending on the species). The LH2 structure contains two rings of Bchl *a* molecules, B800 and B850. The circular symmetry of LH2 complex and small interpigment distances in the B850 ring result in extremely noticeable effects related to excitonic interactions. According to the excitonic calculations, first reported for LH2 in refs 310 and 311, most of the oscillator strength of the B850 ring is concentrated in a doubly degenerate second-lowest energy level. In the ideal ring, the lowest energy level of the B850 is forbidden by symmetry considerations; however, due to diagonal and off-diagonal energy disorder, this level gains some oscillator strength and can be accessed by spectroscopy.[311−313] References 312 and 313 described the first applications of SHB to this lowest state, called B870. The shape of the SDF of this state was uncovered by ZPA spectroscopy, and the temperature dependence of the homogeneous line width has been determined.[312] The latter obeys the well-known $T^{1.3}$ power law, indicative of interaction between the chromophore and the TLS of the amorphous protein environment. The B870 state is also visible in the satellite hole structure resulting from the excitation into the B800 band and subsequent downhill EET.[312] Finally, it has been determined that the el−ph coupling for the B870 state is relatively weak ($S \sim 0.7$).[313] It has been noticed, however, that such a low value of S is inconsistent with the position of the fluorescence spectrum. Detailed SHB and FLN studies[55,314,315] demonstrated the dual nature of the LH2 fluorescence and led to application to LH2 of the concept of self-trapped excitons or excitonic polarons by Freiberg and coworkers.[56,57,102,314] The el−ph coupling for self-trapped excitons has been estimated to be several times higher than for quasifree excitons. Similar conclusions have been reached also for LH1 complexes.[57]

Another issue extensively explored for LH2 by SHB is energy transfer within the B800 ring and from B800 to B850 Chls. HB into the red edge of the B800 band, where B800→B800 EET is not present, allows one to estimate the B800→B850 EET time. Interestingly, this problem was first tackled with SHB[316] even before the structure of LH2 became available in 1995. The ∼2 ps EET time has been confirmed by later SHB experiments.[198,317−319] The narrowest holes in Figure 31 are 4.5 cm^{-1} broad, which corresponds to 2.3 ps EET time. Several times faster EET has been observed within the B800 band.[198,317,319] The dashed curve in Figure 31 is the fit to the ZPA spectrum of the B800 band. Note that it is red-shifted with respect to the B800 band maximum (solid curve), reflecting the fact that the absence of B800→B800 EET for this region results in larger HB yield. One could note, however, that the about 2 ps EET time is somewhat longer than those observed by time domain techniques.[104,317] In principle, according to the equation for HB yield (eq 20), SHB is expected to preferentially probe the longer lifetime side of the EET time distribution if such a distribution is present. It has been also recognized long ago that due to the dispersion of donor−acceptor energy gaps the EET times in PCs complexes in general and in LH2 in particular are subject to distribution.[122] Förster-approximation EET has been considered in refs 122 and 317. The applicability of this approximation to B800→B850 EET in LH2 has later been questioned by multiple researchers.[199−201] Very recently we have confirmed,[70] using extensive HB modeling, that the evolution of the spectral holes burned into the B800 band of the LH2 is indeed in agreement with EET time distributions from refs 199−201 and not with Förster models. Figure 32 depicts the theoretical and experimental dependence of hole width on fractional hole depth. However, the use of the

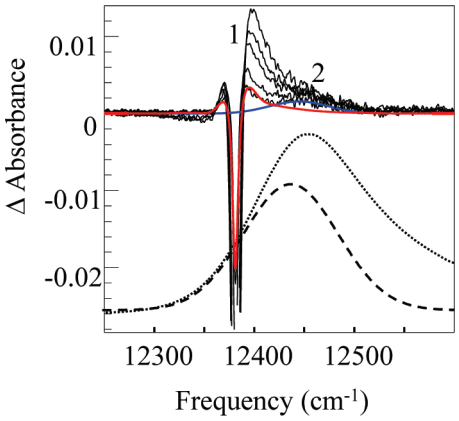

Figure 31. Persistent spectral holes (thin solid curves) burnt with increasing irradiation doses into the B800 band of LH2 complex (dotted curve below) of *R. acidophila* at 807.7 nm. ZPA spectrum (dashed curve below) is depicted for comparison. (1, 2) Two distinct antihole contributions, corresponding to two different tiers of the protein energy landscape. The tips of the deepest holes are eliminated to allow an expanding antihole region. The fractional depth of the deepest holes is ∼40%. The red curve is the hole spectrum calculated taking into account only antihole contribution 1; the blue curve is antihole contribution 2. Reprinted with permission from ref 70. Copyright 2010 American Chemical Society.

distributions of EET times affected by the whole B850 density of states,[199−201] including the upper excitonic components, is in disagreement with the results of pressure-tuning of spectral holes (and bands),[198,319] which suggest that B800→B850 EET time is not dependent on the energy gap between B800 and B850 bands (which is pressure-dependent), i.e., not dependent on the positions of upper excitonic components of B850 manifold. Thus, the exact mechanism of B800→B850 EET still remains a matter of debate.

The expected pressure shifts of the upper components of the B850 manifold have been calculated on the basis of the pressure-induced shifts of the B850 band itself as well as of the spectral holes burned into the B870 band[198,319] (see above). The large pressure-induced shift of the B870 band and of the holes burnt into this band (−0.5 to −0.7 cm^{-1}/MPa depending on the temperature where high pressure was applied) is an expression of the pressure dependence of the distance and electrostatic interactions between the adjacent B850 molecules, not the charge transfer character of the B870 state. The much lower −0.115 cm^{-1}/MPa rate of shift of the B800 holes is a reflection of protein compressibility around well-isolated B800 pigments. These results are in agreement with those of Stark-HB spectroscopy,[320] where relatively low values for change in dipole moment ($\Delta\mu$) and polarizability were observed. Finally, we note that in ref 70 we presented the first study of low-temperature protein dynamics in LH2 by means of SHB and compared it to the SPCS results. Exploration of the HGK and the shape of the NPHB antihole (see Figure 31) allowed for determination of the distribution of the tunneling parameter λ, characterizing "strength" of the barriers between different conformational substates of the protein in the excited state of the chromophore/protein system.

The LH2 antenna complex is the photosynthesis-related protein which is by far the most thoroughly studied by means of SPCS (see ref 62 for review), starting from 1999. The highly symmetric structure of this complex results in a broad range of

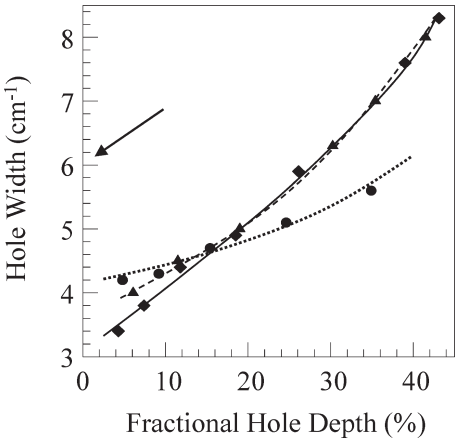

Figure 32. The fractional depth dependence of the hole width in LH2: triangles, experimental data from the same data set as depicted in Figure 31; circles, theoretical prediction for no EET time distribution; and squares, theoretical prediction for EET time distribution from ref 19. The arrow indicates the hole width expected on the basis of time domain data in the absence of EET rate distribution; 1.7 ps was the peak of the EET time distribution employed in the simulation. Reprinted with permission from ref 70. Copyright 2010 American Chemical Society.

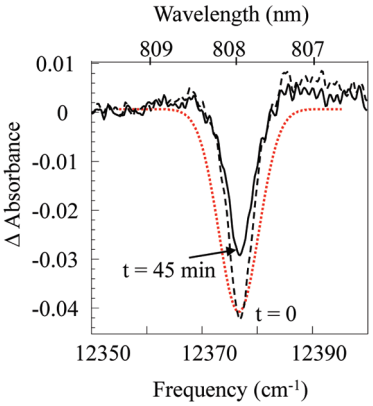

Figure 33. Dashed curve, spectral hole at 808 nm immediately after burning; solid curve, same hole 45 min later, with white light of the FTIR spectrometer on. Despite light-induced hole filling, both holes are 4.9 cm^{-1} broad. T = 5 K. Data taken from ref 70 (the red dashed curve is the 9 cm^{-1} broad distribution of the first cumulant). Reprinted with permission from ref 147. Copyright 2007 American Chemical Society.

interesting physical phenomena manifesting in SPCS experiments. For instance, in ref 321 the direct observation of excitonic bands due to the strongly coupled BChls of the B850 manifold has been reported. This data, along with the elaborate analysis presented in ref 322, indicates that the C_8 (or C_9) symmetry of the LH2 complex may be disturbed, i.e., that these complexes may exhibit elliptical distortion. If this is the case at all and/or if this is an effect of a particular sample preparation procedure is still a matter of debate.[323] Polarization-sensitive measurements on the B800 band, as well as correlated shifts of several lines in the B800 spectrum, convincingly demonstrated that even for relatively weak (~25 cm^{-1}) interactions between the B800 molecules, the respective electronic states can be significantly delocalized.[69,145] The fluorescence spectra of the single LH2 (as well as LH1)[152] complexes have been used to support the idea of exciton self-trapping in B850 (B875 in LH1).[56] Single B800 molecule excitation spectra containing both zero-phonon line and phonon sideband were recently reported.[144] This became possible thanks to the advances in data processing techniques that allowed taking into account the constant shifts of the spectral lines due to light-induced spectral diffusion.

Light-induced spectral diffusion and underlying low-temperature protein dynamics are the key subjects of the majority of recent LH2 SPCS publications.[144−148,188,202] Spectral fluctuations resulting from protein dynamics at room temperature have been considered in refs 77, 78, 80, and 150. Most notably, it has been demonstrated that the spectral diffusion behavior of the B800 spectral lines is in agreement with the models[204] predicting the presence of several hierarchical tiers in the protein energy landscape.[146] The particular conformational changes responsible for spectral shifts of various magnitudes have also been suggested.[62] It remains to be seen if the reported SPCS data are statistically sufficient to serve as representative of the typical or average low-temperature behavior of the LH2 protein and/or if some fractions of these observations reflect the dynamics of the surrounding amorphous host or host−protein interface rather than that of the "pure" LH2 protein. Our preliminary comparison of SPCS and NPHB results (including evolution of ZPH width and of NPHB antihole), indicates that while our NPHB data is in qualitative agreement with SPCS results and the underlying multitier energy landscape models, quantitatively SPCS and SHB data may be in disagreement.[70] Namely, the fastest, smallest-barrier tier dynamics attributed to the surface TLS[324] cannot be reconciled with SHB data, which most likely indicates that the features responsible for this dynamics in SPCS experiments are sample preparation or amorphous host dependent or result from local heating of the sample in the focus of the microscope objective. Figure 33 presents the (lack of) temperature- or light-induced broadening of the spectral hole burnt into the B800 band at 808 nm. While the hole is filling under the influence of the white light of the FTIR spectrometer, it is not broadening within the experimental uncertainty and is not approaching the shape of the first cumulant distribution based on SPCS data,[147] as would be expected if SPCS observations just reflected the protein dynamics at the supposed temperature of the experiment. The above discussion illustrates that HB continues to provide valuable information on EET and protein dynamics in LH2 and provides the average values necessary to determine if SPCS probes statistically relevant features of the protein dynamics of intact protein per se.

5.2. Reaction Centers (RCs)—Electronic Structure and Primary Charge Separation

5.2.1. PSII Reaction Center. The PSII RC, first isolated by Nanba and Satoh in 1987[325] (the isolation procedure was further perfected by Seibert's group,[326,327] and better stability of the samples has been achieved), contains six Chl *a* molecules and two pheophytins *a* (Pheo *a*). At the first glance, the overall arrangement closely resembles the structure of the bacterial RC (see next section), except that two Chl *a* molecules, known as $Chls_Z$, are located at the periphery of the charge separation chain.[4,5,7] On closer inspection, however, one finds that in contrast to the bacterial RC the distances and the next-neighbor electrostatic couplings between the molecules involved in charge separation in PSII are all comparable (there is no well-defined "special pair"), and the system (apart from $Chls_Z$) has to be treated as a multimer,[328] although a pentamer model (where $Pheo_{D2}$ was decoupled from the remaining pigments) has been also discussed.[329] Note that if the site energy of

some pigment belonging to the RC multimer deviates significantly from those of other pigments, this pigment will exhibit quasi-isolated behavior despite relatively large interactions with the nearest neighbors.

The key issues that were addressed for the isolated PSII RC by spectroscopic studies included the time constant(s) and exact mechanism of the primary charge separation, as well as assignments of various spectral features to different pigments. Note that although the couplings between the Chl *a* and Pheo *a* molecules can be determined with sufficient precision, the site excitation energies in the absence of disorder are unknown, and the assignments of these energies can affect the expected mechanisms of EET and charge separation. For example, although it is in general widely believed that both $Chls_Z$ absorb at ~670 nm and transfer energy to the RC multimer, at some point it was suggested[211,330] that one of these $Chls_Z$ may be responsible for the shoulder observable in the absorption spectrum at ~684 nm.[211,330−333] Other pigments have been assigned to varying wavelengths as well.

Concerning the primary charge separation, early time domain studies resulted in charge separation times of 1.5−3 ps.[334,335] These results were corroborated using various techniques,[185,336−339] including HB.[185,339] Interpreting the results concerning charge separation time requires a correct understanding, at the microscopic level, of the charge separation mechanism. By the late 1990s results started to emerge indicating that the charge separation sequence in PSII RC may differ significantly from that in RCs of purple bacteria. Namely, it has been suggested that the first in the chain of events does not involve the "special pair" pigments but rather Chl_{D1} and $Pheo_{D1}$.[340,341] Interestingly, it has also been suggested,[340] on the basis of photon echo experiments and excitonic simulations including simplified charge separation treatment, that the charge separation process is highly dispersive, with respective time constants ranging from 1.5 ps to hundreds of picoseconds and even several nanoseconds. As we demonstrated in 2004,[342] this idea is in agreement with HB results. Very recently, a broad range of charge separation time constants has been reported also by van Grondelle's group.[343,344] Qualitatively, the resonant HB results may be interpreted by assuming that the persistent HB probes the long-lifetime end of the broad charge separation time distribution, while triplet bottleneck HB probes the fastest end. With that assumption, one can fit both resonant persistent and transient hole spectra with λ_B in the 680−686 nm range using the same (moderate, $S_{ph} \sim 0.8 + S_{80} \sim 0.2$) el−ph coupling. This is illustrated in Figure 34. In this model, which was the first crude attempt to employ lifetime distributions in the simulations of the HB data in PC, it was suggested that the apparent large el−ph coupling of the triplet bottleneck holes[211,333,345] is an illusion created by merging of the broadest holes with the phonon sidebands as well as, possibly, by saturation effects (note that transient HB yield in the case of fast charge separation approaches 1; eq 26). It was also noticed in ref 342 that HB behavior is quite similar for the main absorption band of the PSII RC located at 680 nm and for the shoulder located at 684 nm in various other respects as well. For example, Stark HB yielded similar values of $\Delta\mu \sim 1.0$, somewhat larger than those observed for Chl *a* monomer, for both bands. In 2002 Krausz and co-workers[346] recognized that the main band of the PSII RC in the intact core environment is located at ~685 nm.[346,347] Thus, we suggested[342] that the shoulder at 684 nm represents not any particular pigment of the RC but rather the lowest state of a fraction of the least disturbed RCs preserved during the isolation procedure. This idea is in agreement with the sample/preparation-dependent magnitude of this shoulder and with MCD results.[347] Very recently, 2D ES has been employed to shed light on excitonic interactions, charge separation, and energy transfer pathways in PSII RC. A rapid, <100 fs, decay between 680 and 684 nm has been observed, which is consistent with the gross heterogeneity model proposed by us in ref 342, assuming this decay component is due to relaxation in a fraction of the complexes with the lowest excitonic state at 684 nm and higher excitons at 680 nm. Processes with time constants of 1−3 ps and 40−60 ps have also been observed at ~680 nm, but not those with longer[340] characteristic times. Note that in ref 243 the analysis was based on the exciton model of Novoderezhkin et al.,[343] which assigns the 684 nm shoulder to a charge transfer state.[343] It is not clear how the latter assignment is consistent with persistent SHB observations indicating that the 684 nm band exhibits moderate el−ph coupling and permanent dipole moment change, quite atypical for the charge transfer states in other PC.[95,352]

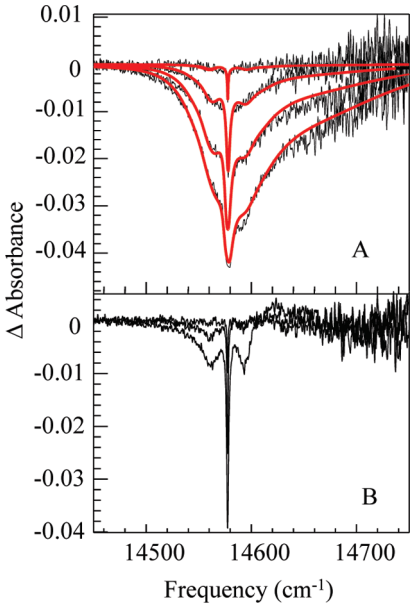

Figure 34. Triplet bottleneck (upper frame) and persistent (lower frame) holes burnt at 686.0 nm. The triplet bottleneck holes are accompanied by the fits (red curves) obtained using $S = 0.7$ and 0.2 for delocalized protein phonons and ~80 cm^{-1} dimer mode, respectively, as well as the fast end of the charge separation time distribution. Data taken from ref 292.

At the time of the submission of this review it appears to be generally accepted that the RC isolation procedure results in the alteration of the structure of the PSII RC and the blue shift of the absorption and emission peaks. Thus, the discussion on the properties of the intact RC will be, to a certain extent, continued in the section on the intact PSII core (section 5.3.2). Nevertheless, the isolated RC serves as a fine example of how static and dynamic disorder result in emergence of several charge separation pathways with widely varying time constants[344] accessible, among other methods, by SHB.

5.2.2. Bacterial Reaction Center. The bacterial reaction center (BRC) constitutes an assembly of four BChl *a* and two BPheo *a* molecules. Of these, two extremely closely coupled Bchls form the primary donor. Due to strong coupling between the molecules of this dimer, the respective lowest excitonic state

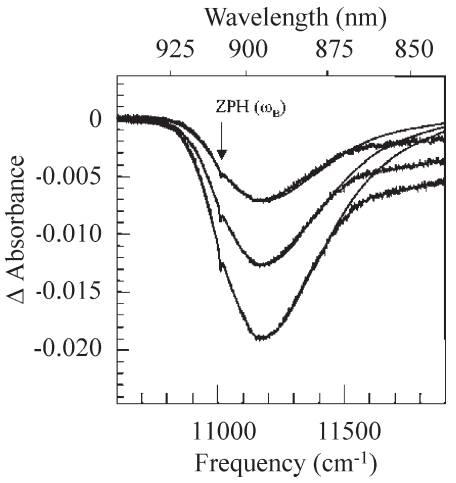

Figure 35. The transient photochemical hole spectra of the RC of R(L135)L mutant of *R. sphaeroides* burnt at 11013 cm^{-1} (908.0 nm) with 10, 20, and 40 mW/cm^2. Reprinted with permission from ref 95. Copyright 2003 American Chemical Society.

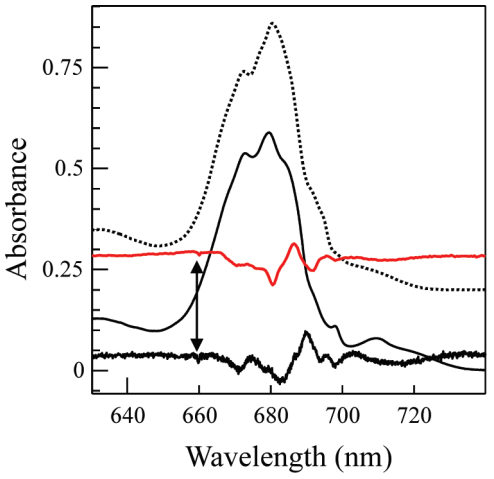

Figure 36. Absorption spectra and nonresonant satellite hole structures (λ_B = 660 nm, arrow) for PSI of *T. elongatus* (solid curves) and *Synechocyctis* PCC6803 (dotted curves). Most of the curves are shifted up for clarity. Data are taken from refs 351 and 352.

is shifted to 870 nm in *R. sphaeroides* (P870) and even to 960 nm in *R. viridis* (P960). The available HB studies of BRCs primarily focused on the properties of this lowest excitonic state. The burning of narrow holes into the higher-energy bands of the BRC is not effective due to the respective EET times being short (<ps). However, excitation into these bands results in effective downhill EET and formation of satellite hole structure.[348] Resonant and nonresonant HB into the lowest-energy P_ state of BRC can be observed both in NPHB[94] and transient HB[95,120,348,349] modes. Interestingly, the conformational change associated with NPHB in the BRC is quite significant and results in ~150 cm^{-1} red shift of the displaced absorption.[94]

The key properties of the lowest state of the BRC, observed in SHB experiments, are fast charge separation (several picoseconds) and extremely strong el−ph coupling, both with delocalized protein phonons and with the so-called dimer marker mode. (Such a mode appears to be present in all photosynthetic RCs, though its parameters somewhat vary.[349]) The phonon sideband is peaked at ~30 cm^{-1} and is characterized by $S_{ph} \sim 2$. The marker mode, with frequency of ~120 cm^{-1} (P870) or ~140 cm^{-1} (P960) has the value of S_{dm} = 1.5 and 1.1, respectively. Figure 35, borrowed from recent work,[95] presents an example of transient photochemical holes (obtained through $P^+Q_A^-$ formation) resonantly burnt into the P_ band of R(L135)L mutant of *R. sphaeroides* and their fits according to eq 20. Here in particular S_{ph} = 2.2 and S_{dm} = 1.7. As these are photochemical holes, no antihole is expected within the spectral region depicted in the figure. Overall the agreement between the spectra is quite satisfactory. The discrepancy on the higher-energy side of the hole spectra is due to intramolecular modes of BChl *a*[216] not being taken into account. Due to extreme el−ph coupling, the resonant ZPH is just a minor contribution to the hole spectrum.

5.3. Large Photosystems and Supercomplexes—Light Harvesting, Electronic Structure, and EET

5.3.1. PSI of Green Plants and Cyanobacteria and the PSI−CP43′ Supercomplex: HB and SMS. As stated in section 2, PSI is a quite complicated entity, with core complex including almost 100 Chl *a* molecules per monomer (i.e., per RC). The Q_y absorption of all these molecules is concentrated in a relatively narrow spectral region, resulting in a high degree of spectral congestion. Thus, most of the SHB studies of PSI so far focused on the so-called "red antenna states", or states absorbing lower in energy than the primary donor P700. While in cyanobacteria these low-energy states are part of the core antenna, in plant PSI they belong to the Lhca peripheral antenna complexes. (Reference 350 contains a recent review on structure and intersubunit EET in plant and cyanobacterial PS I.) Understanding which particular chlorophylls known from structural data are responsible for these states promises to offer insight onto the functioning of the PSI antenna as well as provide benchmarks for excitonic calculations. The 5 K absorption spectra of PSI from *Thermosynechococcus elongatus* and *Synechocystis* PCC6803 are presented in Figure 36 along with the satellite hole structures resulting from high-energy excitation (e.g., at 650 nm). It was the careful analysis of such satellite hole structures, along with their irradiation dose dependence, which first allowed the identification of two separate red states for *Synechocystis*[215,351] and three for *T. elongatus*.[352] The existence of these states has been confirmed by pressure- and Stark-SHB experiments.[215,351−353] As mentioned above, differences in pressure-induced shifts, dipole moment change, and el−ph coupling can be utilized to distinguish between partially overlapping bands. It has been demonstrated that the lowest-energy states of both cyanobacteria (C714 and C719, respectively) exhibit large values of all three of these parameters and therefore they most likely possess significant charge transfer character. Assignments of these states to particular chlorophyll molecules of the complex have been proposed (see next paragraph). The widths of the holes burnt into higher-energy red states allows one to estimate the respective EET times (~5 ps).[353]

The first PSI SPCS results were reported by Jelezko et al.[151] for trimeric PSI from *T. elongatus*. It was demonstrated that the single complex fluorescence spectra are dominated by broad structureless bands peaked at ~730 nm due to emission from the lowest-energy (C719) state. This observation is in agreement with HB data demonstrating that the C719 state possesses significant charge transfer character and, as a result, is characterized by very large el−ph coupling, large permanent dipole moment change (observable in Stark-HB experiments[215,351−353]), and a large pressure-induced spectral shift. In addition to this broad

dx.doi.org/10.1021/cr100234j |*Chem. Rev.* 2011, 111, 4546–4598

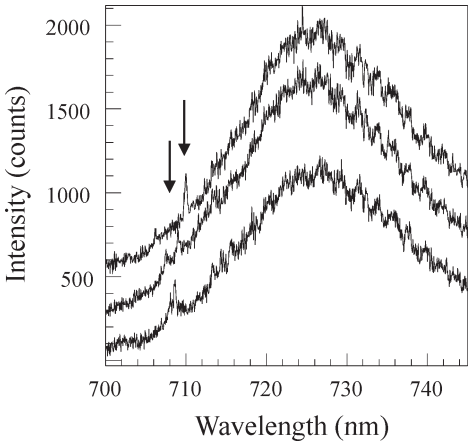

Figure 37. Fluorescence spectra of one single PSI complex from *T. elongatus*, measured consecutively. Note narrow C710 lines which change their position from spectrum to spectrum (arrows) and a broad C719 (F730) band which in this particular complex is peaked at 725 nm. The periodic structure at longer wavelengths is due to the CCD etaloning effect. Reprinted with permission from ref 66. Copyright 2007 American Chemical Society.

band, some relatively narrow lines have been observed at around 710 nm, both in fluorescence and in fluorescence excitation spectra. No attempt to assign these spectral features to particular chlorophylls was made in ref 151. Later we confirmed the results by Jelezko et al. using SPCS and also extended our studies to PSI of another cyanobacterium, *Synechocystis* PCC 6803.[66] Figure 37 depicts several fluorescence spectra of the single trimeric PSI from *T. elongatus* from ref 66. For *Synechocystis* PCC 6803, the broad band peaked at ~722 nm has been observed in the fluorescence spectra of single PSI complexes, in agreement with similarity between the lowest energy states of *T. elongatus* (C719) and *Synechocystis* (C714) first found using SHB.[4] Narrow lines were not observed for *Synechocystis* PSI in our experiments, although Brecht et al. later argued that this was due to experimental imperfections.[73,74] We also observed spectral shifts of the narrow lines in the case of *T. elongatus* PSI, which are a manifestation of light-induced spectral diffusion/protein dynamics. At about the same time Wrachtrup's group produced additional SPCS data on PSI from *T. elongatus*.[75] This time prereduced samples were explored, and an additional emission band at 745 nm was reported. Very recently, Brecht et al.[74] published the chlorophyll/red band assignments by his and Wrachtrup's group. On the basis mainly of the light-induced spectral diffusion behavior, they have assigned C710 to the more tightly bound B7-A32 dimer. The A38−A39 and B37−B38 dimers, which are positioned close to the reaction center, were considered to be good candidates for C719 of *T. elongatus* as well as for C714 in *Synechocystis* PCC 6803. The environment of the B31−B32−B33 trimer allegedly allows for even more flexibility than that of all three dimers mentioned above. Therefore, Brecht et al. assigned this trimer to C715. In 2008, Brecht et al. extended their studies to *Synechocystis* PCC6803 and *Synechococcus* PCC7002.[73] They argue that the pools F699 (*Synechocystis* PCC 6803), F698 (*Synechococcus* PCC 7002), and C710 (*T. elongatus*) as well as the red-most pools C714 (*Synechocystis* PCC 6803), C708 (*Synechococcus* PCC 7002), and C719 (*T. elongatus*) show similar spectroscopic characteristics on the single-molecule level, while C715 of *T. elongatus*, with its very fast spectral diffusion, has no direct analogs in the PSI of other cyanobacteria.

We, on the other hand, have assigned the C719 band (and its analog in *Synechocystis* PCC6803, the C714 band) to the B7−A32 dimer based on its sensitivity to the trimeric/monomeric status of the PSI complex (true also for minus-L mutants) and the narrow C710 band (same as C708 in Brecht/Wrachtrup notation) to the B31−B32−B33 trimer.[352] However, the argument can also be made, on the basis of structure data, for B37−B38 dimer being sensitive to PSI monomerization and thus being responsible for the C719 state. Note that according to SHB data both C710 and C715 exhibit reasonably efficient EET to C719, which is somewhat inconsistent with either of them being due to the B31−B32−B33 trimer, situated relatively far from other proposed candidates for the red band origin. On the other hand, ZPLs belonging to C710 are observed in SPCS spectra by all groups more frequently than ZPLs possibly belonging to the C715. While this may indeed be ascribed to faster spectral diffusion of C715, the possibility remains that the C710 Chls are more isolated from the rest of the red antenna Chls than the C715 ones, which is inconsistent with the C710 chlorophylls being B7 and A32. (In this scenario C715 lines are not observed, since they are broadened by fast EET.) More studies elucidating similarities and differences between various properties of the red bands of PSI are necessary. These may include for example, the studies of EET times and their distributions, spectral hole growth kinetics,[194] NPHB photoproduct shape,[203] and hole thermal cycling experiments, accessing the distribution of the barriers in the protein energy landscape in the ground, rather than the excited, electronic state. In view of our findings for LH2, one may also suggest that the spectral diffusion behavior of different lowest-energy states of PSI is affected not only by the supposed looseness of the respective protein pocket but also by the closeness of the protein/amorphous host interface and by the nature of that host. The final assignment should explain the low-temperature light-induced spectral dynamics,[73,74] as well as other effects accessible by SPCS, SHB, and lower-resolution techniques.

Very recently,[76] low-temperature single molecule studies have revealed strong anticorrelation between the fluorescence of different PSI emitters from *Synechocystis* PCC 6803 and *T. elongatus*, suggesting that there may be no unique EET pathways within a given complex. Rather, it has been suggested that fluctuations of the protein environment may dynamically modify the site energies and couplings of the pigments within the EET chain, producing multiple accessible EET pathways even at low temperatures. These results further support the idea that protein dynamics may play a critical role in the very efficient EET in light-harvesting complexes, in agreement with recent observations from 2D spectroscopic data.[27,116,344]

Little is known about the particular molecular origin of the higher-energy states of the cyanobacterial PSI. At first glance the rich satellite hole structure (see Figure 38) seems to suggest that multiple bands exhibit relatively efficient SHB and could be assigned to chlorophyll molecules somewhat isolated in the structure. However, there is no match to those satellite holes either in fluorescence spectra or in ZPA spectra[292] (Compare Figure 36 and the inset of Figure 38). Thus, most of those satellite features are either higher excitonic components of the red antenna states or, more interestingly, the bands of the chlorophylls located in the vicinity of either the "red states" or P700 and experiencing electrochromic shifts. Work[292] in fact focuses on the SHB study of a PSI−CP43′ supercomplex[354−356] produced by cyanobacteria under iron-stress conditions. Here

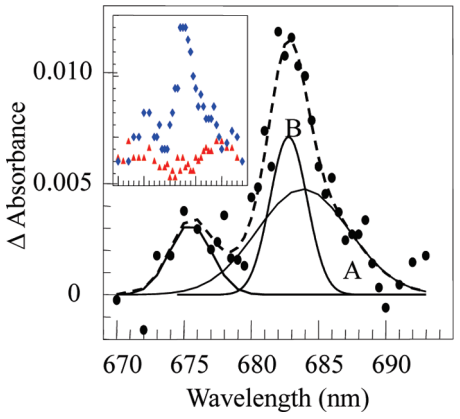

Figure 38. The ZPA spectrum of the CP43′ (circles) with Gaussian deconvolution. Solid lines, individual fit components, labeled according to the CP43 state labeling scheme. Dashed line, sum of the solid lines. Inset: ZPA action spectra of PSI−CP43′ supercomplex (blue diamonds) and matching PSI core (red triangles). The horizontal axes range is the same as in the main frame. Note the lack of structure in the PSI core data set. The ZPA spectrum in the main frame is the difference of the ZPA spectra in the inset. Reprinted with permission from ref 292. Copyright 2006 American Chemical Society.

the ZPA spectrum reveals the lowest-energy states of the CP43′ (IsiA) manifold at ∼683 nm, indicating that at low temperatures the EET from CP43′ to the PSI core is relatively slow (∼50 ps), unlike at physiological temperatures, where it occurs in a few picoseconds.[357] This is corroborated by the presence of the band at ∼685 nm in the supercomplex fluorescence spectrum,[292,358] as well as by direct homogeneous hole width measurements.[292] The quality of the CP43′ ZPA spectrum is high enough to distinguish the analogs of the A and B states of CP43 (see Figure 38). The red shift of the CP43′ fraction of supercomplex emission with respect to that of the isolated CP43 and CP43′[358] has been attributed to EET between adjacent CP43′ subunits. The effect is similar to that described in sections 4.5 and 5.1.2.1 with respect to the analysis of CP43 spectra, with A and B pigments of adjacent CP43′ subunits serving as additional energy acceptors. Assuming that the wavelengths of the pigments of the PSI core located closest to CP43′ are optimized for maximal spectral overlap and fastest CP43′→ PSI core EET at physiological temperatures (i.e., almost isoenergetic with the lowest states of the CP43′ manifold), one can easily imagine the situation where at low temperatures the lowest states of the CP43′ manifold are shifted slightly lower in energy than the closest core pigments, spectral overlaps are drastically reduced, and EET time is increased from ∼2 ps to ∼50 ps.

Concerning the lowest-energy states of Lhca complexes of plant PSI (see ref 359 for a recent review), it has been confirmed by SHB that these states, especially for Lhca3 and Lhca4, exhibit strong el−ph coupling,[360] the strongest for photosynthetic antennae. The same conclusion was reached on the basis of the studies of PSI−LHCI supercomplexes,[221] where large pressure-induced spectral shifts have also been observed, as well as in refs 361 and 362, where FLN has been applied to LHCI complexes (mixture of heterodimers) among other techniques. Stark-SHB has not yet been applied to these systems, although conventional Stark experiments yield high values of polarizability and dipole moment change.[363] Thus, like the lowest states of cyanobacterial PSI, these states exhibit significant charge transfer character.

5.3.2. PSII Intact Oxygen-Evolving Core. The PSII core is the smallest assembly (containing only the RC and the two major antennas, CP43 and CP47 complexes; 35 Chls and 2 Pheos in total) capable of water splitting and oxygen evolution. Assignment of various spectral features of such a complex system has proven a difficult task. Emission spectra of the PSII core show complicated temperature dependence[307] and apparently contain contributions from several emitting traps. Weak emission with a maximum near 740 nm was assigned tentatively to a low-energy charge transfer (CT) state in the PSII core,[307] whose absorption peak appears to be located near 705 nm[364] (our unpublished data on PSII cores are also consistent with a 705 nm absorption peak for the CT state). It was also argued that main contributions to PSII core emission in the 680−700 nm range originate from CP43 and CP47 complexes and not from the RC; that is, so far there is no indication that the RC assembly per se in PSII cores gives rise to a significant emission in the 680−700 nm region.[307,364] This is consistent with the discovery of Krausz et al.[365] that the RC of the core has an optically accessible excited state with excitation energy far lower than previously believed. Krausz et al. showed that this state is both photoactive and energetically ∼0.1 eV below the state absorbing near 680 nm.[366] The presence of the "red tail" absorption in *intact* PSII suggests that narrow holes observed in the PSII core complexes (vide infra) are not associated with absorptions of the RC itself. Relaxation within the RC to the lowest (homogeneously broadened) excited state, which has its purely electronic component in the 700−730 nm region, can be expected to be rapid and would prohibit any narrow HB occurring for higher excited states of the RC, in agreement with experiment.[364,366]

The observation that excitation at wavelengths up to 730 nm can lead to efficient charge separation resulted in the proposal of a new paradigm for P680,[17,307,364−366] suggesting that the lowest excited state of P680 is likely broad and having a dipole strength of less than 0.2 Chl *a*.[364] The discovery that the native PSII enzyme undergoes charge separation via absorption extending to 730 nm stimulated the research of PSII RC preparations.[17,343] As discussed briefly in section 5.2.1, it appears now that the optical spectra of the isolated RC are very different from those still embedded in the intact PSII core.[364,367] Apparently during the isolation procedure the D1 and D2 proteins are slightly shifted apart, leading to weaker coupling between RC pigments, in agreement with the observed blue shift of the isolated RC absorption spectrum.[364,367] But the nature of the *intact* RC (including assignment of site energies for various Chls and Pheos) remains elusive, although many attempts to solve this problem have been made.[112,368−370] The scaled absorption of spinach PSII core complexes (T = 1.7 K) with those of Namba−Satoh RC preparations RC-5 and RC-6 from ref 367 is shown in Figure 39. The inset shows the Q_x region in greater detail. The scaling highlights the contribution from CP43 and CP47 complexes discussed above. Q_y, Q_x, and β-carotene regions are indicated by arrows. Note that there is no "red tail" present in D1/D2/cyt$_{b559}$ RC particles that is comparable to the 700−730 nm absorption in PSII core complexes.[367] In the isolated RCs, according to the analysis of Raszewski et al.,[369] excitations involving Chl$_{D1}$ and Pheo$_{D2}$ become the lowest excited states. Due to substantial *noncorrelated* site energy distributions in these preparations, a range of realizations of the lowest energy excited state may arise. It has been suggested that a component of the persistent spectral HB in these systems may be associated with a subset of ∼20% of realizations in which a Pheo$_{D2}$ exciton is lowest.[368]

dx.doi.org/10.1021/cr100234j |*Chem. Rev.* 2011, 111, 4546–4598

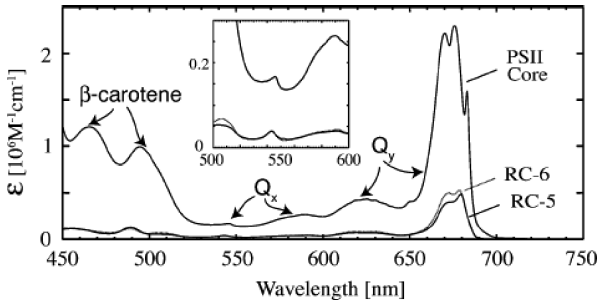

Figure 39. Scaled absorption of spinach PSII core complexes with those of Nanba−Satoh reaction center preparations RC-5 and RC-6 (see the text). Spectra are recorded with the sample immersed in superfluid helium at 1.7 K. The inset shows the Q_x region in greater detail. The region near 630 nm corresponds to vibrational sidelines of Q_y. Reprinted with permission from ref 367. Copyright 2008 Springer.

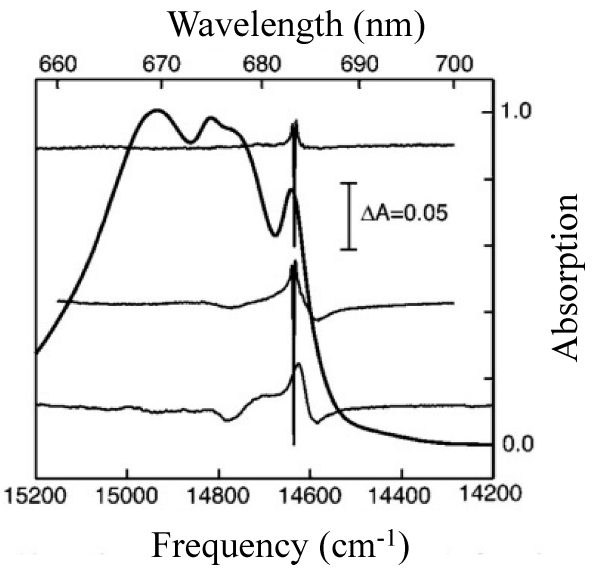

Figure 40. Absorption spectra (thick line) at 1.7 K of a spinach PSII core sample prepared in the $S_1(Q_A)$ state before illumination. Broad band (laser line width ∼2−3 cm^{-1}) HB spectra of a spinach PSII core in the $S_1(Q_A^-)$ state (top) and $S_1(Q_A)$ state (center) at 1.7 K. The hole depths ($\Delta A/A \times 100\%$) are ∼9% and ∼12%, respectively, each attained with ∼3.5 mW/cm^2 for 60 s. The bottom trace shows Q_A^- formation following 630 nm illumination with comparable burn fluence to the hole-burned spectra. Hole-burning with PSII in the $S_1(Q_A)$ state results in a persistent spectral hole superimposed on structure associated with electrochromic shifts due to Q_A^- formation. With PSII in the $S_1(Q_A^-)$ state, difference-spectra after laser illumination at ∼683 nm display persistent spectral HB features only as all PSII centers have been converted to the $S_1(Q_A^-)$ state. Reprinted with permission from ref 17. Copyright 2004 American Chemical Society.

The most efficient HB in PSII core complexes (and equivalently seen in membrane-bound PSII) occurs in the absorption region of lowest energy excitations of the CP43 and CP47 proximal antennas (675−700 nm).[17,371,372] Efficiencies of HB were high and approached 1 when the plastoquinnone Q_A was reduced; the high HB efficiency was attributed to charge separation of P680 in native PSII.[17,364] In other words, the HB behavior of PSII cores was attributed by Krausz and co-workers to a novel charge separation-induced HB mechanism (electrochromic HB). It was suggested that charge separation occurs following (relatively slow) EET from CP43 and CP47.[364] (EET occurs from the lowest-energy pigments of CP43 and CP47 to the RC; recall that the proximal antennas are on opposite sides of the RC proteins). Thus, the lifetime of the burning state is determined by EET, but the HB yield is determined by the quantum efficiency of charge separation. Within this model, lowest energy excitations of both CP43 and CP47, as argued by Krausz et al., must involve pigments capable of performing effective excitation transfer to the RC based on structural considerations ("linker pigments", not to be confused with $Chls_Z$).

An example of HB spectra is shown in Figure 40, where effects of broad band (2−3 cm^{-1}) laser excitation (683.3 nm) of a PSII core poised in the $S_1(Q_A)$ state and also in the photoreduced $S_1(Q_A^-)$ state are illustrated;[17] see the figure caption for details. The structured background is due to Q_A^- formation, as shown by the bottom trace following the 630 nm excitation. The top and center HB spectra were obtained in the $S_1(Q_A^-)$ and $S_1(Q_A)$ state states, respectively (T = 1.7 K). The top spectrum displays the persistent HB feature only, because all PSII centers have been converted to the $S_1(Q_A^-)$ state. Thus, HB in the $S_1(Q_A)$ state results in a persistent spectral hole superimposed on the structure associated with the electrochromic shifts due to Q_A^- formation. Higher resolution data are needed to explain the origin of the narrow antihole distribution near the hole burned at 683.3 nm. The fact that persistent HB is not evident in the 700−730 nm spectral region although charge separation still takes place supports the idea that this region is indeed contributed to by a CT state with very large el−ph coupling.[366] In other words, the "red tail" is predominantly *homogeneously* broadened. The CT excitation most likely involves the special pair of Chls in the RC.[366]

The ZPA spectra of BBY particles (PSII-enriched membrane bound preparations) and core complex samples prepared from spinach and *Synechocystis* 6803 core complexes (from ref 17) are shown in Figure 41. These spectra were obtained in the $S_1(Q_A^-)$ state (holes are not saturated). The narrow SDF near 684 nm dominates the ZPH action spectra. Hole widths burned in the PSII cores (extrapolated to lowest temperatures and fluence) correspond to excited state lifetimes of ∼100 ps.[364] Excitation of the lowest energy states in CP43 and CP47 leads, with probability of ∼90%, to EET to the RC with subsequent charge separation.[364] There was a broader hole width (and higher efficiency HB) in the Q_A state than in the Q_A^- state. This is consistent with PSII emitting more strongly in the open (Q_A) state than the Q_A^- state. Hole widths in the CP47 region were wavelength dependent, with narrower holes appearing at longer wavelengths.[365] This was interpreted as due to progressively slower EET to the RC from these longer-wavelength Chls within the inhomogeneous distribution. This explanation was based on the observed spectral shift of the PSII core[307] and CP47−RC[300] emission bands from ∼690 nm at 5 K to ∼695 nm at 77 K, which has often been interpreted as reflecting decreased emission from high-energy (∼690 nm) pigments in the CP47 lowest-energy band at higher temperatures (∼77 K) due to quenching by EET to the RC. (It was argued that at 5 K, emission originates from the entire distribution of CP47 lowest-energy states, since insufficient thermal energy is present to induce "uphill" energy transfer to the RC, while at ∼77 K, higher-energy pigments from the CP47 lowest-energy state are quenched by rapid transfer to the RC).[300] This interpretation has been recently called into question based on the observation of 695 nm fluorescence from isolated CP47 (for which EET to the RC is obviously impossible) independent of temperature in the range 5−77 K.[9,138] However,

dx.doi.org/10.1021/cr100234j |*Chem. Rev.* 2011, 111, 4546–4598

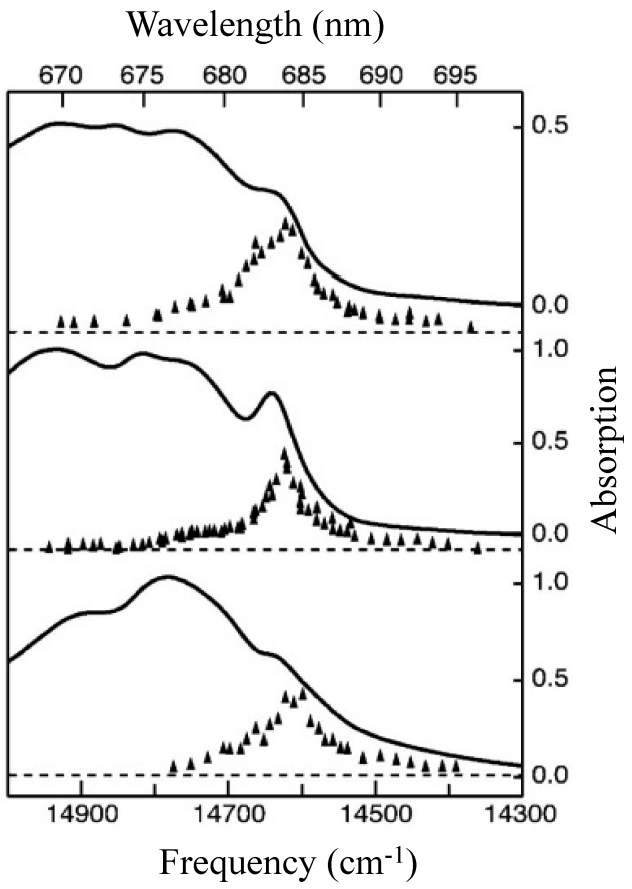

Figure 41. Absorption spectra (thick lines) at 1.7 K of *Synechocystis* 6803 (top) and spinach (center) PSII cores, as well as spinach BBY (bottom) membrane-bound preparations. The triangles are the HB action spectra obtained by burning with constant fluence and plotting the resultant hole area as a function of burn frequency. The horizontal dotted lines indicate the zero of the action spectrum, which are plotted on arbitrary *y*-axis scales. HB for the action spectra was performed at 1.7 K with broad band laser excitation (line width 2−3 cm^{-1}) and with fluence such that holes were not deeply saturated ($\Delta A/A$ <10%). Reprinted with permission from ref 17. Copyright 2004 American Chemical Society.

detailed emission studies of the PSII core and CP47−RC complexes are required to resolve this issue.

It has been shown recently that nonresonant HB spectra obtained for the isolated CP43 and CP47 complexes are in good agreement with HB spectra obtained in the intact PSII core complex.[86] This strongly indicates that the CP43 and CP47 complexes, whose spectra were presented in sections 5.1.2.1 and 5.1.2.2, correspond to intact complexes, i.e. they are not significantly modified by the isolation procedure with respect to the same complexes being part of the intact PSII core. Figure 42 shows the absorption spectrum of the PSII core from spinach (the sample was kindly provided by Dr. E. Krausz) in the $S_1(Q_A^-)$ state (i.e., closed RC at 5 K; the spectrum is indistinguishable from that reported in refs 17, 365). The spectrum was obtained using FTIR spectrometer with a white light (of ~0.125 mW/cm^2) and controlled green light (λ_{ex} = 496.5 nm; fluence = 36 J/cm^2) illumination to ensure nearly 100% reduction of Q_A^-. The difference spectrum between the absorption spectrum from refs 17 and 365 in the $S_1(Q_A)$ state and the absorption spectrum [in the $S_1(Q_A^-)$ state] in the Q_x region (see

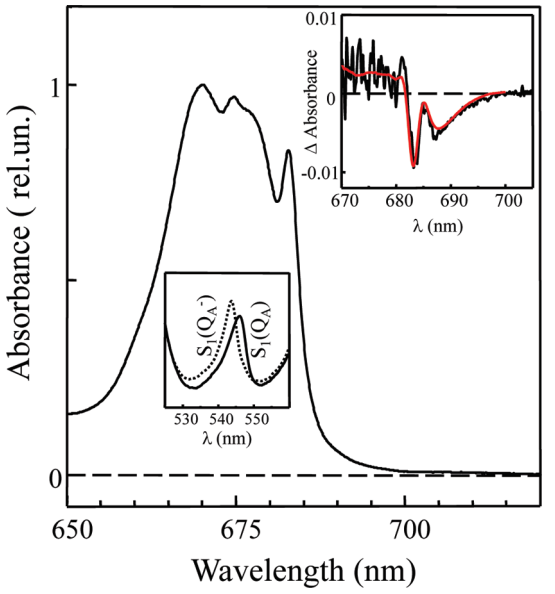

Figure 42. Low-temperature (5 K) absorption spectrum of the PSII core in the $S_1(Q_A^-)$ state. HB spectra for the latter sample (noisy red curve), compared with the sum of HB spectra obtained for the intact CP43 and CP47 complexes, is shown in the top inset. The lower inset shows the Q_x absorption region for the PSII core in $S_1(Q_A^-)$ (dotted curve) and $S_1(Q_A)$ (solid line) states; see the text for details. Reprinted with permission from ref 86. Copyright 2010 American Chemical Society.

the lower inset) shows that the RC is closed under our experimental conditions, as indicated by the ~80 cm^{-1} blue shift of the Q_x transition of the Pheos band. A bleach/shift induced by Q_A^- formation is characterized in detail in ref 366. Such a shift is attributed to the well-known electrochromic effect of $S_1(Q_A^-)$ on the neutral pigments of the RC.[366] In open RCs the effects due to HB have to be disentangled from the electrochromic shifts associated with the $S_1(Q_A^-)$ formation. Performing HB experiments on samples deliberately poised into the $S_1(Q_A^-)$ state makes it possible to circumvent this problem. Once effects due to electrochromic shifts are (mostly) excluded, the sum of the saturated HB spectra (readjusted for relative contributions from CP43 and CP47; λ_B = 496.5 nm) obtained for the intact *isolated* CP47[9] and CP43[10] complexes is very similar to the subtracted saturated nonresonant hole obtained for the PSII core.[86] The extracted HB spectrum for the PSII core is shown in the top inset of Figure 42 as the noisy dotted curve. This spectrum is the difference between the saturated HB spectrum in the $S_1(Q_A^-)$ state and the HB spectrum dominated by the electrochromic shift associated with $S_1(Q_A^-)$ formation. This agreement between the two HB curves discussed above suggests that the optical spectra discussed in section 5.1.2 correspond to the intact CP43 and CP47 complexes as the same low-energy states seem to be observed in intact PSII core system. This is further supported by the fact that any combination of saturated HB spectra for intact CP43[10,85] and sample 1A (i.e., destabilized CP47 complex described in section 5.1.2.2 and discussed in detail in refs 9 and 86 could not fit the extracted nonresonant hole obtained for the PSII core. In fact, the fits were very bad as the HB spectrum obtained for the destabilized CP47 was significantly blue-shifted.

5.4. The Fenna−Matthews−Olson (FMO) Proteins

FMO is the simplest PC found in nature and therefore a useful test object for developing new methods of photosynthesis

dx.doi.org/10.1021/cr100234j |*Chem. Rev.* 2011, 111, 4546–4598

research. It was the first BChl-containing protein to have its structure determined,[373] and the experimental and modeling studies of this protein have been a major source of our understanding regarding pigment−protein interaction and pigment site energies. Although these interesting complexes were studied for more than two decades, they are still a subject of active investigations and new insights continue to emerge.[83,374,375] In brief, the green sulfur photosynthetic bacteria are anoxygeneic phototrophs that contain unique antenna known as chlorosomes.[376] In addition to the chlorosomes, the green sulfur bacteria contain another BChl *a* protein, a peripheral antenna complex called the FMO protein.[377] The FMO connects the chlorosome to the RC in the cytoplasmic membrane and functionally forms a bridge to transfer the excitation energy.[378] Structures of FMO from *Prosthecochloris aestuarii* and *C. tepidum* are trimetric (C_3-symmetry), and each of the three monomers until recently has been thought to contain seven BChl *a* molecules.[373,377,379−383] (It was later suggested that the eighth Bchl *a* molecule is present in FMO; see below.)

Figure 43 from ref 118 depicts linear absorption and 2D electronic spectra (a) as well as mutual arrangement of the seven BChls in the FMO complex (b) of *C. tepidum*. Protein is omitted for clarity. BChl *a* 1 and 2 are on the surface of the monomer protein, while BChl *a* 3, 4, 5, 6, and 7 are buried in the core of the monomer. The recently discovered eighth BChl near the chlorosome,[82,384] not shown in Figure 43, was proposed to serve as an energy-transfer intermediate between the chromosome and the rest of the FMO protein. BChl *a* 1 and 2 are the tightest packed neighboring pair with the closest distance of 3.8 Å between atoms in two tetrapyrrole rings. In contrast to that, BChl *a* 2 and 7 are the farthest-distance pair, with 11.3 Å being the closest distance between any atoms in two tetrapyrrole rings. BChl *a* 7 is in the center of the seven molecules and has the closest average distance toward the other six BChl *a* molecules.[381] Although for a while it was a matter of debate, all recent modeling studies are in agreement that BChl 3 is the main contributor to the lowest-*E* state near 825 nm;[385,386,382] see Figure 43, frame b.

The optical properties of FMO proteins as manifested by various linear and nonlinear spectra of the Q_y band over the last two decades were recently reviewed in ref 401. Data obtained via SHB, pump−probe, photon-echo, and 2D ES (vide infra) were discussed[401] with emphasis on protein structure, site energies of BChls, coupling strengths, line width, and exciton energies, as well as the nature of the lowest energy band. Therefore, in this subsection we limit our comments to several issues related to SHB, FLN, and 2D ES.

Although the relative positions of the BChls are similar, and it has been assumed that Mg coordination and hydrogen-bonding interactions are also similar for individual BChls in FMO of different species,[381] spectroscopic measurements, including absorption and CD, suggest significant differences in the excitonic interactions between BChl *a* molecules in the FMO from *P. aestuarii* and *C. tepidum*.[387−389] Differences in exciton coupling have been confirmed by high-pressure HB studies,[394,395,398] but the origin of these differences is not completely clear. It seems to be widely accepted that it is sufficient to include only one monomer (i.e., not the whole trimer) in simulations of various types of optical spectra of FMO proteins,[401] although SHB data suggests that three states, connected by relatively slow EET, contribute to the lowest energy state near 825 nm.[390] This remains to be proven, but it is likely that these three states could be the lowest-energy states of the three subunits of the trimer. FMO has also been studied by means of FLN,[218] and

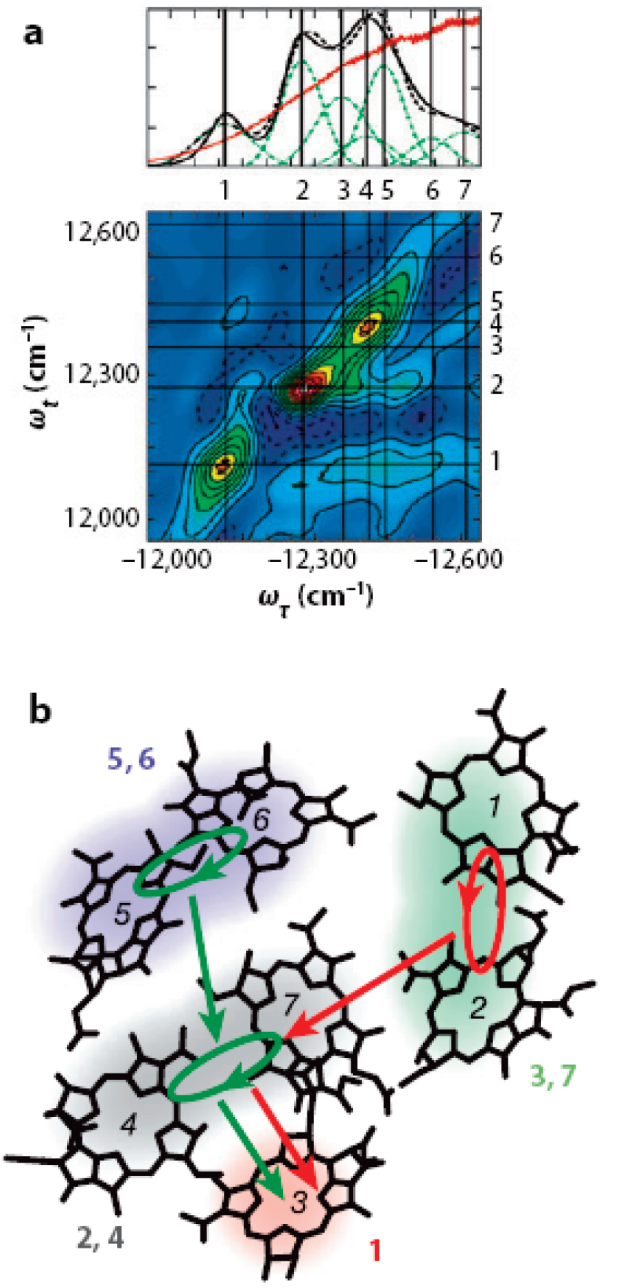

Figure 43. Exciton delocalization and energy flow in the Fenna−Matthews−Olson (FMO) complex. (a) The linear absorption and $T = 0$ fs 2D spectrum of the *C. tepidum* FMO complex. Individual exciton bands are shown in green, and the red curve indicates the laser spectrum in the experiment. (b) The FMO structural arrangement of the seven bacteriochlorophyll molecules (italic numbers) overlaid qualitatively with the delocalization patterns of the excitons (colored shading, bold numbers). Two main excitation energy transfer pathways are indicated by the red and green arrows. Reprinted by permission from ref 118. Copyright 2009 Annual Reviews Inc.

Franck−Condon factors of 30 Bchl *a* modes have been determined. As was common with the early FLN experiments, these factors appear to be significantly lower than those obtained by SHB.[217]

Theoretical and experimental advances in the elucidation of the dynamics of FMO complexes using 2D ES were also reviewed recently in ref 118. The excitonic couplings and site energies of

dx.doi.org/10.1021/cr100234j |*Chem. Rev.* 2011, 111, 4546–4598

excited states in the FMO complex have been used to describe the dynamics of excitation transfer.[385,391] Brixner et al.[28] studied EET in the FMO complex from *C. tepidum* using the 2D technique. 2D spectra were taken at several population times (t_2 or T in section 4.9), providing snapshots of excitation motion within the FMO complex. An example is shown in Figure 43, frame a, which shows the 2D spectrum at T = 0 fs. The cross peaks below the diagonal reveal coupling between excitonic states. The data were combined with theoretical modeling to demonstrate that the energy flow within the FMO complex occurs primarily through two energy transfer pathways (Figure 43, frame b),[28,392] which connect spatially proximate and excitonically coupled dimers. Cho et al.[392] presented a detailed theoretical analysis of the experimental data and suggested that population dynamics in the FMO complex can be described by a combination of Förster theory and modified Redfield equations. Brixner et al.[28] showed that although the two pathways affect an overall funneling of the energy from higher-energy sites to the lowest-energy trap, the energy transport is not a simple process of stepwise energy decrease from one exciton level to the next lowest level. Instead, it depends sensitively on detailed spatial properties of the excited-state wave functions, as predicted by Redfield theory. In addition, BChl 3 was confirmed as the energy trap within the FMO monomer. 2D optical studies by Fleming et al. revealed a long-lasting coherence in FMO complexes,[245] and the strength of the excitonic coupling of the pigments was determined experimentally.[28] Interestingly, these phenomena can also be considered from the viewpoint of quantum entanglement.[393]

Until recently, all spectroscopy data on FMO was interpreted by assuming seven pigments per monomer.[111,118,218,385,386,390,391,394−398] Recent X-ray structures[82,384] (PDB ID 3BSD and 3ENI), as mentioned above, showed an extra eighth BChl *a*, although the occupancy of the respective site appears to be lower than unity.[82] The presence of the eighth Bchl *a* molecule was confirmed in 2009 using X-ray diffraction at 1.3 Å resolution (PDB ID 3EOJ). It is distant from other pigments and located in a cleft in the protein surface, bridging the gap between the base plate pigments and the core BChl *a*, thus increasing EET efficiency.[399] Although both *P. aestuarii* and *C. tepidum* appear to have this eighth pigment, the respective binding interactions are significantly different. In both variants, the carbonyl oxygen of residue 123 binds to the central Mg atom, while *P. aestuarii's* eighth pigment is additionally linked by an Oγ atom of serine 168. Thus, the eighth pigment is pentacoordinated in *C. tepidum*, while hexacoordinated in *P. aestuarii*. Discovery of this new pigment has added a new challenge to reevaluate the relationship between the atomic structure and optical spectra. In recent literature, it has been assumed that the difference in coordination of the eighth pigment is possibly the key to their spectral differences, as the other seven BChl *a* molecules are nearly identical in these two variants.[82,399] Very recently Renger et al.[375] provided structure-based calculations of the optical properties of the FMO protein demonstrating that the eighth pigment is indeed the linker to the baseplate, confirming suggestions from crystallographic studies.[82] It has been shown that the main entrance route for the excitation energy into FMO is via the highest exciton state, which has the largest contribution from the eighth BChl.[375]

6. FINAL REMARKS AND THE FUTURE OF SHB SPECTROSCOPY IN THE ERA OF SINGLE MOLECULE SPECTROSCOPY

It has been demonstrated that SHB remains an active and expanding area of spectroscopy, although some of the key players have passed away in the past decade (e.g., Karl Rebane, Roman Personov, Gerald J. Small, John M. Hayes) or retired (e.g., Josef Friedrich, Urs Wild). Nevertheless, many groups (besides ours) remain active in the application of SHB (e.g., Krausz's, van Grondelle's, Völker's, Freiberg's, and Riesen's groups) and SPCS (e.g., Orrit's, Moerner's, Aartsma's, Brecht's, and Köhler's groups) to various biological systems, including photosynthetic complexes. NPHB data discussed in this review demonstrated that this high-resolution spectroscopy allows studying the excited state electronic structure and excitation and/or electron transfer processes in PC. In summary, SHB spectroscopy provides information on (i) the static inhomogeneous broadening of $S_0 \rightarrow S_1$ transition, (ii) electron−phonon coupling parameters (S and ω_m), (iii) intermolecular Franck−Condon factors via vibronic satellite hole structure, (iv) the extent of correlation between the SDFs of different electronic states, (v) radiative lifetimes, (vi) dephasing time and the excitation energy transfer time, (vii) electron transfer rates from the zero point level, and (viii) energy landscape barrier distribution parameters. In addition, we have discussed several new developments in NPHB spectroscopy emphasizing the description of hole shapes and photoproducts in excitonically coupled systems. The models developed recently and discussed in this review should strengthen and expand this technique as a tool to understand the excitonic structure of complex biological systems. For example, our recent work provided important constraints and parameters for future, more advanced excitonic calculations of LHCII, CP29, CP43, CP47, and PSII core complexes. In addition, we have recently shown that the theoretical description of nonresonant holes is substantially more restrictive (in terms of possible site energies) than those of absorption and emission spectra.[85,86] Excitonic fitting of NPHB spectra can thus be used, together with other types of linear spectra such as CD and LD, to obtain and refine realistic site energies for complex systems. SHB can also provide information on the interaction of the probe with the protein environment, the range of these interactions, and on spectral diffusion, i.e. on the protein motion in conformational phase space (on how this motion is reflected in optical spectra). For example, several examples utilizing SHB and SMS/SPCS have been discussed in this review, where multilevel systems had to be considered, indicating that the mechanism of NPHB spectroscopy is due to a hierarchy of configurational relaxation events triggered by electronic excitation.

Below we provide some of our thoughts as to what further research should hope to accomplish in the field of NPHB and SPCS, regarding application of these techniques in the area of photosynthesis research. For example, assigning chlorophylls (Chls) to various excitonic states is crucial for understanding how these systems work. By using recently developed computational models,[40,85,86] analyzing the unique redistribution of absorption intensity in nonresonant HB spectra should ease this process by providing a rigorous test for Chl site energy assignments. For high-level studies, however, these models must be adapted to include a more advanced description of both energy transfer broadening and coupling to phonons and vibrational modes. In addition, challenges remain in applying these methods to *resonant* HB spectra; although the theoretical description is not difficult, for complex systems (with multiple overlapping pigment distributions) the computational challenges can be daunting. The extension of excitonic HB theories to resonant HB spectra (and especially ΔFLN spectra) will be a key challenge to fully realize the power of these techniques. A related problem in NPHB and SPCS modeling is the treatment of photoproduct

distribution (in NPHB) and spectral diffusion (both NPHB and SPCS), each of which may provide important insight into the structural dynamics of the pigment−protein complexes studied (for example, the characterization of multiple-level systems and the apparent hierarchy of disorder in protein systems).[70] Another possible future development is the combination of phonon spectroscopy by SHB and ΔFLN with inelastic neutron scattering[178] in order to separate contributions to the one-phonon profile arising from the protein phonon density of states (DOS) and from el−ph coupling. This approach may provide further insight into the interaction of electronic or excitonic transitions with protein dynamics. Only through detailed theoretical modeling of high-resolution experimental data can such important problems be assessed.

We anticipate that SHB and SPCS will also provide more insight into the mechanisms and the pathways of primary charge transfer in PSII core. It remains to be confirmed whether PSII core possesses parallel primary charge transfer pathways. For example, recently Renger and Schlodder[11] suggested that the primary charge separation in PSII core from Chl_{D1} could compete with exciton relaxation into a low-lying charge-transfer/excited state of the "special pair". The work on protein dynamics of various PC may provide additional insight on fine-tuning of the energy of the excited states which, as suggested by Fleming et al.[27,116] and recently discussed by Brecht et al.[76] and Romero et al.,[344] could optimize the extremely efficient EET in PC. In summary, NPHB and SPCS may be utilized to develop a joint comprehensive picture of protein dynamics and related spectral diffusion phenomena in various PCs.

The role of quantum entanglement in biomolecular systems has been recently reviewed in ref 393 with the focus on recent theoretical calculations and the relationship between entanglement and other quantum mechanical features that are observed and predicted in light-harvesting complexes via 2D ES. A number of possible extensions of the current work have also been proposed.[393] New types of 2D techniques can be developed; it has been proposed that by looking at a smarter representation of the 2D spectra using a particular set of pulses, the correlated dynamics of the double excited states could be probed.[400] The latter is very important, as 2D spectra can be obscured by overlapping contributions of single and double exciton resonances.[401] It is anticipated that new coherent control strategies with shaped excitation pulses will be developed,[401] providing new insight into quantum mechanical phenomena in biologically functional structures,[393] in particular in light-harvesting components of photosynthetic organisms.[402]

Finally, we note one of the very recent developments in SHB. Namely, it has been demonstrated that SHB can be performed on electronic transition *in diffuse reflection* mode[403] (what is believed to be the first time). SHB (at T = 3 K) was applied to the electronic origin of the $^4A_2(F) \rightarrow {}^4T_1(P)$ transition of a 400 μm thick film of nanocrystalline $LiGa_5O_8$:Co(II) (average particle size ≈ 50 nm). For this particular material, the authors observed signal-to-noise ratios about 16 times better in diffuse reflection compared to HB spectra in luminescence excitation measurements. This opens new possible applications; for example, one could easily measure charge transfer processes in opaque nanocrystalline materials and molecules adsorbed on various surfaces used in various photovoltaic devices. In particular, the diffuse reflection SHB should be used to study opaque materials with very low luminescence quantum yield. Thus, we anticipate that SHB will continue to provide insight into the electronic structure in complex biological and nonbiological systems.

AUTHOR INFORMATION

Corresponding Author

*E-mail: ryszard@ksu.edu.

BIOGRAPHIES

Ryszard Jankowiak is a Professor of Physical Chemistry at Kansas State University (Manhattan, KS). After earning his doctoral degree in condensed matter physics/spectroscopy from Poland's Technical University of Gdańsk in 1981, he worked for the Technical University of Gdańsk, Camerino University in Italy (1981), Philipps University in Germany (1981−1985), and the U.S. Department of Energy's Ames Laboratory (1985−2005), which is associated with Iowa State University, Ames, Iowa. He worked as a senior scientist at Ames Laboratory USDOE until 2005. He was also an Adjunct Professor at Iowa State University (Department of Chemistry) from 2002 to 2005. In June 2005, he joined Kansas State University in Manhattan, KS. His research interests include molecular electronic spectroscopy, laser-based spectroscopies, low-temperature protein dynamics, and excitation energy and electron transfer processes in photosynthesis using hole-burning spectroscopy. He is also a research affiliate of the Photosynthetic Antenna Research Center (PARC), Washington University, Saint Louis, and a member of the Johnson Center for Basic Cancer Research (Manhattan, KS), where he continues to develop methods for early diagnosis of cancer risk. He has published over 190 research papers, including several invited reviews and 10 book chapters.

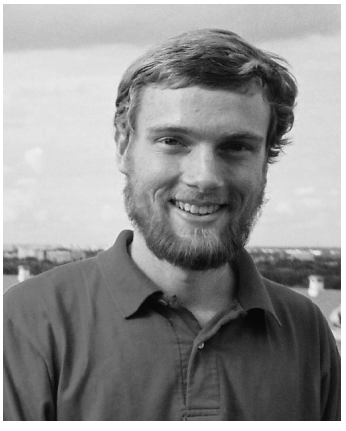

Mike Reppert began research in 2005 as a sophomore at Kansas State University (KSU) during a summer undergraduate internship in the laboratory of Prof. Ryszard Jankowiak at Ames Laboratory USDOE. As an undergraduate at KSU, he continued research under

Prof. Jankowiak (KSU Chemistry) and Prof. Virginia Naibo (KSU Mathematics) until graduating in 2009 with B.S. degrees in Chemistry, Biochemistry, and Mathematics. He spent the next year on a Fulbright scholarship conducting research in the laboratory of Prof. Bolesław Kozankiewicz at the Institute of Physics (Polish Academy of Sciences) in Warsaw, Poland. He is currently a doctoral student at the Massachusetts Institute of Technology in Cambridge, MA. His current research interests include the theoretical description of energy/electron transfer processes in complex biological systems, particularly as probed using various laser-based spectroscopic techniques. He has coauthored 10 papers.

Valter Zazubovich received his Ph.D. in condensed matter physics from the University of Tartu, Estonia, in 1999. His graduate work, performed under supervision of Prof. Jaak Kikas, focused on impurity center spectroscopy in amorphous and incommensurate solids and included short-term research stays at the Universities of Helsinki and Bayreuth and Technical University of Munich (the latter two with Prof. Josef Friedrich). He then joined the group of Prof. Gerald J. Small (led by Prof. Ryszard Jankowiak after G.J.S. passed away in 2004) at Iowa State University and Ames Laboratory, USDOE. There he employed various high-resolution spectroscopic techniques to study energy and charge transfer processes and pigment−protein interactions in photosynthetic pigment−protein complexes. In 2005 Dr. Zazubovich joined the Physics Department of Concordia University in Montreal, Canada, where he is an Associate Professor of Biophysics. In addition to photosynthesis research by means of high-resolution optical spectroscopy, his interests include low-temperature protein dynamics and the development of novel biosensors and biomimetic sensors for the detection of explosives.

Jörg Pieper is a Professor of Biological Physics at the University of Tartu, Estonia. He received his Ph.D. in biological and condensed matter physics from Humboldt University, Berlin, Germany, in 2000. His thesis on energy level structure and electron−phonon-coupling of the light-harvesting complex II of green plants was supervised by Prof. J. Voigt. It was carried out in cooperation with the group of Prof. Gerald J. Small and Prof. Ryszard Jankowiak, including two research visits at Iowa State University, Ames, IA, where he applied hole-burning spectroscopy to photosynthetic pigment−protein complexes of green plants. In 2000, he joined the Hahn-Meitner Institute Berlin, studying protein dynamics and structure−dynamics−function relationships in proteins using quasielastic neutron scattering partly combined with laser excitation in laser−neutron pump−probe experiments. From 2005 to 2010 Dr. Pieper was a researcher at Max-Volmer Laboratory of the Technical University (TU) Berlin, Germany. In September 2010 he joined the University of Tartu, Estonia. His research interests include the study of excitation energy transfer processes and electron−phonon coupling in photosynthesis using low-temperature site-selective and hole-burning spectroscopies, as well as the functional significance of protein dynamics at physiological temperatures as revealed by neutron scattering.

Tonu Reinot received his Ph.D. in condensed matter physics from the University of Tartu, Estonia, in 1993. His graduate work was performed under the supervision of Prof. Jaak Aaviksoo; it focused on polariton features of molecular crystals and on impurity center behavior in different solid matrices. He then joined the group of Prof. Gerald J. Small (led by Prof. Ryszard Jankowiak after G.J.S. passed away in 2004) at Iowa State University and Ames Laboratory, USDOE. There he employed high-resolution hole-burning and single molecule spectroscopic techniques to study various hyperquenched glasses and light-harvesting biological complexes, as well as cellular systems and tissues in order to distinguish between their normal and cancerous states. Currently, he works in the Center for Sustainable Environmental Technologies in Iowa State University.

ACKNOWLEDGMENT

R.J. (and in part M.R./T.R.) acknowledges support from the DOE EPSCoR (DE-FG02-08ER46504) and National Science Foundation under grants CHE-0907958 and EPS-0903806 and matching support from the State of Kansas through Kansas Technology Enterprise Corp. V.Z. acknowledges support from

NSERC and CFI. J.P. gratefully acknowledges support from Deutsche Forschungsgemeinschaft at TU Berlin (SFB 429, TP A1). We are thankful for many discussions with the late Dr. John M. Hayes and the late Prof. Gerald J. Small during our employment at Ames Laboratory USDOE, Iowa State University. Authors also acknowledge useful discussions with Prof. Elmars Krausz from the Research School of Chemistry, Australian National University; Prof. Arvi Freiberg and Dr. Margus Rätsep from the Institute of Physics, University of Tartu, Estonia; Dr. Michael Seibert from NREL, Golden, CO; Prof. Petra Fromme, Arizona State University; Dr. David Tiede, Argonne National Laboratory; Prof. Robert Blankenship, Washington University; and Dr. Rafael Picorel from the Aula Dei, Zaragoza, Spain. In addition, we thank past (Kerry J. Riley) and present graduate students (Bhanu Neupane, Khem Acharya, Nicoleta Herascu) and past postdoctoral fellows [in particular Dr. Nhan Dang (currently at Los Alamos National Laboratory, NM)], who have contributed to our recent research on NPHB and SPCS. Particular appreciation is extended to R.J.'s current group members for careful reading of the manuscript (Dr. X. Feng, B. Neupane, K. Acharya, M. Koirala, and Ch. Lin) and help with references (B. Neupane and K. Acharya).

ABBREVIATIONS:

BChl	bacteriochlorophyll
BPheo	bacteriopheophytine
BRC	bacterial reaction centers
ω_B	burn frequency
CS	charge separation
Chl	chlorophyll
$V_{1,2}$	coupling matrix element
α	Debye−Waller factor
ΔFLN	delta FLN
DOS	density of states
el−ph	electron−phonon
ET	electron transfer
el−vibr	electron vibrational
EET	excitation energy transfer
λ_{ex}	excitation wavelength
FLN	fluorescence line narrowing
FLNS	fluorescence line narrowing spectroscopy
FC	Franck−Condon
fwhm	full width at half-maximum
HB	hole-burning
HGK	hole growth kinetics
Γ_{hom}	homogeneous line width
S	Huang−Rhys factor
Γ_{inh}	inhomogeneous broadening
IDF	inhomogeneous distribution function
TLS	two level systems
TLS_{int}	intrinsic TLS
LHCI	light harvesting complex I
LHCII	light harvesting complex II
MLS	multilevel system
NLN	nonline narrowed
NPHB	nonphotochemical hole-burning
Pheo	pheophytin
PSB	phonon sideband
PSBH	phonon sideband hole
PHB	photochemical hole-burning
PSI	photosystem I
PSII	photosystem II
PC	photosynthetic complexes
RC	reaction center
SHB	spectral hole-burning
SMS	single molecule spectroscopy
SPCS	single photosynthetic complex spectroscopy
SDF	site distribution function
2D ES	two-dimensional electronic spectroscopy
λ	tunneling parameter
TLS	two-level systems
ZPH	zero-phonon hole
ZPL	zero-phonon line
ZPA	zero-phonon action

REFERENCES

(1) Witt, H. T.; Müller, A.; Rumberg, B.*Nature* **1963**, *197*, 987.
(2) Barber, J. *Q. Rev. Biophys.* **2003**, *36*, 71.
(3) Ferreira, K. N.; Iverson, T. M.; Maghlaoui, K.; Barber, J.; Iwata, S. *Science* **2004**, *303*, 1831.
(4) Loll, B.; Kern, J.; Saenger, W.; Zouni, A.; Biesiadka, J. *Nature* **2005**, *438*, 1040.
(5) Zouni, A.; Witt, H. T.; Kern, J.; Fromme, P.; Krauβ, N.; Saenger, W.; Orth, P. *Nature* **2001**, *409*, 739.
(6) Jordan, P.; Fromme, P.; Witt, H. T.; Klukas, O.; Saenger, W.; Krauss, N. *Nature* **2001**, *411*, 909.
(7) Guskov, A.; Kern, J.; Gabdulkhakov, A.; Broser, M.; Zouni, A.; Saenger, W. *Nat. Struct. Mol. Biol.* **2009**, *16*, 334.
(8) Deisenhofer, J.; Epp, O.; Sinning, I.; Michel, H. *J. Mol. Biol.* **1995**, *246*, 429.
(9) Neupane, B.; Dang, N. C.; Acharya, K.; Reppert, M.; Zazubovich, V.; Picorel, R.; Seibert, M.; Jankowiak, R. *J. Am. Chem. Soc.* **2010**, *132*, 4214.
(10) Dang, N. C.; Zazubovich, V.; Reppert, M.; Neupane, B.; Picorel, R.; Seibert, M.; Jankowiak, R. *J. Phys. Chem. B* **2008**, *112*, 9921.
(11) Renger, T.; Schlodder, E. *ChemPhysChem* **2010**, *11*, 1141.
(12) Hughes, J. L.; Picorel, R.; Seibert, M.; Krausz, E. *Biochemistry* **2006**, *45*, 12345.
(13) Tumino, G.; Casazza, A. P.; Engelmann, E.; Garlaschi, F. M.; Zucchelli, G.; Jennings, R. C. *Biochemistry* **2008**, *47*, 10449.
(14) Årsköld, S., P. A.; Prince, B. J.; Krausz, E.; Smith, P. J.; Pace, R. J.; Picorel, R.; Seibert, M. *J. Lumin.* **2004**, *108*, 97.
(15) de Weerd, F. L.; van Stokkum, I. H. M.; van Amerongen, H.; Dekker, J. P.; van Grondelle, R. *Biophys. J.* **2002**, *82*, 1586.
(16) Miloslavina, Y.; Szczepaniak, M.; Müller, M. G.; Sander, J.; Nowaczyk, M.; Rögner, M.; Holzwarth, A. R. *Biochemistry* **2006**, *45*, 2436.
(17) Hughes, J. L.; Prince, B. J.; Krausz, E.; Smith, P. J.; Pace, R. J.; Riesen, H. *J. Phys. Chem. B* **2004**, *108*, 10428.
(18) Vasil'ev, S.; Orth, P.; Zouni, A.; Owens, T. G.; Bruce, D. *Proc. Natl. Acad. Sci. U. S. A.* **2001**, *98*, 8602.
(19) Pawlowicz, N. P.; Groot, M. L.; van Stokkum, I. H. M.; Breton, J.; van Grondelle, R. *Biophys. J.* **2007**, *93*, 2732.
(20) Fromme, P. *Photosynthetic Protein Complexes: A Structural Approach*; Wiley-VCH Verlag: Weinheim, Germany, 2008; p 1.
(21) Deisenhofer, J.; Michel, H. *New Compr. Biochem.* **1992**, *23*, 103.
(22) Hu, X.; Ritz, T.; Damjanović, A.; Autenrieth, F.; Schulten, K. *Q. Rev. Biophys.* **2002**, *35*, 1.
(23) Hu, X.; Schulten, K. *Phys. Today* **1997**, *50*, 28.
(24) Ermler, U.; Fritzsch, G.; Buchanan, S. K.; Michel, H. *Structure* **1994**, *2*, 925.
(25) Kálmán, L.; Williams, J. C.; Allen, J. P. *Photosynth. Res.* **2008**, *98*, 643.
(26) Berlin, Y.; Burin, A.; Friedrich, J.; Köhler, J. *Phys. Life Rev.* **2006**, *3*, 262.
(27) Read, E. L.; Lee, H.; Fleming, G. R. *Photosynth. Res.* **2009**, *101*, 233.
(28) Brixner, T.; Stenger, J.; Vaswani, H. M.; Cho, M.; Blankenship, R. E.; Fleming, G. R. *Nature* **2005**, *434*, 625.

(29) Berera, R.; van Grondelle, R.; Kennis, J. T. M. *Photosynth. Res.* **2009**, *101*, 105.
(30) Edington, M. D.; Riter, R. E.; Beck, W. F. *J. Phys. Chem. B* **1997**, *101*, 4473.
(31) Salverda, J. M.; Vengris, M.; Krueger, B. P.; Scholes, G. D.; Czarnoleski, A. R.; Novoderezhkin, V.; van Amerongen, H.; van Grondelle, R. *Biophys. J.* **2003**, *84*, 450.
(32) De Vries, H.; Wiersma, D. A. *J. Chem. Phys.* **1980**, *72*, 1851.
(33) Rebane, K. K. *Impurity Spectra of Solids*; Plenum: New York, 1970; p 1.
(34) Jankowiak, R.; Hayes, J. M.; Small, G. J. *Chem. Rev* **1993**, *93*, 1471.
(35) Jankowiak, R.; Small, G. J. *Photosynth. React. Cent.* **1993**, *2*, 133.
(36) Völker, S. In *Relaxation Processes in Molecular Excited States*; Fünfschilling, J., Ed.; Kluwer Academic Publishers: Dordrecht, 1989; p 113.
(37) Moerner, W. E. *Topics in Current Physics. Persistent Spectral Hole Burning: Science and Applications*; Springer-Verlag: New York, 1987; p 1.
(38) Reinot, T.; Zazubovich, V.; Hayes, J. M.; Small, G. J. *J. Phys. Chem. B* **2001**, *105*, 5083.
(39) Reppert, M.; Naibo, V.; Jankowiak, R. *Chem. Phys.* **2010**, *367*, 27.
(40) Reppert, M.; Naibo, V.; Jankowiak, R. *J. Chem. Phys.* **2009**, *131*, 234104.
(41) Sigl, A.; Orrit, M.; Reinot, T.; Jankowiak, R.; Friedrich, J. *J. Chem. Phys.* **2007**, *127*, 084510.
(42) Vo-Dinh, T.; Velthorst, N. H.; Moore, D. S.; Schräder, B. *Pure Appl. Chem.* **1997**, *69*, 1435.
(43) Köhler, B. E. In *Chemical and Biochemical Applications of Lasers*; Moore, C. B., Ed.; Academic Press: New York, 1979; p 31.
(44) van Amerongen, H.; Valkunas, L.; van Grondelle, R. *Photosynthetic Excitons*; World Scientific: Singapore, 2000; p 168.
(45) Fidy, J.; Laberge, M.; Kaposi, A. D.; Vanderkooi, J. M. *Biochim. Biophys. Acta* **1998**, *1386*, 331.
(46) Jankowiak, R. In *Shpol'skii Spectroscopy and Related Site Selective Methods*; Gooijer, C., Ariese, F., Hofstraat, J. W., Eds.; John Wiley & Sons: New York, 2000; p 235.
(47) Hughes, J. L.; Krausz, E. In *Applications of Physical Methods to Inorganic and Bioinorganic Chemistry*;Scott, R. A., Lukehart, C. M., Eds.; John Wiley and Sons: New York, 2007; p 42.
(48) Purchase, R.; Völker, S. *Photosynth. Res.* **2009**, *101*, 245.
(49) Kharlamov, B. M.; Personov, R. I.; Bykovskaya, L. A. *Opt. Commun.* **1974**, *12*, 191.
(50) Gorokhovskii, A. A.; Kaarli, R. K.; Rebane, L. A. *JETP Lett.* **1974**, *20*, 216.
(51) Bogner, U.; Schwarz, R. *Phys. Rev. B* **1981**, *24*, 2846.
(52) Jaaniso, R. *Proc. Acad. Sci. Estonian SSR Phys. Math.* **1985**, *34*, 277.
(53) Yaaniso, R. V.; Avarmaa, R. A. *J. Appl. Spectrosc.* **1986**, *44*, 365.
(54) Fünfschilling, J.; Glatz, D.; Zschokke-Gränacher, I. *J. Lumin.* **1986**, *36*, 85.
(55) Rätsep, M.; Freiberg, A. *Chem. Phys. Lett.* **2003**, *377*, 371.
(56) Timpmann, K.; Rätsep, M.; Hunter, C. N.; Freiberg, A. *J. Phys. Chem. B* **2004**, *108*, 10581.
(57) Freiberg, A.; Rätsep, M.; Timpmann, K.; Trinkunas, G. *Chem. Phys.* **2009**, *357*, 102.
(58) Rätsep, M.; Linnanto, J.; Freiberg, A. *J. Chem. Phys.* **2009**, *130*, 194501.
(59) Rätsep, M.; Pajusalu, M.; Freiberg, A. *Chem. Phys. Lett.* **2009**, *479*, 140.
(60) Rätsep, M.; Pieper, J.; Irrgang, K. D.; Freiberg, A. *J. Phys. Chem. B* **2008**, *112*, 110.
(61) Rätsep, M.; Freiberg, A. *J. Lumin.* **2007**, *127*, 251.
(62) Berlin, Y.; Burin, A.; Friedrich, J.; Köhler, J. *Phys. Life Rev.* **2007**, *4*, 64.
(63) Ponkratov, V. V.; Friedrich, J.; Vanderkooi, J. M.; Burin, A. L.; Berlin, Y. A. *J. Low Temp. Phys.* **2004**, *137*, 289.
(64) Rigler, R.; Orrit, M.; Basché, Th. *Single Molecule Spectroscopy (Nobel Conference Lectures—Springer Series in Chemical Physics)*; Springer: Berlin, 2001; p 67.
(65) Barkai, E.; Jung, Y.; Silbey, R. *Annu. Rev. Phys. Chem.* **2004**, *55*, 457.
(66) Riley, K. J.; Reinot, T.; Jankowiak, R.; Fromme, P.; Zazubovich, V. *J. Phys. Chem. B* **2007**, *111*, 286.
(67) Richter, M. F.; Baier, J.; Southall, J.; Cogdell, R. J.; Oellerich, S.; Köhler, J. *Proc. Natl. Acad. Sci. U. S. A.* **2007**, *104*, 20280.
(68) Oellerich, S.; Ketelaars, M.; Segura, J.; Margis, G.; de Ruijter, W.; Köhler, J.; Schmidt, J.; Aartsma, T. J. *Single Mol.* **2002**, *3*, 319.
(69) Hofmann, C.; Ketelaars, M.; Matsushita, M.; Michel, H.; Aartsma, T. J.; Köhler, J. *Phys. Rev. Lett.* **2003**, *90*, 013004.
(70) Grozdanov, D.; Herascu, N.; Reinot, T.; Jankowiak, R.; Zazubovich, V. *J. Phys. Chem. B* **2010**, *114*, 3426.
(71) Bopp, M. A.; Jia, Y.; Li, L.; Cogdell, R. J.; Hochstrasser, R. M. *Proc. Natl. Acad. Sci. U. S. A.* **1997**, *94*, 10630.
(72) Goldsmith, R. H.; Moerner, W. E. *Nat. Chem.* **2010**, *2*, 179.
(73) Brecht, M.; Radics, V.; Nieder, J. B; Studier, H.; Bittl, R. *Biochemistry* **2008**, *47*, 5536.
(74) Brecht, M.; Studier, H.; Elli, A. F.; Jelezko, F.; Bittl, R. *Biochemistry* **2007**, *46*, 799.
(75) Elli, A. F.; Jelezko, F.; Tietz, C.; Studier, H.; Brecht, M.; Bittl, R.; Wrachtrup, J. *Biochemisty* **2006**, *45*, 1454.
(76) Brecht, M.; Radics, V.; Nieder, J. B.; Bittl, R. *Proc. Natl. Acad. Sci. U. S. A.* **2009**, *106*, 11857.
(77) Novoderezhkin, V. I.; Rutkauskas, D.; van Grondelle, R. *Biophys. J.* **2006**, *90*, 2890.
(78) Rutkauskas, D.; Novoderezhkin, V.; Cogdell, R. J.; van Grondelle, R. *Biophys. J.* **2005**, *88*, 422.
(79) Saga, Y.; Tamiaki, H. *Cell Biochem. Biophys.* **2004**, *40*, 149.
(80) Janusonis, J.; Valkunas, L.; Rutkauskas, D.; van Grondelle, R. *Biophys. J.* **2008**, *94*, 1348.
(81) Krüger, T. P. J.; Novoderezhkin, V. I.; Ilioaia, C.; van Grondelle, R. *Biophys. J.* **2010**, *98*, 3093.
(82) Tronrud, D. E.; Wen, J.; Gay, L.; Blankenship, R. E. *Photosynth. Res.* **2009**, *100*, 79.
(83) Wen, J.; Zhang, H.; Gross, M.; Blankenship, R. E. *Proc. Natl. Acad. Sci. U. S. A.* **2009**, *106*, 6134.
(84) Jaschke, P. R.; Beatty, J. T. *Biochemistry* **2007**, *46*, 12491.
(85) Reppert, M.; Zazubovich, V.; Dang, N. C.; Seibert, M.; Jankowiak, R. *J. Phys. Chem. B* **2008**, *112*, 9934.
(86) Reppert, M.; Acharya, K.; Neupane, B.; Jankowiak, R. *J. Phys. Chem. B* **2010**, *114*, 11884.
(87) Deisenhofer, J.; Epp, O.; Miki, K.; Huber, R.; Michel, H. *J. Mol. Biol.* **1984**, *180*, 385.
(88) Amunts, A.; Drory, O.; Nelson, N. *Nature* **2007**, *447*, 58.
(89) Nield, J.; Barber, J. *Biochim. Biophys. Acta* **2006**, *1757*, 353.
(90) Liu, Z.; Yan, H.; Wang, K.; Kuang, T.; Zhang, J.; Gui, L.; An, X.; Chang, W. *Nature* **2004**, *428*, 287.
(91) Breton, J.; Vermeglio, V. *The Photosynthetic Bacterial Reaction Center II*; NATO ASI Sciences, Series A, Life Sciences; Plenum: New York, 1992; p 1.
(92) Kalitius, E.; Babendure, J. L.; Kalitene, Z.; Lin, S.; Taguchi, A. K. W.; Woodbury, N. W. *J. Phys. Chem. B* **2003**, *107*, 12029.
(93) Haffa, A. L. M.; Lin, S.; Williams, J. C.; Bowen, B. P.; Taguchi, A. K. W.; Allen, J. P.; Woodbury, N. W. *J. Phys. Chem. B* **2004**, *108*, 4.
(94) Reddy, N. R. S.; Kolaczkowski, S. V.; Small, G. J. *Science* **1993**, *260*, 68.
(95) Johnson, E. T.; Nagarajan, V.; Zazubovich, V.; Riley, K.; Small, G. J.; Parson, W. W. *Biochemistry* **2003**, *42*, 13673.
(96) Roszak, A. W.; Howard, T. D.; Southall, J.; Gardiner, A. T.; Law, C. J.; Isaacs, N. W.; Cogdell, R. J. *Science* **2003**, *302*, 1969.
(97) McDermott, G.; Prince, S. M.; Freer, A. A.; Hawthorntwaite-Lawless, A. M.; Papiz, M. Z.; Cogdell, R. J.; Isaacs, N. W. *Nature* **1995**, *374*, 517.
(98) Schulten, K. In *Simplicity and Complexity in Proteins and Nucleic Acids*, Frauenfelder, H., Deisenhofer, J., Wolynes, P. G., Eds.; Dahlem University Press: Berlin,1995; p 227.
(99) Hu, X.; Ritz, T.; Damjanovic, A.; Schulten, K. *J. Phys. Chem. B* **1997**, *101*, 3854.

(100) Pullerits, T.; Chachisvilis, M.; Sundström, V. *J. Phys. Chem.* **1996**, *100*, 10787.
(101) Dahlbom, M.; Pullerits, T.; Mukamel, S.; Sundström, V. *J. Phys. Chem. B* **2001**, *105*, 5515.
(102) Trinkunas, G.; Freiberg, A. *J. Lumin.* **2006** *119−120*, 105.
(103) Wendling, M.; van Mourik, F.; van Stokkum, I. H. M.; Salverda, J. M.; Michel, H.; van Grondelle, R. *Biophys. J.* **2003**, *84*, 440.
(104) Pullerits, T.; Hess, S.; Herek, J. L.; Sundström, V. *J. Phys. Chem. B* **1997**, *101*, 10560.
(105) Shreve, A. P.; Trautman, J. K.; Frank, H. A.; Owens, T. G.; Albrecht, A. C. *Biochim. Biophys. Acta* **1991**, *1058*, 280.
(106) Davydov, A. S. *Theory of Molecular Excitons*; Plenum: New York, 1971; p 1.
(107) Frenkel, J. *Phys. Z. Sowjetunion* **1936**, *9*, 158.
(108) Renger, G. In *Bioenergetics*; Gräbner, P. Malazzio, G., Eds.; Birkhäuser Verlag: Basel, 1997; p 311.
(109) Förster, T. *Ann. Phys. (Leipzig)* **1984**, *2*, 55.
(110) Struve, W. S. In *Anoxygenic Photosynthetic Bacteria*; Blankenship, R. E., Madigan, M. T., Bauer, C. E., Eds.; Kluver Academic Publishers: Dordrecht, Netherlands, 1995; p 297.
(111) Adolphs, J.; Muh, F.; Madjet, M. E.A. *Photosynth. Res.* **2008**, *95*, 197.
(112) Raszewski, G.; Renger, T. *J. Am. Chem. Soc.* **2008**, *130*, 4431.
(113) van Grondelle, R.; Novoderezhkin, V. I. *Phys. Chem. Chem. Phys.* **2006**, *8*, 793.
(114) Dexter, D. *J. Chem. Phys.* **1953**, *21*, 836.
(115) Blankenship, R. E. *Molecular Mechanisms of Photosynthesis*; Blackwell Science Ltd.: London, 2008; p 42.
(116) Ishizaki, A.; Fleming, G. R. *J. Chem. Phys.* **2009**, *130*, 234110.
(117) May, V.; Kühn, O. *Charge and Energy Transfer Dynamics in Molecular Systems*; Wiley-VCH: New York, 2000; p 227.
(118) Cheng, Y.-C; Fleming, G. R. *Annu. Rev. Phys. Chem.* **2009**, *60*, 241.
(119) Berg, M.; Walsh, C. A.; Narasimhan, R.; Littau, K. A.; Fayer, M. D. *J. Chem. Phys. B* **1983**, *88*, 1564.
(120) Lyle, P. A.; Kolaczkowski, S. V.; Small, G. J. *J. Phys. Chem.* **1993**, *97*, 6924.
(121) Hayes, J. M.; Gillie, J. K.; Tang, D.; Small, G. J. *J. Biochim. Biophysics. Acta* **1988**, *932*, 287.
(122) Kolaczkowski, S. V.; Hayes, J. M.; Small, G. J. *J. Phys. Chem.* **1994**, *98*, 13418.
(123) Personov, R. I. In *Spectroscopy and Excitation Dynamics of Condensed Molecular Systems*; Agranovich, V. M., Hochstrasser, R. M., Eds.; Elsevier Science Ltd: Amsterdam, 1983; p 1.
(124) Osadko, I. S. In *Adv. Polym. Sci.*; Dusek, K., Ed.; Springer-Verlag: Berlin, 1994; p 123.
(125) Hofstrat, J. W.; Gooijer, C.; Velthorst, N. H. In *Molecular Luminescence Spectroscopy: Methods and Applications*; Schulman, S. G., Ed.; John Wiley & Sons: New York, 1988; p 383.
(126) Selzer, P. M. In *Topics in Applied Physics*; Yen, W. M., Selzer, P. M., Eds.; Springer Verlag: New York, 1986; p 113.
(127) Weber, M. J. In *Topics in Applied Physics*; Yen, W. M., Selzer, P. M., Eds.; Springer Verlag: New York, 1986; p 189.
(128) Fidy, J.; Vanderkooi, J. M. In *Light in Biology and Medicine*; Douglas, R. H., Moan, J., Rontó, Gy., Eds.; Plenum Press: New York, 1991; p 367.
(129) Weber, J. M. *J. Lumin.* **1987**, *36*, 179.
(130) Jankowiak, R.; Small, G. J. *Anal. Chem.* **1989**, *61*, 1023A.
(131) Price, B. P.; Wright, J. C. *Anal. Chem.* **1990**, *62*, 1989.
(132) Jankowiak, R.; Small, G. J. *Chem. Res. Toxicol.* **1991**, *4*, 256.
(133) Riesen, H. *Comments Inorg. Chem.* **1993**, *14*, 323.
(134) Denisov, Yu. V.; Kizel, V. A. *Opt. Spectrosc.* **1967**, *23*, 251.
(135) Szabo, A. *Phys. Rev. Lett.* **1970**, *25*, 924.
(136) Personov, R. I.; Al'Shitz, E. I.; Bykovskaya, L. A. *Opt. Commun.* **1972**, *6*, 169.
(137) Small, G. J.; Hayes, J. M.; Silbey, R. J. *J. Phys. Chem.* **1992**, *96*, 7499.
(138) Acharya, K.; Neupane, B.; Reppert, M.; Feng, X.; Jankowiak, R. *J. Phys. Chem. Lett.* **2010**, *1*, 2310.
(139) Boxer, S. G.; Lockhart, D. J.; Kirmaier, C.; Holten, D. In *Proceedings of the 22nd Jerusalem Symposium on Quantum Chemistry and Biochemistry*; Jortner, J., Pullman, B., Eds.; Kluwer Academic Publishers: Dordrecht, Netherlands, 1990; p 39.
(140) Hammes, S.; Mazzola, L.; Boxer, S. G.; Gaul, D. F.; Schenck, C. C. *Proc. Natl. Acad. Sci. U.S.A.* **1990**, *87*, 5682.
(141) Reddy, N. R. S.; Wu, H.-M.; Jankowiak, R.; Picorel, R.; Cogdell, R. J.; Small, G. J. *Photosynth. Res.* **1996**, *48*, 277.
(142) Rätsep, M., Small, G. J. In *Shpol'skii Spectroscopy and Other Site-Selection Methods*; Gooijer, C., Ariese, F., Hofstraat, J. W., Eds.; Wiley-Interscience: New York, 2000; p 381.
(143) Ketelaars, M.; Hofmann, C.; Köhler, J.; Howard, T. D.; Cogdell, R. J.; Schmidt, J.; Aartsma, T. J. *Biophys. J.* **2002**, *83*, 1701.
(144) Hofmann, C.; Michel, H.; van Heel, M.; Köhler, J. *Phys. Rev. Lett.* **2005**, *94*, 195501.
(145) Hofmann, C.; Aartsma, T. J; Michel, H.; Köhler, J. *New J. Phys.* **2004**, *6*, 8.
(146) Hofmann, C.; Aartsma, T. J; Michel, H.; Köhler, J. *Proc. Natl. Acad. Sci. U. S. A.* **2003**, *100*, 15534.
(147) Baier, J.; Richter, M. F.; Cogdell, R. J.; Oellerich, S.; Köhler, J. *J. Phys. Chem. B* **2007**, *111*, 1135.
(148) Baier, J.; Richter, M. F.; Cogdell, R. J.; Oellerich, S.; Köhler, J. *Phys. Rev. Lett.* **2008**, *100*, 018108.
(149) Janusonis, J.; Valkunas, L.; Rutkauskas, D.; van Grondelle, R. *Biophys. J.* **2008**, *94*, 1348.
(150) Rutkauskas, D.; Novoderezkhin, V.; Cogdell, R. J.; van Grondelle, R. *Biochemistry* **2004**, *43*, 4431.
(151) Jelezko, F.; Tietz, C.; Gerken, U.; Wrachtrup, J.; Bittl, R. *J. Phys. Chem. B* **2000**, *104*, 8093.
(152) Gerken, U.; Jelezko, F.; Götze, B.; Branschädel, M.; Tietz, C.; Ghosh, R.; Wrachtrup, J. *J. Phys. Chem. B* **2003**, *107*, 338.
(153) Tietz, C; Jelezko, F.; Gerken, U.; Schuler, S.; Schubert, A.; Rogl, H.; Wrachtrup, J. *Biophys. J.* **2001**, *81*, 556.
(154) de Boeij, W.; Pshenichnikov, M. S.; Wiersma, D. A. *Annu. Rev. Phys. Chem.* **1998**, *49*, 99.
(155) Hesselink, W. H.; Wiersma, D. A. In *Modern Problems in Condensed Matter*; Agranovich, V. M., Maradudin, A. A., Eds; Elsevier Science Ltd: Amsterdam, 1983; p 249.
(156) Walsh, C. A.; Berg, M.; Narasimhan, L. R.; Fayer, M. D. *Acc. Chem. Res.* **1987**, *20*, 120.
(157) Narasimhan, L. R.; Littau, K. A.; Pack, D. W.; Bai, Y. S.; Elschner, A.; Fayer, M. D. *Chem. Rev.* **1990**, *90*, 439.
(158) Mukamel, S. *Principles of Nonlinear Optical Spectroscopy*; Oxford University Press: New York, 1995; p 261.
(159) Stoneham, A. M. *Rev. Mod. Phys.* **1969**, *41*, 82.
(160) Friedrich, J.; Haarer, D. *Angew. Chem., Int. Ed. Engl.* **1984**, *23*, 113.
(161) Jankowiak, R.; Small, G. J. *Science* **1987**, *237*, 618.
(162) Kane, A. O. *Phys. Rev.* **1960**, *119*, 40.
(163) Dzyub, I. P.; Lubchenko, A. F. *Fiz. Tverd. Tela* **1961**, *3*, 3602.
(164) Silsbee, R. H. *Phys. Rev.* **1962**, *128*, 1726.
(165) Hayes, J. M.; Lyle, P. A.; Small, G. J. *J. Phys. Chem.* **1994**, *98*, 7337.
(166) Flecher, G.; Friedrich, J. *Chem. Phys. Lett.* **1977**, *50*, 32.
(167) Kikas, J. *Chem. Phys. Lett.* **1978**, *57*, 511.
(168) Koedijk, J. M. A.; Wannemacher, R.; Silbey, R. J.; Völker, S. *J. Phys. Chem.* **1996**, *100*, 19945.
(169) Jankowiak, R.; Small, G. J. In *Disorder Effects on Relaxation Processes*; Blumen, A., Richard, R., Eds.; Springer-Verlag: Berlin, 1994; p 425.
(170) Littau, K. A.; Fayer, M. D. *Chem. Phys. Lett.* **1991**, *176*, 551.
(171) Leeson, D. T.; Wiersma, D. A.; Fritsch, K.; Friedrich, J. *Phys. Chem.* **1997**, *101*, 6331.
(172) Jankowiak, R.; Small, G. J. *Phys. Rev.* **1993**, *B97*, 14805.
(173) Meijers, H. C.; Wiersma, D. A. *Phys. Rev. Lett.* **1992**, *68*, 381.
(174) Sapozhnikov, M. N. *Phys. Status Solidi B* **1976**, *75*, 11.
(175) Skinner, J. L. *Annu. Rev. Phys. Chem.* **1988**, *39*, 463.
(176) Di Bartolo, B. D. *Optical Interactions in Solids*; John Wiley and Sons: New York, 1968; p 222.

(177) Keil, T. *Phys. Rev.* **1965**, *140*, A601.
(178) Pieper, J.; Irrgang, K.-D.; Renger, G.; Lechner, R. E. *J. Phys. Chem. B.* **2004**, *108*, 10556.
(179) Orecchini, A.; Paciaroni, A.; Bizzarri, A. R.; Cannistraro, S. *J. Phys. Chem. B* **2002**, *106*, 12150.
(180) Paciaroni, A.; Orecchini, A.; Cinelli, S.; Onori, G.; Lechner, R. E.; Pieper, J. *Chem. Phys.* **2003**, *292*, 397.
(181) Kurkal, V.; Smith, J. C. *J. Am. Chem. Soc.* **2006**, *128*, 2356.
(182) Völker, S.; Macfarlane, R. M. *J. Chem. Phys.* **1980**, *73*, 4476.
(183) Shu, L.; Small, G. J. *Chem. Phys.* **1990**, *141*, 447.
(184) Shu, L.; Small, G. J. *J. Opt. Soc. Am. B* **1992**, *9*, 724.
(185) Jankowiak, R.; Tang, D.; Small, G. J.; Seibert, M. *J. Phys. Chem.* **1989**, *93*, 1649.
(186) Reppert, M.; Naibo, V.; Jankowiak, R. *J. Chem. Phys.* **2010**, *132*, 1.
(187) Reinot, T.; Small, G. J. *J. Chem. Phys* . **2001**, *114*, 9105.
(188) Oikawa, H.; Fujiyoshi, S.; Dewa, T.; Nango, M.; Matsushita, M. *J. Am. Chem. Soc.* **2008**, *130*, 4590.
(189) Baier, J.; Richter, M. F.; Cogdell, R. J.; Oellerich, S.; Köhler, J. *J. Phys. Chem. B* **2007**, *111*, 1135.
(190) Baier, J.; Richter, M. F.; Cogdell, R. J.; Oellerich, S.; Köhler, J. *Phys. Rev. Lett.* **2008**, *100*, 018108.
(191) Hughes, J. L.; Prince, B. J.; Peterson Årsköld, S.; Krausz, E.; Smith, P. J.; Pace, R. J.; Picorel, R.; Seibert, M. *J. Lumin.* **2004**, *108*, 131.
(192) Jankowiak, R.; Richert, R.; Bässler, H. *J. Phys. Chem.* **1985**, *89*, 4569.
(193) Kenney, M. J.; Jankowiak, R.; Small, G. J. *Chem. Phys.* **1990**, *146*, 47.
(194) Reinot, T.; Small, G. J. *J. Chem. Phys.* **2000**, *113*, 10207.
(195) Köhler, W.; Breinl, W.; Friedrich, J. *J. Phys. Chem.* **1985**, *89*, 2473.
(196) Elschner, A.; Bässler, H. *Chem. Phys.* **1988**, *123*, 305.
(197) Dang, N. C.; Reinot, T.; Reppert, M.; Jankowiak, R. *J. Phys. Chem. B* **2007**, *111*, 1582.
(198) Zazubovich, V.; Jankowiak, R.; Small, G. J. *J. Lumin.* **2002**, *98*, 123.
(199) Jang, S.; Newton, M. D.; Silbey, R. J. *Phys. Rev. Lett.* **2004**, *92*, 218301.
(200) Scholes, G. D.; Fleming, G. R. *J. Phys. Chem. B* **2000**, *104*, 1854.
(201) Mukai, K.; Abe, S.; Sumi, H. *J. Phys. Chem. B* **1999**, *103*, 6096.
(202) Baier, J.; Gabrielsen, M.; Oellerich, S.; Michel, H.; van Heel, M.; Cogdell, R. J.; Köhler, J. *Biophys. J.* **2009**, *97*, 2604.
(203) Reinot, T.; Dang, N. C.; Small, G. J. *J. Chem. Phys.* **2003**, *119*, 10404.
(204) Frauenfelder, H.; Sligar, S. G.; Wolynes, P. G. *Science* **1991**, *254*, 1598.
(205) Fenimore, P. W.; Frauenfelder, H.; McMahon, B. H.; Young, R. D. *Physica A* **2005**, *351*, 1.
(206) Reddy, N. R. S.; Picorel, R.; Small, G. J. *J. Phys. Chem.* **1992**, *96*, 6458.
(207) Zazubovich, V.; Jankowiak, R. *J. Lumin.* **2007**, *127*, 245.
(208) Avarmaa, R. A.; Rebane, K. K. *Spectrochim. Acta A* **1985**, *41*, 1365.
(209) Gillie, J. K.; Small, G. J.; Golbeck, J. H. *J. Phys. Chem.* **1989**, *93*, 1620.
(210) Kühn, O.; Renger, T.; May, V.; Voigt, J.; Pullerits, T.; Sundström, V. *Trends Photochem. Photobiol.* **1997**, *4*, 213.
(211) Chang, H.-C.; Small, G. J.; Jankowiak, R. *Chem. Phys.* **1995**, *194*, 323.
(212) den Hartog, F. T. H.; Dekker, J. P.; van Grondelle, R.; Völker, S. *J. Phys. Chem. B* **1998**, *102*, 11007.
(213) Pieper, J.; Rätsep, M.; Jankowiak, R.; Irrgang, K.-D.; Voigt, J.; Renger, G.; Small, G. J. *J. Phys. Chem. A* **1999**, *103*, 2412.
(214) Pieper, J.; Irrgang, K.-D.; Rätsep, M.; Voigt, J.; Renger, G.; Small, G. J. *Photochem. Photobiol.* **2000**, *71*, 574.
(215) Hayes, J. M.; Matsuzaki, S.; Rätsep, M.; Small, G. J. *J. Phys. Chem. B* **2000**, *104*, 5625.
(216) Zazubovich, V.; Tibe, I.; Small, G. J. *J. Phys. Chem. B* **2001**, *105*, 12410.
(217) Peterman, E. J. G.; Pullerits, T.; van Grondelle, R.; van Amerongen, H. *J. Phys. Chem. B* **1997**, *101*, 4448.
(218) Wendling, M.; Pullerits, T.; Przyjalogowski, M. A.; Vulto, S. I.; Aartsma, T. J.; van Grondelle, R.; van Amerongen, H. *J. Phys. Chem. B* **2000**, *104*, 5825.
(219) Pieper, J.; Schödel, R.; Irrgang, K.-D.; Voigt, J.; Renger, G. *J. Phys. Chem. B.* **2001**, *105*, 7115.
(220) Creemers, T. M. H.; De Caro, C. A.; Visschers, R. W.; van Grondelle, R.; Völker, S. *J. Phys. Chem. B* **1999**, *103*, 9770.
(221) Ihalainen, J. A.; Rätsep, M.; Jensen, P. E.; Scheller, H. V.; Croce, R.; Bassi, R.; Korppi-Tommola, J. E. I.; Freiberg, A. *J. Phys. Chem. B* **2003**, *107*, 9086.
(222) Pieper, J.; Rätsep, M.; Irrgang, K.-D.; Freiberg, A. *J. Phys. Chem. B* **2009**, *113*, 10870.
(223) Brecht, M.; Studier, H.; Radics, V.; Nieder, J. B.; Bittl, R. *J. Am. Chem. Soc.* **2008**, *130*, 17487.
(224) Mc Colgin, W. C.; Marchetti, A. P; Eberly, J. H. *J. Am. Chem. Soc.* **1978**, *100*, 5622.
(225) Pieper, J. Ph.D. Thesis, Humboldt Universität zu Berlin, 2000.
(226) Lee, I.; Hayes, J. M.; Small, G. J. *J. Chem. Phys.* **1989**, *91*, 3463.
(227) Pieper, J.; Voigt, J.; Renger, G.; Small, G. J. *Chem. Phys. Lett.* **1999**, *310*, 296.
(228) Reddy, N. R. S.; van Amerongen, H.; Kwa, S. L. S.; van Grondelle, R.; Small, G. J. *J. Phys. Chem.* **1994**, *98*, 4729.
(229) Jankowiak, R.; Cooper, R. S.; Zamzow, D.; Small, G. J.; Doskocil, G.; Jeffrey, A. M. *Chem. Res. Toxicol.* **1988**, *1*, 60.
(230) Zamzow, D.; Jankowiak, R.; Cooper, R. S.; Small, G. J. *Chem. Res. Toxicol.* **1989**, *2*, 29.
(231) Hofstraat, J. W.; Engelsma, M.; Gooijer, C.; Velthorst, N. H. *Spectrochim. Acta* **1989**, *45A*, 491.
(232) Wolf, J.; Myers, A. B. *Mol. Cryst. Liq. Cryst.* **1996**, *291*, 135.
(233) Jankowiak, R.; Rogan, E.; Cavalieri, E. L. *J. Phys. Chem. B* **2004**, *108*, 10266.
(234) van Oijen, A. M.; Ketelaars, M.; Köhler, J.; Aartsma, T. J.; Schmidt, J. *Biophys. J.* **2000**, *78*, 1570.
(235) Cho, M. *Chem. Rev.* **2008**, *108*, 1331.
(236) Tokmakoff, A. *J. Phys. Chem. A* **2000**, *104*, 4247.
(237) Jonas, D. M. *Annu. Rev. Phys. Chem.* **2003**, *54*, 425.
(238) Wagner, W.; Li, C.; Semmlow, J.; Warren, W. S. *Optics Express* **2005**, *13*, 3697.
(239) Yang, L.; Abramavicius, D.; Mukamel, S. *New J. Phys.* **2010**, *12*, 065046.
(240) Ginsberg, N. S.; Cheng, Y.-C.; Fleming, G. R. *Acc. Chem. Res.* **2009**, *42*, 1352.
(241) Abramavicius, D.; Mukamel, S. *J. Phys. Chem. B* **2009**, *113*, 6097.
(242) Abramavicius, D.; Mukamel, S. *J. Chem. Phys.* **2010**, *113*, 184501.
(243) Myers, J. A.; Lewis, K. L. M.; Fuller, F. D.; Tekavec, P. F.; Yocum, C. F.; Ogilvie, J. P. *J. Phys. Chem. Lett.* **2010**, *1*, 2774.
(244) Chen, Y.-C.; Fleming, G. R. *J. Phys. Chem. A* **2008**, *112*, 4254.
(245) Engel, G. S.; Calhoun, T. R.; Read, E. L.; Ahn, T.-K.; T. Mančal, T.; Cheng, Y.-.C; Blankenship, R. E.; Fleming, G. R. *Nature Lett.* **2007**, *446*, 782.
(246) Lee, H.; Cheng, Y.-C.; Fleming, G. R. *Science* **2007**, *316*, 1462.
(247) Scholes, G. D. *J. Phys. Chem. Lett.* **2010**, *1*, 2.
(248) Collini, E.; Wong, C. Y.; Wilk, K. E.; Curmi, P. M. G.; Brumer, P.; Scholes, G. D. *Nature* **2010**, *463*, 644.
(249) Palewska, K.; Meister, E. C.; Wild, U. P. *J. Lumin.* **1991**, *50*, 47.
(250) Christensson, N.; Milota, F.; Nemeth, A.; Sperling, J.; Kauffmann, H. F.; Pullerits, T.; Hauer, J. *J. Phys. Chem. B* **2009**, *113*, 16409.
(251) Nemeth, A.; Milota, F.; Mančal, T.; Lukeš, V.; Kauffmann, H. F. *Chem. Phys. Lett.* **2008**, *459*, 94.
(252) Jansson, S. *Biochim. Biophys. Acta* **1994**, *1184*, 1.
(253) Paulsen, H. *Photochem. Photobiol.* **1995**, *62*, 367.

(254) Green, B. R.; Durnford, D. G. *Annu. Rev. Plant Physiol. Plant Mol. Biol.* **1996**, *47*, 685.
(255) Ruban, A. V.; Young, A. J.; Horton, P. *Biochemistry* **1996**, *35*, 674.
(256) van Amerongen, H.; Croce, R. In *Primary Processes of Photosynthesis: Basic Principles and Apparatus*; Renger, G., Ed.; RSC Publication: Cambridge, UK, 2008; p 329.
(257) Bassi, R.; Giuffra, R. E.; Croce, R.; Dainese, P.; Bergantino, E. In *Light as an Energy Source and Information Carrier in Plant Physiology*; Jennings, R. C., Ed.; Plenum Press: New York, 1996; p 41.
(258) Horton, P.; Ruban, A. V.; Walters, R. G. *Annu. Rev. Plant Physiol. Plant Mol. Biol.* **1996**, *47*, 655.
(259) Kühlbrandt, W.; Wang, D. N.; Fujiyoshi, Y. *Nature* **1994**, *367*, 614.
(260) Renger, T.; May, V. *Phys. Rev. Lett.* **2000**, *84*, 5228.
(261) Remelli, R.; Varotto, C.; Sandona, D.; Croce, R.; Bassi, R. *J. Biol. Chem.* **1999**, *274*, 33510.
(262) Rogl, H.; Kühlbrandt, W. *Biochemistry* **1999**, *38*, 16214.
(263) Rogl, H.; Schödel, R.; Lokstein, H.; Kühlbrandt, W.; Schubert, A. *Biochemistry* **2002**, *41*, 2281.
(264) Standfuss, J.; Lamborghini, M.; Kühlbrandt, W.; van Scheltinga, A. C. T. *EMBO J.* **2005**, *24*, 919.
(265) Standfuss, J.; Kühlbrandt, W. *J. Biol. Chem.* **2004**, *279*, 36884.
(266) Irrgang, K.-D.; Slowik, D.; Miao, J.; Scharf, K.; Weiβ, M.; Kussin, S. In *Photosynthesis: Fundamental Aspects to Global Perspectives*; van der Est, A., Bruce, D., Eds.; Alliance Communications Group: Burbank, CA, 2005; p 689.
(267) Giuffra, E.; Zucchelli, G.; Sandona, D.; Croce, R.; Cugini, D.; Garlaschi, F. M.; Bassi, R.; Jennings, R. C. *Biochemistry* **1997**, *36*, 12984.
(268) Sandona, D.; Croce, R.; Pagano, A.; Crimi, M.; Bassi, R. *Biochim. Biophys. Acta* **1998**, *1365*, 207.
(269) Pesaresi, P.; Sandona, D.; Giuffra, E.; Bassi, R. *FEBS Lett.* **1997**, *402*, 151.
(270) Gibasiewicz, K.; Rutkowski, M.; van Grondelle, R. *Photosynthetica* **2009**, *47*, 232.
(271) Pieper, J.; Irrgang, K.-D.; Rätsep, M.; Jankowiak, R.; Voigt, J.; Schrötter, T.; Small, G. J.; Renger, G. *J. Phys. Chem. A* **1999**, *103*, 2412.
(272) Vasil'ev, S.; Irrgang, K.-D.; Schrötter, T.; Bergmann, A.; Eichler, H.-J.; Renger, G. *Biochemistry* **1997**, *36*, 7503.
(273) Herascu, N.; Najafi, M.; Amunts, A.; Pieper, J.; Irrgang, K.-D.; Picorel, R.; Seibert, M.; Zazubovich, V. *J. Phys. Chem. B* **2011**, *115*, 2737.
(274) Pieper, J.; Irrgang, K.-D.*J. Phys. Chem. B* **2011**, submitted.
(275) Linnanto, J.; Martiskainen, J.; Lehtovuori, V.; Ihalainen, J.; Kananavicius, R.; Barbato, R.; Korppi-Tommola, J. *Photosynth. Res.* **2006**, *87*, 267.
(276) Novoderezhkin, V. I.; Palacios, M. A.; van Amerongen, H.; van Grondelle, R. *J. Phys. Chem. B* **2005**, *109*, 10493.
(277) Madjet, M. E.; Abdurahman, A.; Renger, T. *J. Phys. Chem. B* **2006**, *110*, 17268.
(278) Ishizaki, A.; Calhoun, T. R.; Schlau-Cohen, G. S.; Fleming, G. R. *Phys. Chem. Chem. Phys.* **2010**, *12*, 7319.
(279) Calhoun, T. R.; Ginsberg, N. S.; Schlau-Cohen, G. S.; Cheng, Y.-C.; Ballottari, M.; Bassi, R.; Fleming, G. R. *J. Phys. Chem. B* **2009**, *113*, 16291.
(280) Schlau-Cohen, G. S.; Calhoun, T. R.; Ginsberg, N. S.; Read, E. L.; Ballottari, M.; Bassi, R.; van Grodelle, R.; Fleming, G. R. *J. Phys. Chem. B* **2009**, *113*, 15352.
(281) Schlau-Cohen, G. S.; Calhoun, T. R.; Ginsberg, N. S.; Ballottari, M.; Bassi, R.; Fleming, G. R. *Proc. Natl. Acad. Sci. U.S.A.* **2010**, *107*, 13276.
(282) Müh, F.; Madjet, M. E.; Renger, T. *J. Phys. Chem. B* **2010**, *114*, 13517.
(283) Du, M.; Xie, X.; Mets, L.; Fleming, G. R. *J. Phys. Chem.* **1994**, *98*, 4736.
(284) Bittner, T.; Irrgang, K.-D.; Renger, G.; Wasielewski, M. R. *J. Phys. Chem.* **1994**, *98*, 11821.
(285) Connelly, J. P.; Müller, M. G.; Hucke, M.; Gatzen, G.; Mullineaux, C. W.; Ruban, A. V.; Horton, P.; Holzwarth, A. R. *J. Phys. Chem.* **1997**, *101*, 1902.
(286) Kleima, F. J.; Gradinaru, C.; Calkoen, F.; van Stokkum, I. H. M.; van Grondelle, R.; van Amerongen, H. *Biochemistry* **1997**, *36*, 15262.
(287) Gradinaru, C. C.; van Grondelle, R.; van Amerongen, H. *J. Phys. Chem. B* **2003**, *107*, 3938.
(288) Palacios, M. A.; Standfuss, J.; Vengris, M.; van Oort, B. F.; van Stokkum, I. H. M.; Kühlbrandt, W.; van Amerongen, H.; van Grondelle, R. *Photosynth. Res.* **2006**, *88*, 269.
(289) Bittner, T.; Wiederrecht, G. P.; Irrgang, K.-D.; Renger, G.; Wasielewski, M. R. *Chem. Phys.* **1995**, *194*, 311.
(290) Groot, M.; Frese, R. N.; De Weerd, F. L.; Bromek, K.; Pettersson, A.; Peterman, E. J. G.; Van Stokkum, I. H. M.; Van Grondelle, R.; Dekker, J. P. *Biophys. J.* **1999**, *77*, 3328.
(291) Di Donato, M.; van Grondelle, R.; van Stokkum, I. H.; Groot, M. L. *J. Phys. Chem. B* **2007**, *111*, 7345.
(292) Riley, K. J.; Zazubovich, V.; Jankowiak, R. *J. Phys. Chem. B* **2006**, *110*, 22436.
(293) Vasil'ev, S.; Bruce, D. *Biophys. J.* **2006**, *90*, 3062.
(294) Saito, K.; Kikuchi, T.; Nakayama, M.; Mukai, K.; Sumi, H. *J. Photochem. Photobiol., A: Chem.* **2006**, *178*, 271.
(295) Groot, M.; Peterman, E. J. G.; van Stokkum, I. H. M.; Dekker, J. P.; van Grondelle, R. *Biophys. J.* **1995**, *68*, 281.
(296) de Paula, J. C.; Liefshitz, A.; Hinsley, S.; Lin, W.; Chopra, V.; Long, K.; Williams, S. A.; Betts, S.; Yocum, C. F. *Biochemistry* **1994**, *33*, 1455.
(297) de Weerd, F. L.; Palacios, M. A.; Andrizhiyevskaya, E. G.; Dekker, J. P.; van Grondelle, R. *Biochemistry* **2002**, *41*, 15224.
(298) Huyer, J.; Eckert, H. J.; Irrgang, K.-D.; Miao, J.; Eichler, H. J.; Renger, G. *J. Phys. Chem. B* **2004**, *108*, 3326.
(299) van Dorssen, R. J.; Breton, J.; Plijter, J. J.; Satoh, K.; van Gorkom, H. J.; Amesz, J. *Biochim. Biophys. Acta, Bioenerg.* **1987**, *893*, 267.
(300) Andrizhiyevskaya, E. G.; Chojnicka, A.; Bautista, J. A.; Diner, B. A.; van Grondelle, R.; Dekker, J. P. *Photosynth. Res.* **2005**, *84*, 173.
(301) Chang, H.-C.; Jankowiak, R.; Yocum, C. F.; Picorel, R.; Alfonso, M.; Seibert, M.; Small, G. J. *J. Phys. Chem.* **1994**, *98*, 7717.
(302) Pólivka, T.; Kroh, P.; Psencik, J.; Engst, D.; Komenda, J.; Hála, J. *J. Lumin.* **1997**, *72*−*74*, 600.
(303) den Hartog, F. T. H.; van Papendrecht, C.; Störkel, U.; Völker, S. *J. Phys. Chem. B* **1999**, *103*, 1375.
(304) Alfonso, M.; Montoya, G.; Cases, R.; Rodriguez, R.; Picorel, R. *Biochemistry* **1994**, *33*, 10494.
(305) Shen, G.; Vermaas, W. F. J. *Biochemisty* **1994**, *33*, 7379.
(306) Krausz, E.; Hughes, J. L.; Smith, P.; Pace, R.; Peterson Ársköld, S. *Photochem. Photobiol. Sci.* **2005**, *4*, 744.
(307) Krausz, E.; Hughes, J. L.; Smith, P. J.; Pace, R. J.; Ársköld, S. P. *Photosynth. Res.* **2005**, *84*, 193.
(308) Hughes, J. L.; Krausz, E.; Smith, P. J.; Pace, R. J.; Riesen, H. *Photosynth. Res.* **2005**, *84*, 93.
(309) Jankowiak, R.; Rätsep, M.; Hayes, J.; Zazubovich, V.; Picorel, R.; Seibert, M.; Small, G. J. *J. Phys. Chem. B* **2003**, *107*, 2068.
(310) Sauer, K.; Cogdell, R. J.; Prince, S. M.; Freer, A.; Isaacs, N. W.; Scheer, H. *Photochem. Photobiol.* **1996**, *64*, 564.
(311) Alden, R. G.; Johnson, E.; Nagarajan, V.; Parson, W. W.; Law, C. J.; Cogdell., R. J. *J. Phys. Chem. B* **1997**, *101*, 4667.
(312) Wu, H.-M.; Rätsep, M.; Lee, I.-J.; Cogdell, R. J.; Small, G. J. *J. Phys. Chem. B* **1997**, *101*, 7654.
(313) Wu, H.-M.; Reddy, N., R. S.; Small, G. J. *J. Phys. Chem. B* **1997**, *101*, 651.
(314) Freiberg, A.; Rätsep, M.; Timpmann, K.; Trinkunas, G. *J. Lumin.* **2003**, *102*, 363.
(315) Freiberg, A.; Rätsep, M.; Timpmann, K.; Trinkunas, G. *J. Lumin.* **2003**, *108*, 107.
(316) Reddy, N. R.; S.; Small, G., J.; Seibert, M.; Picorel, R. *Chem. Phys. Lett.* **1991**, *181*, 391.
(317) Wu, H.-M.; Savikhin, S.; Reddy, N. R. S.; Jankowiak., R.; Cogdell, R. J.; Struve, W. S.; Small, G. J. *J. Phys. Chem.* **1996**, *100*, 12022.
(318) Matsuzaki, S.; Zazubovich, V.; Fraser, N. J.; Cogdell, R. J.; Small, G. J. *J. Phys. Chem. B* **2001**, *105*, 7049.

(319) Zazubovich, V.; Jankowiak, R.; Small, G, J. *J. Phys. Chem. B* **2002**, *106*, 6802.
(320) Rätsep, M.; Wu, H.-M.; Hayes, J. M.; Small, G. J. *Spectrochem. Acta. A* **1998**, *54*, 1279.
(321) Ketelaars, M.; van Oijen, A. M.; Matsushita, M.; Köhler, J.; Schmidt, J.; Aartsma, T. J. *Biophys. J.* **2001**, *80*, 1591.
(322) Matsushita, M.; Ketelaars, M.; van Oijen, A. M.; Köhler, J.; Aartsma, T. J.; Schmidt, J. *Biophys. J.* **2001**, *80*, 1604.
(323) Hofmann, C.; Aartsma, T. J.; Köhler, J. *Chem. Phys. Lett.* **2004**, *395*, 373.
(324) Neu, P.; Silbey, R. J.; Heuer, A.; Zilker, S. J.; Haarer, D. *J. Lumin.* **1998**, *76*−*77*, 619.
(325) Nanba, O.; Satoh, N. *Proc. Natl. Acad. Sci. U.S.A.* **1987**, *84*, 109.
(326) Seibert, M.; Picorel, R.; Rubin, A. B.; Connolly, J. S. *Plant Physiol.* **1988**, *87*, 303.
(327) McTavish, H.; Picorel, R.; Seibert, M. *Plant Physiol.* **1989**, *89*, 452.
(328) Durrant, J.; R.; Klug, D. R.; Kwa, S. L. S.; van Grondelle, R.; Perter, G.; Dekker, J. P. *Proc. Natl. Acad. Sci. U.S.A.* **1995**, *92*, 4798.
(329) Jankowiak, R.; Hayes, J. M.; Small, G. J. *J. Phys. Chem. B* **2002**, *106*, 8803.
(330) Jankowiak, R.; Rätsep, M.; Picorel, R.; Seibert, M.; Small, G. J. *J. Phys. Chem. B* **1999**, *103*, 9759.
(331) Peterman, E. J. G.; van Amerongen, H.; van Grondelle, R.; Dekker, J. P. *Proc. Natl. Acad. Sci. U.S.A.* **1998**, *95*, 6128.
(332) den Hartog, F. T. H.; Vacha, F.; Lock, A. J.; Barber, J.; Dekker, J. P.; Völker, S. *J. Phys. Chem. B* **1998**, *102*, 9174.
(333) Kwa, S. L. S.; Eijckelhoff, C.; van Grondelle, R.; Dekker, J. P. *J. Phys. Chem.* **1994**, *98*, 7702.
(334) Wasielewski, M. R.; Johnson, D. G.; Seibert, M.; Govindjee *Proc. Natl. Acad. Sci. U.S.A.* **1989**, *86*, 524.
(335) Wasielewski, M. R.; Johnson, D. G.; Govindjee; Preston, C.; Seibert, M. *Photosynth. Res.* **1989**, *22*, 89.
(336) Schelvis, J. P. M.; van Noort, P. I.; Aartsma, T. J.; van Gorkom, H. J. *Biochim. Biophys. Acta* **1994**, *1184*, 242.
(337) Greenfield, S. R.; Seibert, M.; Wasielewski, M. R. *J. Phys. Chem. B* **1999**, *103*, 8364.
(338) Greenfield, S. R.; Seibert, M.; Govindjee; Wasielewski, M. R. *J. Phys. Chem. B* **1997**, *101*, 2251.
(339) Tang, D.; Jankowiak, R.; Seibert, M.; Small, J. G. *Photosynth. Res.* **1991**, *29*, 19.
(340) Prokhorenko, V. I.; Holzwarth, A. R. *J. Phys. Chem. B* **2000**, *104*, 11563.
(341) Dekker, J. P.; van Grondelle, R. *Photosynth. Res.* **2000**, *63*, 195.
(342) Riley, K. J.; Jankowiak, R.; Rätsep, M.; Small, G. J.; Zazubovich, V. J. *Phys. Chem. B* **2004**, *108*, 10346.
(343) Novoderezhkin, V. I.; Dekker, J. P; van Grondelle, R. *Biophys. J.* **2007**, *93*, 1293.
(344) Romero, E.; van Stokkum, I. H. M.; Novoderezhkin, V. I.; Dekker, J. P.; van Grondelle, R. *Biochemistry* **2010**, *49*, 4300.
(345) Chang, H.-C.; Jankowiak, R.; Reddy, N. R. S.; Yocum, C. F.; Picorel, R.; Seibert, M.; Small, G. J. *J. Phys. Chem.* **1994**, *98*, 7725.
(346) Peterson Årsköld, S.; Masters, V. M.; Prince, B. J.; Smith, P. J.; Pace, R., J.; Krausz, E. *J. Am. Chem. Soc.* **2003**, *123*, 13063.
(347) Smith, P. J.; Peterson, S.; Masters, V. M.; Wydrzynski, T.; Styring, S.; Krausz, E.; Pace, R. *Biochemistry* **2002**, *41*, 1981.
(348) Johnson, S. G.; Tang, D.; Jankowiak, R.; Hayes, J. M.; Small, G. J. *J. Phys. Chem.* **1990**, *94*, 5849.
(349) Small, G. J. *Chem. Phys.* **1995**, *197*, 239.
(350) Sener, M. K.; Jolley, C.; Ben-Shem, A.; Fromme, P.; Nelson, N.; Croce, R.; Schulten, C. *Biophys. J.* **2005**, *89*, 1630.
(351) Rätsep, M.; Johnson, T. W.; Chitnis, P. R.; Small, G. J. *J. Phys. Chem. B* **2000**, *104*, 836.
(352) Zazubovich, V.; Matsuzaki, S.; Johnson, T. W.; Hayes, J. M.; Chitnis, P. R.; Small, G. J. *Chem. Phys.* **2002**, *275*, 47.
(353) Hsin, T.-M.; Zazubovich, V.; Hayes, J. M.; Small, G. J. *J. Phys. Chem. B* **2004**, *108*, 10515.
(354) Bibby, T. S.; Nield, J.; Barber, J. *Nature* **2001**, *412*, 743.
(355) Nield, J.; Morris, E., P.; Bibby, T. S.; Barber, J. *Biochemistry* **2003**, *42*, 3180.
(356) Boekema, E. J.; Hifney, A.; Yakushevska, A. E.; Piotrowski, M.; Keegstra, W.; Berry, S.; Michel, K.-P.; Pistorius, E. K.; Kruip, J. *Nature* **2001**, *412*, 745.
(357) Melkozernov, A. N.; Bibby, T. S.; Lin, S.; Barber, J.; Blankenship, R. E. *Biochemistry* **2003**, *42*, 3893.
(358) Andrizhiyevskaya, E. G.; Schwabe, T. M. E.; Germano, M.; D'Haene, S.; Kruip, J.; van Grondelle, R.; Dekker, J. P. *Biochim. Biophys. Acta* **2002**, *1556*, 265.
(359) Melkozernov, A. N.; Barber, J.; Blankenship, R. E. *Biochemistry* **2006**, *45*, 331.
(360) Croce, R., Zazubovich, V. Unpublished.
(361) Gibasiewicz, K.; Szrajner, A.; Ihalainen, J. A.; Germano, M.; Dekker, J. P.; van Grondelle, R. *J. Phys. Chem. B* **2005**, *109*, 21180.
(362) Croce, R.; Chojnicka, A.; Morosinotto, T.; Ihalainen, J. A.; van Mourik, F.; Dekker, J. P.; Bassi, R.; van Grondelle, R. *Biophys. J.* **2007**, *93*, 2418.
(363) Romero, E.; Mozzo, M.; van Stokkum, I. H. M.; Dekker, J. P.; van Grondelle, R.; Croce, R. *Biophys. J.* **2008**, *96*, L35.
(364) Hughes, J. L.; Prince, B. J.; Peterson Årsköld, S.; Smith, P. J.; Pace, R. J.; Riesen, H.; Krausz, E. *Aust. J. Chem.* **2004**, *57*, 1179.
(365) Hughes, J. L.; Krausz, E. *J. Lumin.* **2007**, *127*, 239.
(366) Hughes, J. L.; Smith, P.; Pace, R.; Krausz, E. *Biochim. Biophys. Acta* **2006**, *1757*, 841.
(367) Krausz, E.; Cox, N.; Årsköld, S. *Photosynth. Res.* **2008**, *98*, 207.
(368) Cox, N.; Hughes, J.; Rutherford, A. W.; Krausz, E. *Phys. Procedia* **2010**, *3*, 1601.
(369) Raszewski, G.; Saenger, W.; Renger, T. *Biophys. J.* **2005**, *88*, 986.
(370) Cox, N.; Hughes, J. L.; Steffen, R.; Smith, P. J.; Rutherford, W.; Pace, R. J.; Krausz, E. *J. Phys. Chem. B* **2009**, *113*, 12364.
(371) Prince, B. J.; Krausz, E.; Peterson Årsköld, S.; Smith, P. J.; Pace, R. J. *J. Lumin.* **2004**, *108*, 101.
(372) Hughes, J. L.; Krausz, E.; Smith, P. J.; Pace, R. J. In *PS2004: 13th International Congress of Photosynthesis*; van der Est, A., Bruce, D., Eds.; Montreal, Canada, 2004; p S6A.
(373) Fenna, R. E.; Matthews, B. W. *Nature* **1975**, *258*, 573.
(374) Tsukatani, Y.; Wen, J.; Blankenship, R. E; Bryant, D. A. *Photosynth. Res.* **2010**, *104*, 201.
(375) Busch, M. S.; Müh, F.; Madjet, M. E-A.; Renger, T. *J. Phys. Chem.Lett.* **2011**, *2*, 93.
(376) Garrity, G. M.; Holt, J. G. In *Bergey's Manual of Systematic Bacteriology*, 2nd ed.; Boone, D. R., Castenholz, R. W., Eds, Springer: New York, 2001; p 427.
(377) Olson, J. M. *Photosynth. Res.* **2004**, *80*, 181.
(378) Blankenship, R. E. *Molecular Mechanism of Photosynthesis*, Blackwell Science Ltd.: London, 2002; p 1.
(379) Matthews, B. W.; Fenna, R. E. *Acc. Chem. Res.* **1980**, *13*, 309.
(380) Matthews, B. W.; Fenna, R. E.; Bolognesi, M. C.; Schmid, M. F.; Olson, J. M. *J. Mol. Biol.* **1979**, *131*, 259.
(381) Li, Y.; Zhou, W.; Blankenship, R. E.; Allen, J. P. *J. Mol. Biol.* **1997**, *271*, 456.
(382) Tronrud, D. E.; Schmid, M. F.; Matthews, B. W. *J. Mol. Biol.* **1986**, *188*, 443.
(383) Camara-Artigas, A.; Blankenship, R. E.; Allen, J. P. *Photosynth. Res.* **2003**, *75*, 49.
(384) Ben-Shem, A.; Frolow, F.; Nelson, N. *FEBS Lett.* **2004**, *564*, 274.
(385) Louwe, R. J. W.; Vrieze, J.; Hoff, A. J.; Aartsma, T. J. *J Phys. Chem. B* **1997**, *101*, 11280.
(386) Vulto, S. I. E.; De Baat, M. A.; Louwe, R. J. W.; Permentier, H. P.; Neef, T.; Miller, M.; Van Amerongen, H.; Aartsma, T. J. *J. Phys. Chem. B* **1998**, *102*, 9577.
(387) Olson, J. M. In *Methods in Enzymology*; San Pietro, A, Ed.; Academic Press: New York, 1971; Vol. 23, part A, pp 636.
(388) Olson, J. M.; Ke, B.; Thompson, K. H. *Biochim. Biophys. Acta, Bioenerg.* **1976**, *430*, 524.

(389) Blankenship, R. E.; Cheng, P.; Causgrove, T. P.; Brune, D. C.; Wang, S. H. H.; Choh, J. U.; Wang, J. *Photochem. Photobiol.* **1993**, *57*, 103.
(390) Matsuzaki, S.; Zazubovich, V.; Rätsep, M.; Hayes, J. M.; Small, G. J. *J. Phys. Chem. B* **2000**, *104*, 9564.
(391) Adolphs, J.; Renger, T. *Biophys. J.* **2006**, *91*, 2778.
(392) Cho, M.; Vaswani, H. M.; Brixner, T.; Stenger, J.; Fleming, G. R. *J. Phys. Chem.* **2005**, *109*, 10542.
(393) Whaley, K. B.; Sarovar, M.; Ishizaki, A. *arXiv:1012.4059v1*.
(394) van Mourik, F.; Verwijst, R. R.; Mulder, J. M.; van Grondelle, R. *J. Phys. Chem.* **1994**, *98*, 10307.
(395) Reddy, N. R. S.; Jankowiak, R.; Small, G. J. *J. Phys. Chem.* **1995**, *99*, 16168.
(396) Louwe, R. J. W.; Aartsma, T. J.; Gast, P.; Hulsebosch, R. J.; Nan, H. M.; Vrieze, J.; Hoff, A. J. *Biochim. Biophys. Acta, Bioenerg.* **1998**, *1365*, 373.
(397) Iseri, E. I.; Gulen, D. *Eur. Biophys. J. Biophys. Lett.* **1999**, *28*, 243.
(398) Wendling, M.; Przyjalgowski, M. A.; Gulen, D.; Vulto, S. I. E.; Aartsma, T. J.; van Grondelle, R.; van Amerongen, H. *Photosynth. Res.* **2002**, *71*, 99.
(399) Shibata, Y.; Saga, Y.; Tamiaki, H.; Itoh, S. *Biochemistry* **2007**, *46*, 7062.
(400) Abramavicius, D.; Voronine, D. V.; Mukamel, S. *Proc. Natl. Acad. Sci. U.S.A.* **2008**, *105*, 8525.
(401) Milder, M. T. W.; van Grondelle, R.; Herek, J. L. *Photosynth. Res.* **2010**, *104*, 257.
(402) Sarovar, M.; Ishizaki, A.; Fleming, G. R.; Whaley, K. B. *Nat. Phys.* **2010**, *6*, 462.
(403) Riesen, H; Yildirim, B. J. *Phys. Chem. Lett.* **2010**, *1*, 2380.

NOTE ADDED IN PROOF

While this review was being written, direct information on the CP29 structure was not available. All structural models were based on the high sequence homology among the Lhcb proteins. Very recently, however, the first crystal structure of spinach CP29 was reported at 2.8 Å resolution by Pan et al. (*Nature Structural & Molecular Biology* **2011**, *18*, 309). According to this work CP29 binds 13 Chl and 3 carotenoid molecules.